Bergman's Comprehensive Encyclopedia of Human Anatomic Variation

Bergman's Comprehensive Encyclopedia of Human Anatomic Variation

R. Shane Tubbs, MS, PA-C, PhD

Professor and Chief Scientific Officer,
Seattle Science Foundation,
Seattle, Washington, United States
Professor of Anatomy
Department of Anatomical Sciences
St. George's University, Grenada
Centre of Anatomy and Human Identification
University of Dundee, Scotland, United Kingdom

Mohammadali M. Shoja, MD

Tuberculosis and Lung Disease Research Center
Tabriz University of Medical Sciences
Tabriz, Iran

Marios Loukas, MD, PhD

Professor and Chair
Department of Anatomical Sciences,
Dean of Research, School of Medicine
St. George's University, Grenada

WILEY Blackwell

Published by John Wiley & Sons, Inc., Hoboken, New Jersey
Published simultaneously in Canada

Library of Congress Cataloging-in-Publication Data

Names: Tubbs, R. Shane. | Shoja,
Mohammadali M. | Loukas, Marios.
Title: Bergman's comprehensive encyclopedia of human anatomic variation /
[edited by] R. Shane Tubbs, MS, PA-C, PhD, Professor and Chief Scientific Officer,
Seattle Science Foundation, Seattle, Washington, United States, Professor of
Anatomy, Department of Anatomical Sciences, St. George's University,
Grenada, Centre of Anatomy and Human Identification, University of Dundee,
Scotland, United Kingdom, Mohammadali M. Shoja, MD, Tuberculosis and Lung Disease Research Center,
Tabriz University of Medical Sciences, Tabriz, Iran, Marios Loukas,
MD, PhD, Professor and Chair, Department of Anatomical Sciences, Dean of
Research, School of Medicine, St. George's University, Grenada.
Other titles: Comprehensive encyclopedia of human anatomic variation |
Encyclopedia of human anatomic variation
Description: Hoboken, New Jersey : John Wiley & Sons, Inc., [2016] | Includes
index.
Identifiers: LCCN 2015039645 | ISBN 9781118430354 (cloth)
Subjects: LCSH: Human anatomy—Variation—Encyclopedias. | Human
anatomy—Encyclopedias.
Classification: LCC QM24 .C65 2016 | DDC 612.003—dc23 LC record available at http://lccn.loc.gov/2015039645

Set in 9.5/12pt Minion Pro by Aptara Inc., New Delhi, India

10 9 8 7 6 5 4 3 2 1

As the reader sees from the title of this textbook, it is dedicated to Dr. Ronald Bergman. Dr. Bergman was not the first to collect and publish on the variations of the human anatomy (e.g. Henle, Macalister, Adachi). However, he was the first to publish on this topic at such an in depth and comprehensive scale. My first introduction to Dr. Bergman's *Compendium of Human Anatomic Variation* was as a graduate student. As any dissector will eventually do, I came across something unusual in one of our cadavers during a routine dissection. I asked by my mentor, Dr. George Salter, about this who said, "You know there used to be a book in the lab office that focused on the anatomic variations of the body." After some digging, I was delighted to find this book, which I set out to memorize as best as I could. From that day on, Dr. Bergman's book and *Gray's Anatomy* were my main resources for studying anatomy. Therefore, this current text is not only an updated resource but also a tribute to the pioneering efforts of Dr. Ronald Bergman who reminded us that no two bodies are the same!

R. Shane Tubbs

I would like to dedicate my work on this enormous project to my son, Isaiah. Isaiah you are the light of my life! To my wife, Susan, you are the best. Many thanks to Drs. Rod Oskouian and Johnny Delashaw for their encouragement. Also, Dr. W. Jerry Oakes has supported this project and my other academic endeavors and I sincerely thank him. Lastly, I thank Dr. E. George Salter for persuading me to take on a career in anatomy and for first introducing me to the *Compendium of Human Anatomic Variation*!

R. Shane Tubbs

To Susan and Shane Tubbs, a very beautiful couple.

Mohammadali M. Shoja

To the love of my life, my wife Joanna Loukas

Marios Loukas

Contents

List of contributors

Nimer Adeeb
Children's of Alabama
Birmingham, Alabama, USA

Anjali Aggarwal
Postgraduate Institute of Medical Education & Research
Chandigarh, India

Sadakazu Aiso
Keio University
Tokyo, Japan

Veysel Akgun
Gulhane Military Medical Academy
Ankara, Turkey

Keiichi Akita
Tokyo Medical and Dental University
Tokyo, Japan

Soner Albay
Suleyman Demirel University Faculty of Medicine
Isparta, Turkey

Nihal Apaydin
Ankara University Faculty of Medicine
Ankara, Turkey

Takamitsu Arakawa
Kobe Graduate School of Health Sciences
Kobe, Japan

Mohammad Reza Ardalan
Tabriz University of Medical Sciences
Tabriz, Iran

Ian L. Aveytua
New York College of Podiatric Medicine
New York, New York, USA

Barclay W. Bakkum
Illinois College of Optometry
Chicago, Illinois, USA

Mustafa K. Başkaya
University of Wisconsin
Madison, Wisconsin, USA

Bilal Battal
Gulhane Military Medical Academy
Ankara, Turkey

Brion Benninger
Western University of Health Sciences
Portland, Oregon, USA

Frederic J. Bertino
St George's University, School of Medicine
St Georges, Grenada

Marius C. Bosman
University of Pretoria
Pretoria, South Africa

Yalcin Bozkurt
Golcuk Military Hospital
Kocaeli, Turkey

Michaël Bruneau
Hôpital Erasme
Brussels, Belgium

Gianluca Bullitta
"Sapienza" University of Rome
Rome, Italy

Alper Cesmebasi
St George's University, School of Medicine
St Georges, Grenada

David W. Chang
The University of Texas MD Anderson Cancer Center
Houston, Texas, USA

Kunal Chawla
Postgraduate Institute of Medical Education & Research
Chandigarh, India

Ulaş Cikla
University of Wisconsin
Madison, Wisconsin, USA

Jarrod A. Collins
Children's of Alabama
Birmingham, Alabama, USA

Michael Conklin
Children's of Alabama
Birmingham, Alabama, USA

Patrick Courtis
University College Dublin
Dublin, Ireland

Anthony D'Antoni
New York College of Podiatric Medicine
New York, New York, USA

Zubin J. Daruwalla
Beaumont Hospital
Dublin, Ireland

Ross Dawkins
University of Alabama at Birmingham
Birmingham, Alabama, USA

Aman Deep
Children's of Alabama
Birmingham, Alabama, USA

Arpan Deep
Postgraduate Institute of Medical Education & Research
Chandigarh, India

John P. Deveikis
University of Alabama at Birmingham
Birmingham, Alabama, USA

Sedat Develi
Gulhane Military Medical Academy
Ankara, Turkey

Anthony C. DiLandro
New York College of Podiatric Medicine
New York, New York, USA

Benjamin J. Ditty
University of Alabama at Birmingham
Birmingham, Alabama, USA

Maira du Plessis
St George's University
St Georges Grenada

Amr E. El-Shazly
Liège University Hospital
Liège, Belgium

Juntima Euathrongchit
Chiang Mai University
Chiang Mai, Thailand

Regina C. Fiacco
New York College of Podiatric Medicine
New York, New York, USA

David Fitzpatrick
University College Dublin
Dublin, Ireland

Clare Fitzpatrick
University College Dublin
Dublin, Ireland

Natasha Flack
University of Otago
Dunedin, New Zealand

Paul Foreman
University of Alabama at Birmingham
Birmingham, Alabama, USA

Shallu Garg
Postgraduate Institute of Medical Education & Research
Chandigarh, India

Dustin T. Gayheart
University of Alabama at Birmingham
Birmingham, Alabama, USA

Bernard George
Hôpital Lariboisière
Paris, France

Giuseppe Giannicola
"Sapienza" University of Rome
Rome, Italy

Mirtha A. Gonzalez
Baylor College of Medicine
Houston, Texas, USA

Dylan Goodrich
St George's University, School of Medicine
St Georges, Grenada

Christoph J. Griessenauer
University of Alabama at Birmingham
Birmingham, Alabama, USA

Richa Gupta
Postgraduate Institute of Medical Education & Research
Chandigarh, India

Tulika Gupta
Postgraduate Institute of Medical Education & Research
Chandigarh, India

Mark N. Hadley
University of Alabama at Birmingham
Birmingham, Alabama, USA

Mohammad R. Haffajee
University of KwaZulu-Natal
Durban, South Africa

Matthew Haffner
St George's University, School of Medicine
St Georges, Grenada

Salih Hamcan
Agri Military Hospital
Agri, Turkey

Mark Harrigan
University of Alabama at Birmingham
Birmingham, Alabama, USA

Munawar Hayat
St George's University, School of Medicine
St Georges, Grenada

Nobuaki Imanishi
Keio University
Tokyo, Japan

Paul Anthony Irwin
Children's of Alabama
Birmingham, Alabama, USA

Mohammad Jaber
Children's of Alabama
Birmingham, Alabama, USA

Masahiro Jinzaki
Keio University
Tokyo, Japan

David B. Joseph
Children's of Alabama
Birmingham, Alabama, USA

Shamfa C. Joseph
St George's University, School of Medicine
St Georges, Grenada

Rene M. Kafka
New York College of Podiatric Medicine
New York, New York, USA

Harjeet Kaur
Postgraduate Institute of Medical Education & Research
Chandigarh, India

Kazuo Kishi
Keio University
Tokyo, Japan

Necdet Kocabiyik
Gulhane Military Medical Academy
Ankara, Turkey

Gregory C. Kujoth
University of Wisconsin
Madison, Wisconsin, USA

Sachio Kuribayashi
Keio University
Tokyo, Japan

Clare Lamb
University of Dundee
Dundee, UK

H. Wayne Lambert
West Virginia University School of Medicine
Morgantown, West Virginia, USA

Hye Yeon Lee
Yonsei University College of Medicine
Seoul, Korea

Howe Liu
University of North Texas Health Science Center
Fort Worth, Texas, USA

Marios Loukas
St George's University, School of Medicine
St Georges, Grenada

Michael C. Lysek
University of Alabama at Birmingham
Birmingham, Alabama, USA

Thandinkosi E. Madiba
University of KwaZulu-Natal
Durban, South Africa

Mark A. Mahan
University of Utah
Salt Lake City, Utah, USA

Niladri Kumar Mahato
Ohio University
Athens, Ohio, USA

R. Malhotra
Beaumont Hospital
Dublin, Ireland

Eva Maranillo
Complutense University of Madrid
Madrid, Spain

Tarik F. Massoud
Stanford University School of Medicine
Stanford, California, USA

Joseph H. Miller
University of Alabama at Birmingham
Birmingham, Alabama, USA

Nathan Miller
National University of Health Sciences
Lombard, Illinois, USA

Priti L. Mishall
Albert Einstein College of Medicine
Bronx, New York, USA

Martin M. Mortazavi
University of Washington School of Medicine
Seattle, Washington, USA

Hannan Mullett
Beaumont Hospital
Dublin, Ireland

Horia Muresian
Cardiovascular Surgery
San Donato Milan, Italy
University Hospital of Bucharest
Bucharest, Romania

Pedro B. Nava
Loma Linda University School of Medicine
Riverside, California, USA

David T. Netscher
Baylor College of Medicine
Houston, Texas, USA
Weill Medical College, Cornell University
New York, New York, USA

Helen Nicholson
University of Otago
Dunedin, New Zealand

Akimoto Nimura
Tokyo Medical and Dental University
Tokyo, Japan

W. Jerry Oakes
Children's of Alabama
Birmingham, Alabama, USA

Jean Oakes
University of Alabama at Birmingham
Birmingham, Alabama, USA

Anthony Olinger
Kansas City University of Medicine and Biosciences
Kansas City, Missouri, USA

Nidal B. Omar
University of Alabama at Birmingham
Birmingham, Alabama, USA

Deepali Onkar
NKP Salve Institute of Medical Sciences and Research Centre
Nagpur, India

Gülnur Özgüner
Suleyman Demirel University
Isparta, Turkey

Arán Pascual-Font
Complutense University of Madrid
Madrid, Spain

Akshal Patel
Pennsylvania State University
Hershey, Pennsylvania, USA

Swetal Patel
St George's University, School of Medicine
St Georges, Grenada

Toral Patel
Children's of Alabama
Birmingham, Alabama, USA

David Polimanti
"Sapienza" University of Rome
Rome, Italy

Benjamin Todd Raines
University of Alabama at Birmingham
Birmingham, Alabama, USA

Megha Rapotra
Postgraduate Institute of Medical Education & Research
Chandigarh, India

Joel Raborn
University of Alabama at Birmingham
Birmingham, Alabama, USA

Garen M. Ream
New York College of Podiatric Medicine
New York, New York, USA

Elias Rizk
Pennsylvania State University
Hershey, Pennsylvania, USA

Fareed Rizq
Children's of Alabama
Birmingham, Alabama, USA

José Francisco Rodríguez-Vázquez
Complutense University of Madrid
Madrid, Spain

Matthew Rubacha
St George's University, School of Medicine
St Georges, Grenada

Federico Maria Sacchetti
"Sapienza" University of Rome
Rome, Italy

Alireza Sadighi
University of Wisconsin
Madison, Wisconsin, USA

Daisy Sahni
Postgraduate Institute of Medical Education & Research
Chandigarh, India

Tsuyoshi Saga
Kurume University School of Medicine
Fukuoka, Japan

Narbada Saini
Postgraduate Institute of Medical Education & Research
Chandigarh, India

Yujiro Sakamoto
Tokyo Medical and Dental University
Tokyo, Japan

Santosh Sangari
Weill Cornell Medical College
New York, New York, USA

Jose Sanudo
Complutense University of Madrid
Madrid, Spain

Marco Scacchi
"Sapienza" University of Rome
Rome, Italy

Albert van Schoor
University of Pretoria
Pretoria, South Africa

Pietro Sedati
"Sapienza" University of Rome
Rome, Italy

Harsimran Jit Singh
Postgraduate Institute of Medical Education & Research
Chandigarh, India

Anjali Singla
Postgraduate Institute of Medical Education & Research
Chandigarh, India

Devendra Shekhawat
Postgraduate Institute of Medical Education & Research
Chandigarh, India

Courtney L. Shepard
University of Alabama at Birmingham
Birmingham, Alabama, USA

Mohammadali M. Shoja
Tuberculosis and Lung Disease Research Center
Tabriz University of Medical Sciences
Tabriz, Iran

M. Cumhur Sivrikoz
Eskişehir Osmangazi University Medical Faculty
Eskişehir, Turkey

Michael Snosek
St George's University, School of Medicine
St Georges, Grenada

Young-Bin Song
Children's of Alabama
Birmingham, Alabama, USA

Robert J. Spinner
Mayo Clinic
Rochester, Minnesota, USA

Jonathan Spratt
University Hospital of North Durham
Durham, UK

Mark D. Stringer
Christchurch Hospital
University of Otago
Dunedin, New Zealand

Kelley A. Strothmann
Indiana University
Fort Wayne, Indiana, USA

Hiroo Suami
The University of Texas MD Anderson Cancer Center
Houston, Texas, USA

Nagahiro Takahashi
Kurume University School of Medicine
Fukuoka, Japan

Satoshi Tsutsumi
Juntendo University Urayasu Hospital
Chiba, Japan

R. Shane Tubbs
Seattle Science Foundation
Seattle, Washington, USA
St George's University, School of Medicine
St Georges, Grenada
University of Dundee
Dundee, UK

Richard Isaiah Tubbs
Children's of Alabama
Birmingham, Alabama, USA

Selcuk Tunali
TOBB University of Economics and Technology
Ankara, Turkey
University of Hawaii
Honolulu, Hawaii, USA

Richard Tunstall
The University of Warwick
Coventry, UK

Senem T. Ozdemir
Uludag University
Bursa, Turkey

Ivan Varga
Comenius University in Bratislava
Bratislava, Slovakia

Teresa Vazquez
Complutense University of Madrid
Madrid, Spain

Joel Vilensky
Indiana University
Fort Wayne, Indiana, USA

Jenna R. Voirol
Indiana University
Fort Wayne, Indiana, USA

Yutthaphan Wannasopha
Chiang Mai University
Chiang Mai, Thailand

Peter J. Ward
West Virginia School of Osteopathic Medicine
Lewisburg, West Virginia, USA

Robert Ward
Tufts Medical Center,
Boston, Massachusetts, USA

Koichi Watanabe
Kurume University School of Medicine
Fukuoka, Japan

Louise Wing
John Radcliffe Hospital
Oxford, UK

Stephanie Woodley
University of Otago
Dunedin, New Zealand

Candace R. Wooten
St George's University, School of Medicine
St Georges, Grenada

Daniel J. Won
Loma Linda University School of Medicine
Riverside, California, USA

Bulent Yalcin
Gulhane Military Medical Academy
Ankara, Turkey

Shoko M. Yamada
Loma Linda University School of Medicine
Riverside, California, USA

Shokei Yamada
Loma Linda University School of Medicine
Riverside, California, USA

Minoru Yamada
Keio University
Tokyo, Japan

Shun Yamazaki
Keio University
Tokyo, Japan

Jennifer Yang
University of Alabama at Birmingham
Birmingham, Alabama, USA

Hee Jun Yang
Gachon Graduate School of Medicine
Incheon, South Korea

Anthony Zandian
St George's University, School of Medicine
St Georges, Grenada

Preface

Since the beginning of time, differences between humans have made us identifiable to those around us. Some extreme forms of morphological variation have even resulted in individuals being either unique or outcasts. For example, dwarfs have been revered in various cultures and even represented in royal courts and some cultures have bestowed a god status on children born with multiple limbs. Other variations, however, have been viewed as "different" enough to warrant being ostracized. Children being born with a caudal appendage (tail) who were considered offspring of Satan exemplify this.

Human anatomic variation can be defined as human form that is outside of the normal. However, what is normal? This question is often very difficult to answer. For example, most would agree that having two breasts is normal but what about a woman with accessory breasts? Is this normal, abnormal or even pathologic? Is it a variant or an anomaly? Sometimes, the answer to these questions is based on cultural norms or societal acceptance.

Obviously, hair color is certainly varied among individuals with many having a color that doesn't fit into the classic brown, black, red, or blonde categories. But are various hair colors that one of these terms does not apply to have a variation or is this simply an issue of definition e.g. red in the broader sense would include auburn, strawberry, etc.? In other words, our definition of normal is the gauge by which an anatomic trait is considered a variation or not. Some have tried to shed light on this by using such words as "borderlands." Beyond the "border" a trait is thereby considered a variation. To confuse these issues, the term anomaly is and has been used interchangeably in regard to both variation and pathology. Herein, we have attempted to avoid pathologic anatomy but often, the line between an anatomic variation that is pathologic or predisposes one to pathology and one that is just a trait that is outside of what is considered normal is very gray. Moreover, as the term "anomaly" is often used to denote a variation that results in dysfunction or disease, we have tried to avoid this term when possible. However, the form of a structure may cause dysfunction in one person and not another. Therefore, "anomalies" do not always result in dysfunction or disease. The terms "abnormal" and "aberrant" have each been used loosely in the medical literature to describe anatomy that is non-pathologic or results in dysfunction.

Confoundedly, there are variations within variations. Where does one draw the line between a variation that is accepted as "normal" (the so-called normal variant) and a variation that is considered "abnormal"? In this text, we have attempted to be more inclusive than not. If the majority of individuals do not have an anatomic trait, then we have considered it a variation. With this however, the definition of majority has to be defined.

A quarter of a century ago, Dr. Ronald Bergman set forth to collect and publish a compendium of human variation. His textbook soon became the gold standard in human anatomic variation. As anatomists, we consulted this text almost daily. However, in the interim since its publication, radiologic technology and improved optics such as the surgical microscope have allowed us to see into the body with better accuracy than ever before. As a result, many more variations have come to the anatomist's and clinician's attention. Therefore, an updated textbook devoted to human anatomic variation seemed timely. However, as no single text on human anatomy can include all of the intricate details and structures of the body, so too can no single text on human anatomic variation capture all known or reported variants of the body, although we have tried. This tome will attempt to capture many of the known variants of the human form.

Nothing is pleasant that is not spiced with variety.
Francis Bacon

Through every rift of discovery some seeming anomaly drops out of the darkness, and falls, as a golden link into the great chain of order.
Edwin Hubbel Chapin

Variety's the very spice of life that gives it all its flavor.
William Cowper

The essence of the beautiful is unity in variety.
W. Somerset Maugham

I have called this principle, by which each slight variation, if useful, is preserved, by the term of Natural Selection.
Charles Darwin

Variety of mere nothings gives more pleasure than uniformity of something.
Jean Paul

The gifts of nature are infinite in their variety, and mind differs from mind almost as much as body from body.
Quintilian

To such an extent does nature delight and abound in variety that among her trees there is not one plant to be found which is exactly like another; and not only among the plants, but among the boughs, the leaves and the fruits, you will not find one which is exactly similar to another.

Leonardo DaVinci

The catalogue of forms is endless: until every shape has found its city, new cities will continue to be born. When the forms exhaust their variety and come apart, the end of cities begins.

Italo Calvino

R. Shane Tubbs

Foreword

With the possible exception of a few pairs of identical twins, the anatomy of every human being on this planet is unique. That means that there are as many anatomical variations as there are people! Obviously, only a small percentage of these variations are of clinical significance. There are subtle variations in facial anatomy that will allow a clinical anatomist to tell one person from another, but that is not the type of variation that this textbook is about. Instead, this textbook is a resource for the clinical anatomist who needs a single comprehensive source for all the variations that have been published in peer-reviewed journals or web sites.

This new text is the first of its kind since *Compendium of Human Anatomic Variation: Text, Atlas, and World Literature* by Ronald A. Bergman, Sue Ann Thompson, and Adel K. Afifi published in 1988. There have been many published accounts of variations since that time. In fact, this text contains thousands of published variations. This update is clinically important in view of recent advances in surgery and radiologic imaging. For a surgical example, endoscopic surgery makes what was previously an insignificant variation now necessary for the surgeon to recognize in order to perform a procedure safely. Improved resolution of radiologic images in all modalities makes it more important to be able to recognize what is pathologic and what is a normal variation.

Bergman's "Compendium" was the "gold standard" of its day. This text will soon become the new gold standard. Even Dr. Bergman would agree with that!

Respectfully submitted,
Stephen W. Carmichael, Ph.D., D.Sc.
Professor Emeritus of Anatomy and Orthopedic Surgery,
Mayo Clinic
Editor Emeritus, *Clinical Anatomy*

Foreword

This book, with great personal pride for me, provides elegant confirmation of the proven fact that the human body (as well as every living thing) is not created without variability. To paraphrase a profound statement by Sir William Osler, "variability is the rule of life"! The present book complements and extends a previous compendium, and an internet edition of human anatomic variation. Dr. Shane Tubbs conceived and developed this revision. He and his co-editors expand our knowledge and are to be very highly commended for keeping the concepts fresh in the minds of all who are interested in the structure and function of the human body.

Ronald A. Bergman, PhD
Emeritus Professor of Anatomy
The University of Iowa

1 Skull

Selcuk Tunali
TOBB University of Economics and Technology, Ankara, Turkey
University of Hawaii, Honolulu, Hawaii, United States

Frontal bone

The frontal sinus ostium is sometimes absent. In a cadaveric study, Ozgursoy et al. (2010) reported absence of right frontal sinus ostium in 3.6% of cases when there was a connection between the right and left frontal sinuses. They also noted that if one of the frontal sinus ostia cannot be found during sinus surgery, although this sinus and its recess can be seen on thick-sliced coronal computed tomographic scans, there could be an agenetic frontal sinus hidden by the extensive pneumatization of the contralateral sinus that crosses the midline (3.6%).

The frontal sinus itself can be absent. Computed tomographic scans in the axial and coronal planes of the frontal sinuses of 565 patients were examined. There was bilateral agenesis of the frontal sinus in 8.32% of these cases and unilateral absence of the frontal sinus in 5.66% (Danesh-Sani et al. 2011).

Another study investigated the prevalence of agenesis of the frontal sinuses using dental volumetric tomography (DVT) in Turkish individuals. The frontal sinuses of 410 patients were examined by DVT scans in the coronal plane. There was bilateral and unilateral absence of the frontal sinuses in 0.73% and 1.22% of cases, respectively (Çakur et al. 2011a). Aydinlioğlu et al. (2003) studied computed tomography (CT) scans of the paranasal sinuses in the axial and coronal planes from a series of 1200 cases. Bilateral and unilateral absences of the frontal sinuses were noted in 3.8% and 4.8%, respectively.

In a study on the septation of the frontal sinuses, Comer et al. (2013) concluded that frontal sinus septations appear to be significantly associated with and predictive of the presence of supraorbital ethmoid cells. Identifying frontal sinus septations on sinus CT could therefore imply a more complex anatomy of the frontal recess.

In a study by Bajwa et al. (2013), all patients older than 15 months and 23 days had completely fused metopic sutures. The estimated median age for the start of the fusion process was 4.96 months (95% confidence interval, 3.54–6.76 months), and the estimated median age for completion of fusion was 8.24 months (95% confidence interval, 7.37–9.22 months). The fusion process was complete between 2.05 and 14.43 months of age in 95% of the normal population. There was no significant difference between sexes. This study demonstrated wide variation in the timing of normal fusion, which can complete as early as two months of age (Bajwa et al. 2013).

Persistent metopic sutures can be misdiagnosed as vertical traumatic skull fractures extending down the midline in head trauma patients. The surgeon should therefore be aware of this anatomical variant during primary and secondary surveillance of the traumatized patient and during surgical intervention, especially including frontal craniotomy. A reconstructed tomography scan demonstrating sutural closuring status could provide useful additional information in the diagnostic sequence, superior to a plain X-ray in the emergency setting (Bademci et al. 2007). Nakatani et al. (1998) encountered a complete ectometopic suture in a 91-year-old Japanese male cadaver during a gross anatomy course. It was observed in 1 of 26 skulls aged 62–92 years and was about 13 cm long from the bregma to the nasion. A metopic suture is rare in a person of advanced age, as in their case.

In another study, 1276 adult Indian skulls were examined for the incidence of metopic sutures. There was metopism in 2.66% of the skulls and metopic sutures were present in 38.17% (35.27% in the lower part of the frontal bone in various shapes); the incidences in the upper, upper middle and lower middle parts of the frontal bone were 0.8% in each location. As well as the abovementioned findings, a peculiar shape (inverted Y) was seen in 0.63% and a radiating type in 0.31% of the skulls (Agarwal et al. 1979).

Hyperostosis frontalis interna is a condition of bony overgrowth of the frontal region of the endocranial surface, appearing in the scientific literature as early as 1719. During routine dissection of a donor's calvaria it was noted that she had significant bony overgrowth of the endocranium. Such overgrowth was diffuse throughout the frontal bone, extending slightly into the parietal region with midline sparing (Fig. 1.1). It ranged from 1.0 cm thickness in the temporal region to 1.3 cm adjacent to the midline in the frontal region. Large individual nodules were located along either side of the frontal crest at the intersection of the frontal and parietal bones. The largest nodules measured 2.08 cm in thickness on the right and 1.81 cm on the left (Fig. 1.2). As a result, the pathway of the middle meningeal artery was tortuous. In addition there was significant bilateral depression of the frontal lobes and surrounding neural tissues (Fig. 1.3) (Champion and Cope 2012).

Bergman's Comprehensive Encyclopedia of Human Anatomic Variation, First Edition. Edited by R. Shane Tubbs, Mohammadali M. Shoja and Marios Loukas.

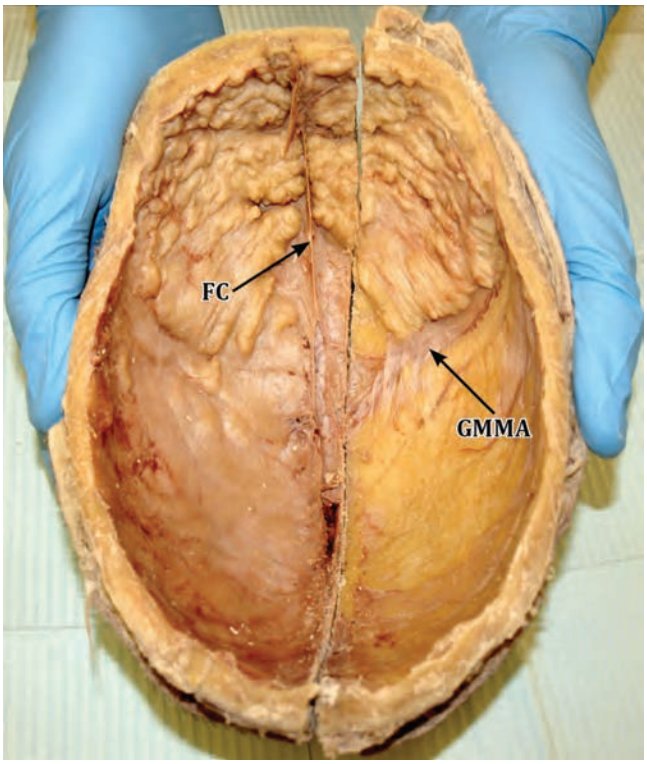

Figure 1.1 Severe case of hyperostosis frontalis interna with typical midline sparing along the frontal crest. Notice the tortuous pathway of the middle meningeal artery. FC: frontal crest; GMMA: groove for middle meningeal artery.

Source: Champion and Cope (2012). Reproduced with permission from International Journal of Anatomical Variations.

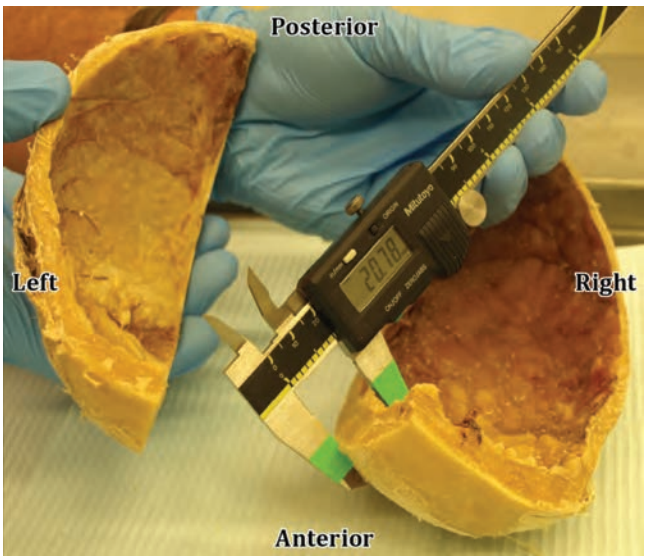

Figure 1.2 Picture shows the measurement of a large nodule (2.08 cm) located adjacent to the frontal crest at the juncture of the frontal and parietal bones.

Source: Champion and Cope (2012). Reproduced with permission from International Journal of Anatomical Variations.

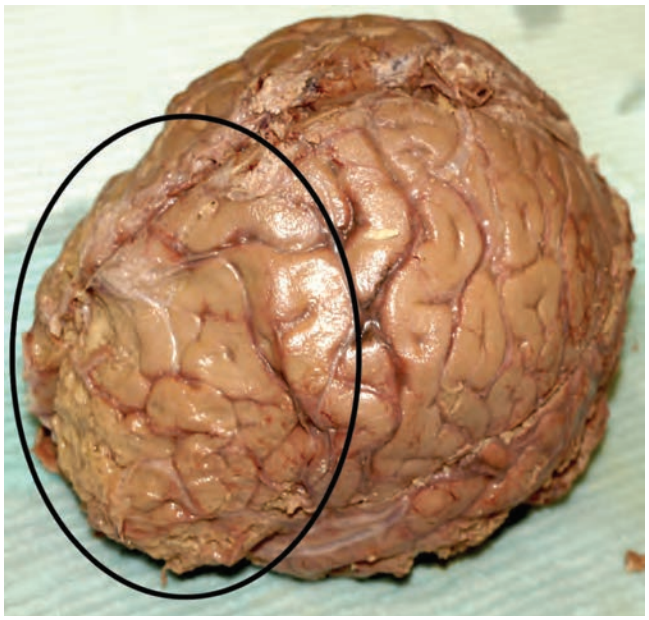

Figure 1.3 Notice the significant compression of the frontal lobes.

Source: Champion and Cope (2012). Reproduced with permission from International Journal of Anatomical Variations.

Nikolić et al. (2010) determined the rate of occurrence and appearance of hyperostosis frontalis interna (HFI) in females and correlated this phenomenon with aging. The sample included 248 deceased females, 45 with different types of HFI and 203 without HFI, average ages 68.3±15.4 (range 19–93) and 58.2±20.2 years (range 10–101), respectively. The rate of HFI was 18.14%. The older the woman, the higher the possibility of HFI (Pearson correlation 0.211, N=248, P=0.001), but the type of HFI did not correlate with age (Pearson correlation 0.229, N=45, P=0.131). The frontal and temporal bones were significantly thicker in women with HFI than in women without it (t=–10.490, DF=246, P=0.000, and t=–5.658, DF=246, P=0.000, respectively). These bones became thicker with aging (Pearson correlation 0.178, N=248, P=0.005 and 0.303, N=248, P=0.000, respectively). The best predictors of HFI were frontal bone thickness, temporal bone thickness, and age (respectively: Wald coefficient=35.487, P=0.000; Wald coefficient=3.288, P=0.070, and Wald coefficient=2.727, P=0.099). Diagnosis of HFI depends not only on frontal bone thickness but also on the waviness of the internal plate of the frontal bone and the involvement of the inner bone surface (Nikolić et al. 2010). May et al. (2011) studied two female populations separated by a period of 100 years: 992 historical and 568 present-day females. HFI was detected by direct observation or CT images. HFI was significantly more prevalent in the present-day than the historical females (P<0.05). The risk of developing it was approximately 2.5 times greater in present-day females than in those who lived 100 years ago (P<0.05). HFI tended to appear at a younger age in the present-day population. The last two decades have witnessed an increase in prevalence (from 55.6% to 75%); prevalence has also increased during the past century, especially among

young individuals, possibly indicating a profound change in human fertility patterns together with the introduction of various hormonal treatments and new dietary habits (May et al. 2011).

A accessory spine of the zygomatic process of the frontal bone is referred to as the spine of Broca.

Occipital bone

The occipital condyle can be oval, triangular, circular, or two-portioned in shape. Ozer et al. (2011) reported the most common type as oval or ovoid (59.67%), whereas the most unusual type was a two-portioned condyle (0.32%). In another study, occipital condyles were classified according to shape: type 1: oval-like; type 2: kidney-like; type 3: S-like; type 4: eight-like; type 5: triangular; type 6: ring-like; type 7: two-portioned; and type 8: deformed. The most common type was type 1 (50%) and the most unusual was type 7 (0.8%) (Naderi et al. 2005).

In some cases a median or third occipital condyle is present. This is occasionally located on the anterior margin of the foramen magnum. Some instances are expressed as a simple rounded tubercle, but in more developed cases an articular facet receives the tip of the odontoid process forming a true diarthrosis (Bergman et al. 1996; Figueiredo et al. 2008). The "condylus tertius" or "third occipital condyle" is an embryological remnant of the proatlas sclerotome. Anatomically, it is attached to the basion and often articulates with the anterior arch of the atlas and the odontoid apex; it is therefore also called the "median occipital condyle" (Udare et al. 2014). It varies in length (0.65 cm in this case); Hadley mentioned that a third condyle with a length of 13–14 mm had been reported in the literature (Rao 2002).

Various structures similar to parts of the atlas have been seen around the foramen magnum and have been described as occipital vertebrae ("manifestation of occipital vertebra"). The atlas can be fused in whole or in part with the occipital bone ("assimilation of the atlas"). This variation occurs in about 0.5–1% of skeletons and has been interpreted by some authors as a cranial shift in the regional grouping of vertebrae in the vertebral column. Signs believed to be associated with assimilated or occipital vertebrae around the foramen magnum include: (a) a massive paramastoid process; (b) an enlarged jugular process; (c) the anterior margin of the foramen magnum thickened and raised to form a bar of bone between the condyles; (d) the hypoglossal canal divided by a bony bridge; and (e) a tertiary condyle and a facet or other marking for the apex of the dens on the anterior margin of the foramen magnum (Bergman et al. 1996).

Bony elements extending towards the foramen magnum are partly attributable to occipital vertebrae. Prakash et al. (2011) reported a single median tubercle situated at the anterior margin of foramen magnum (basion), with the apex facing backwards into the foramen magnum. The tubercle measured 5 mm anteroposteriorly and 3 mm transversely (Fig. 1.4).

Occipitalization of the atlas can be detected incidentally at autopsies or during routine cadaveric dissections, or in dry skulls

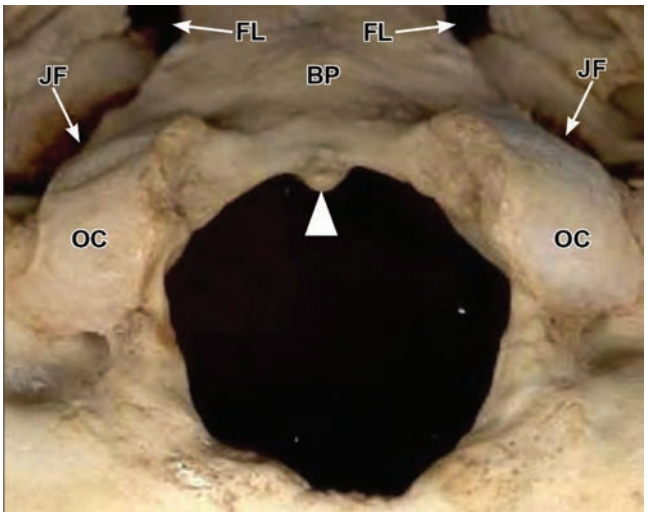

Figure 1.4 Photograph showing the tubercle at anterior margin of foramen magnum. BP: basilar part occipital bone; OC: occipital condyle; JF: jugular foramen; FL: foramen lacerum; white arrowhead: the tubercle.

Source: Prakash et al. (2011). Reproduced with permission from International Journal of Anatomical Variations.

in osteology classes. Fusion of the atlas with the occipital bone can result in compression of the vertebral artery and first cervical nerve. Occipitalization of the atlas (atlanto-occipital fusion, assimilation of the atlas) is a congenital osseous variation found in the craniovertebral junction. It is caused by assimilation of the first cervical vertebra (the atlas) to the basicranium (Bose and Shrivastava 2013).

Bose and Shrivastava (2013) reported a case where the atlas vertebra was almost completely fused with the occipital bone at the base of the skull, except at the transverse processes on both sides. The lateral masses had fused completely with the occipital condyles (Fig. 1.5).

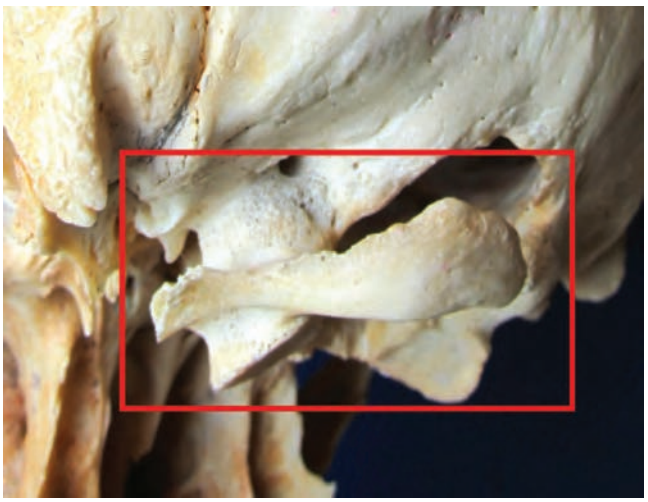

Figure 1.5 Illustration shows the side view of the skull to show the occipitalization of the atlas, shown in box.

Source: Bose and Shrivastava (2013). Reproduced with permission from International Journal of Anatomical Variations.

If there is duplication of the atlas, the condyles are of the occipitoatlantal type. In a series of 1246 skeletons, 13 (1.04%) exhibited two or more characteristics of manifestations of an occipital vertebra; 2 (0.16%) revealed assimilation of the atlas and were among 10 (0.80%) that manifested definite cranial shifting of the intersegmental boundaries of the vertebral column (Bergman et al. 1996).

Occipitalization is a congenital synostosis of the atlas to the occiput, which is a result of failure of segmentation and separation of the most caudal occipital sclerotome and the first cervical sclerotome during the first few weeks of fetal life. The degree of bony fusion between the atlas and occiput can vary; complete and partial assimilation have been described. In most cases assimilation occurs between the anterior arch of the atlas and the anterior rim of the foramen magnum, and is associated with other skeletal malformations such as basilar invagination, occipital vertebra, spina bifida of the atlas, or fusion of the second and third cervical vertebrae (Klippel-Feil syndrome). The incidence of atlanto-occipital fusion ranges from 0.14% to 0.75% of the population, both sexes being equally affected (Saini et al. 2009) (Fig. 1.6).

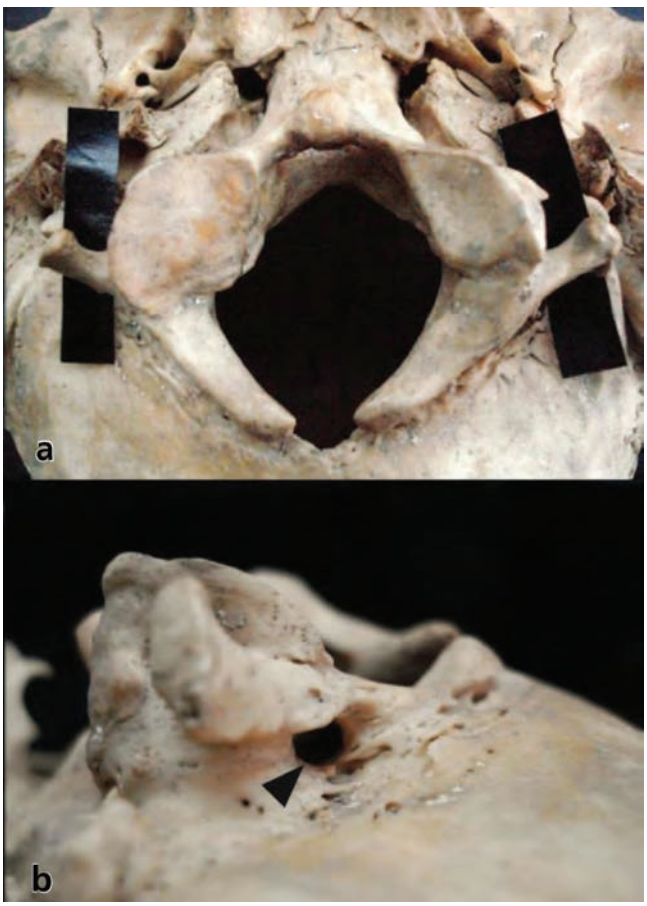

Figure 1.6 Total occipitalization of the atlas, with bifid posterior arch. (a) Incomplete foramen transversarium (black paper). (b) A foramen on the right side (arrowhead).

Source: Saini et al. (2009). Reproduced with permission from International Journal of Anatomical Variations.

Rarely, there is a bony canal in the clivus. This canal probably represents a persisting remnant of the notochord. Chauhan et al. (2010) reported a bony canal in the clivus traversing through the basilar part of the occipital bone from its superior to inferior surface. Considering the direction and location of the canal, they suggested two explanations for its formation: a connecting vein between the basilar plexus and pharyngeal venous plexus could pass through it, or it could have contained the remnant of the notochord (Fig. 1.7).

The hypoglossal canal exhibits variations. Five types can be distinguished: type 1, no evidence of division (typical single canal) (65.4%); type 2, one osseous spur located at either the inner or the outer orifice of the canal or inside it (16.1%); type 3, two or more osseous spurs along the canal (2.3%); type 4, complete osseous bridging in either the internal or external portion of the canal (13.1%); and type 5, complete osseous bridging occupying the entire extent of the canal (3.1%). Berry and Berry (1967) examined 585 skulls and discovered a double hypoglossal canal in 14.6%. The hypoglossal canal has been described as triple or quadruple in rare cases (Bergman et al. 1996; Paraskevas et al. 2009).

The jugular foramen can be divided into parts by intrajugular processes (Bergman et al. 1996). Six processes, arising from the petrous and the occipital bones, were identified and demonstrated in a study by Athavale (2010). The most prominent and common was the posterior petrous process toward the endocranial side, which has been described in the literature as an intrajugular process of the occipital bone and has formed the basis of previous classifications of the compartments of the jugular foramen. The tendency towards septation was more common near the endocranial side (Athavale 2010). Unusual bony projections can narrow the jugular foramen. Rastogi and Budhiraja (2010) reported a case in which a bony growth had converted the jugular foramen into a slit (Fig. 1.8). Such a narrow jugular foramen could cause neurovascular symptoms. Involvement of the ninth, tenth and eleventh cranial nerves at the jugular foramen is known as Vernet's syndrome, and could occur in such foramina (Rastogi and Budhiraja 2010). The right jugular foramen is usually larger than the left jugular foramen.

The grooving on the inner surface of the occipital bone is variable. In about 17% of cases the sagittal sulcus turns to join the left transverse sulcus. The sagittal sulcus can bifurcate, the larger groove turning to join the right transverse sulcus and the smaller one joining the left transverse sulcus (about 15% of cases). In rare cases, the larger groove joins the left and the smaller the right. In very rare cases, the right and left grooves appear equal in size (Bergman et al. 1996).

The shape of the foramen magnum varies in both children and adults. Lang (1990) classified the shapes into five groups: two semicircles (adults in 41.2% and children in 18.4%); elongated circle (adults in 22.4% and children in 20.4%); egg-shaped (adults in 17.6% and children in 25.5%); rhomboidal (adults in 11.8% and in children 31.6%); and rounded (adults

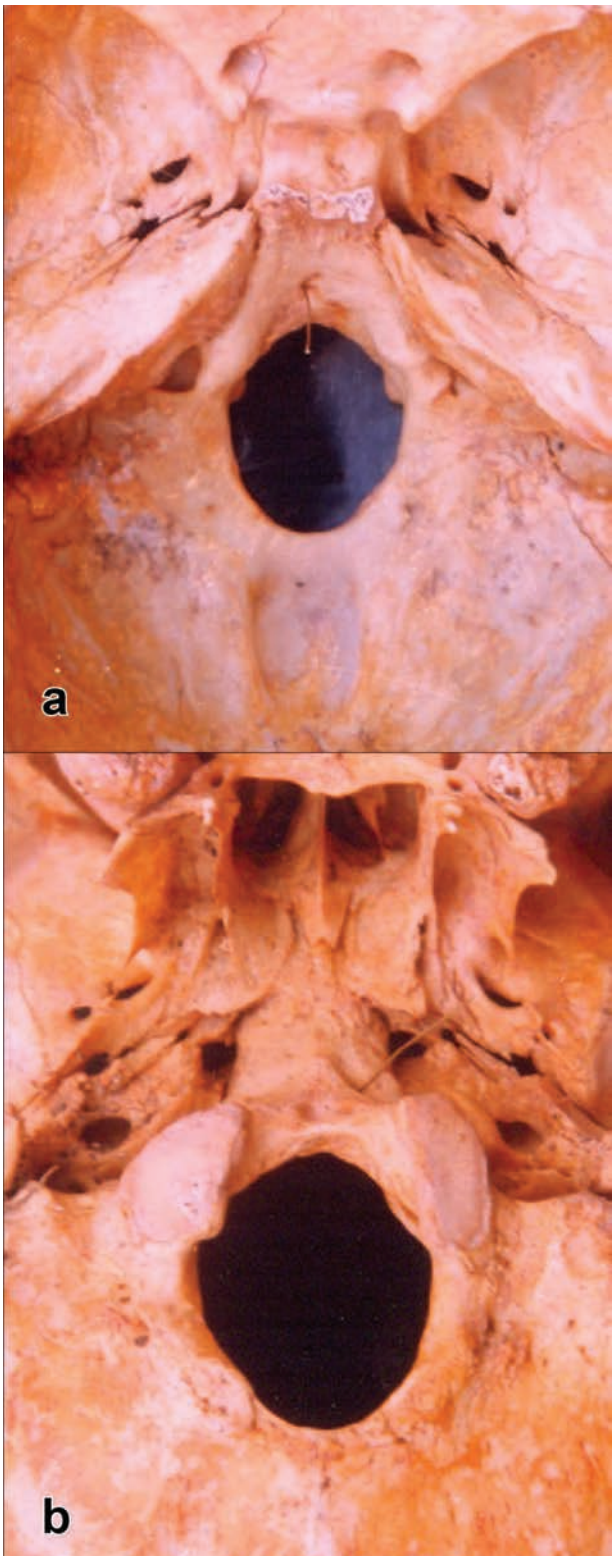

Figure 1.7 (a) Basis cranii interna showing inner opening of clival canal (wire in the canal). (b) Basis cranii externa showing outer opening of clival canal (wire in the canal).

Source: Chauhan et al. (2010). Reproduced with permission from International Journal of Anatomical Variations.

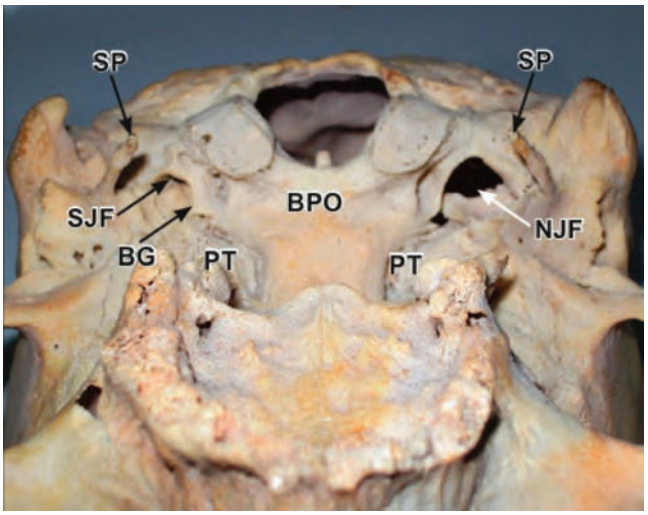

Figure 1.8 Skull base showing slit-like jugular foramen and the abnormal bone growth in the jugular fossa. NJF: normal jugular foramen; SJF: slit-like jugular foramen; BG: bone growth in jugular fossa; BPO: basilar part of the occipital bone; PT: petrous part of the temporal bone; SP: styloid process.

Source: Rastogi and Budhiraja (2010). Reproduced with permission from International Journal of Anatomical Variations.

in 7% and in children in 4%) (Bergman et al. 1996). Göçmez et al. (2014) determined the morphology of the foramen magnum using three-dimensional (3D) computed tomography and distinguished eight types of shape. In order of frequency, these were: round (18.8%); two semicircles (17.8%); egg-shaped (14.9%); hexagonal (13.9%); tetragonal (10.9%); oval (10.9%); pentagonal (8.9%); and irregular (4%). Burdan et al. (2012) examined Eastern European individuals using computed tomography. They found all the cranial and foramen measurements were significantly higher in individuals with the round type of foramen magnum. There was sexual dimorphism, related mainly to the linear diameters and area (not to the shape). There was a greater correlation between the examined parameters of the foramen and proper external cranial measurements in females than in males, which indicates more homogeneous growth in girls. Chethan et al. (2012) reported that in 20.7% of skulls the occipital condyle protruded into the foramen.

A Kerckring ossicle or pseudoforamen is sometimes seen. An accessory fontanelle can also be seen behind the foramen magnum and is known as the fontanelle of Hamy. A notch of the anterior rim of the foramen magnum is termed a keyhole foramen magnum.

Elevation of an area between the supreme and superior nuchal lines is termed a "torus occipitalis." Other names include "occipital spur." In these cases the inion can be greatly enlarged. It is the insertion site of the ligamentum nuchae (Bergman et al. 1996). The portion of the occipital bone between the superior and highest nuchal lines develops in membrane or in cartilage. This portion of the bone, which is denser, smoother, and

sometimes prominently bulged, is known as the torus occipitalis transversus; it forms a distinct projection in anthropoids and to a lesser extent in earlier races of man (Srivastava 1992).

Sutural bones are usually small, irregularly shaped ossicles, often found in the sutures of the cranium, especially in the parietal bones. When the lateral portions of the transverse occipital sutures persist, the situation is termed sutura mendosa. This starts from both lambdoidal sutures and represents the remnant of a transverse occipital suture. This suture forms an interparietal bone (Inca bone or intercalary bone or sutural bone). As many as 172 sutural or Wormian bones have been found in one skull (e.g., Bonthier D'Andernach's ossicle near the obelion). They are rarely found in the sutures of the face (Bergman et al. 1996). True interparietal bones or Inca bones are bounded by the lambdoid suture and sutura mendosa (transverse occipital suture). They were previously known as os Incae, os interparietale, or Goethe's ossicles. An Inca bone resembles the triangular architectural monument design of the Inca tribe; it is rare, ranging between 0.8% and 2.5%. Inca bones occur due to nonfusion of the multiple ossification centers in the membranous portion of the squamous part of the occipital bone (Udupi and Srinivasan 2011) (Fig. 1.9).

Other variants of the basiocciput include clefts, fissures, notochordal remnants, and intrasynchondrosal ossified bodies. Near the basioccipital junction, accessory ossicles known as the basiotic bone of Albrecht can sometimes be found. Accessory air cells of the jugular process of the occipital bone are known as the occipitojugular air cells of Mouret.

Figure 1.9 Photograph showing Inca (interparietal) bone.

Source: Udupi and Srinivasan (2011). Reproduced with permission from International Journal of Anatomical Variations.

Parietal bone

Accessory intraparietal or subsagittal sutures are rare but can be seen dividing the parietal bone. They can be explained on the basis of incomplete union of the two separate ossification centers. These are usually bilateral and fairly symmetrical, but can occasionally be unilateral. The pattern of development can give rise to numerous accessory sutures that could be mistaken for fractures, especially with plain film evaluation alone. A CT scan with 3D reconstruction is vital for further characterization of a questionable fracture (Sanchez et al. 2010).

In the anterior between the paired frontal and parietal bones there is sometimes an accessory ossicle, os bregmaticum, either free or fused with one of the frontals or parietals (Bergman et al. 1996). The anterior fonatanelle may remain open and the normal time to closure of this area is between 4 and 26 months of age (Tunnessen 1990).

A 14-week-old girl presented with characteristic signs of metopic craniosynostosis and frontal cranioplasty was recommended. Upon inspection of the cranium at the time of surgery, a large symmetrical bregmatic accessory bone (measuring 4.5 cm^2, pentagonal) was discovered. The cranium was broadly examined, including the area posterior to the region of the lambda and the area inferior to the squamosal sutures. No other unusual bones were present (Stotland et al. 2012).

Sutural or Wormian bones are small irregularly shaped bones found at the cranial sutures. Their size, shape, and number differ from skull to skull. A sutural bone is occasionally present at the pterion or junction of the parietal, frontal, greater wing of the sphenoid, and the squamous portion of the temporal bone. It is called "pterion ossicle," "epipteric bone," or Flower's bone. Nayak and Soumya (2008) reported a case of three sutural bones at the pterion (Figs 1.10, 1.11).

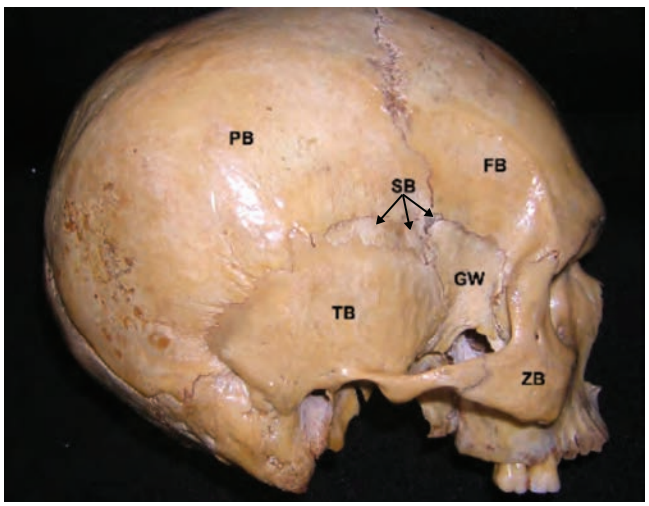

Figure 1.10 Lateral view of the skull showing sutural bones at the pterion. PB: parietal bone; FB: frontal bone; TB: temporal bone; GW: greater wing of sphenoid bone; SB: sutural bones; ZB: zygomatic bone.

Source: Nayak and Soumya (2008). Reproduced with permission from International Journal of Anatomical Variations.

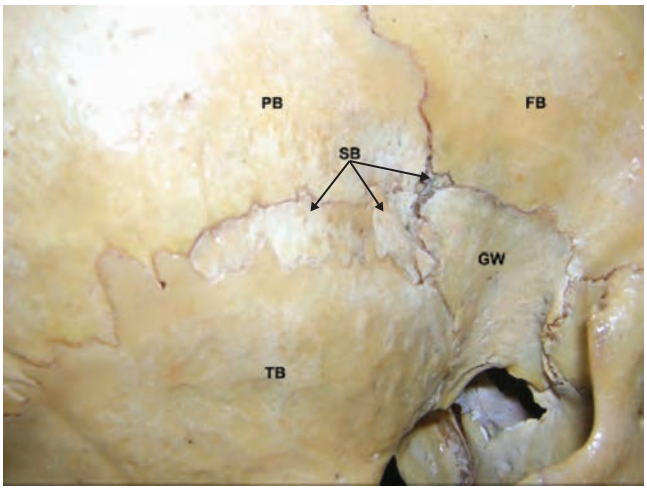

Figure 1.11 Closer view of the pterion with the sutural bones. PB: parietal bone; FB: frontal bone; TB: temporal bone; GW: greater wing of sphenoid bone; SB: sutural bones.

Source: Nayak and Soumya (2008). Reproduced with permission from International Journal of Anatomical Variations.

Sphenoid bone

The sphenoidal sinus varies in size, septation, and extensions. The dimensions of the average sinus are 20 mm (height), 18 mm (width), and 12 mm (length). The capacity of the sphenoidal sinus varies from 0.5 to 30 mL, averaging about 7.5 mL. The bony plate separating the sphenoidal sinus from the optic nerve, maxillary division of the trigeminal nerve, the nerve of the pterygoid canal, the cavernous sinus, the carotid artery, and the hypophysis is sometimes very thin or absent, rendering these structures vulnerable in chronic sinus infections (Bergman et al. 1996). Idowu et al. (2009) reported a main single intersphenoid septum in 95% of patients. Poirier et al. (2011) studied high-resolution computed tomographic scans of patients undergoing endoscopic trans-sphenoidal pituitary tumor resection. They reported a mean of 1.57 septations for each sphenoid sinus. Çakur et al. (2011a, b) investigated the prevalence of sphenoid sinus hypoplasia and agenesis using dental volumetric computed tomography in an adult population. They reported no bilateral agenesis of the sphenoid sinus, though there was unilateral agenesis in 0.26% of the sample and sphenoid sinus hypoplasia was seen in 0.52% (unilateral in 0.26%, bilateral in 0.26%).

A bony bridge sometimes connects the anterior and posterior clinoid processes, which are more usually connected by the fibrous interclinoid ligaments. If these ossify they give rise to the anatomical variation, which some authors consider rare. Its nomenclature in the literature is still vague; it has been variously named the interclinoid tenia, sella bridge, or interclinoid bony bridge. Its prevalence could be as high as 5% (Bergman et al. 1996; Aragão et al. 2013).

The sella turcica can be absent, hypoplastic, enlarged, and/or empty (i.e., empty sella syndrome). It has been reported to be duplicated or to have an intrasellar tubercle or spike.

The caroticoclinoid foramen is an inconstant structure located in the anterior cranial fossa. It is formed by the ossification of a fibrous ligament that begins on the anterior clinoid process and binds to the middle clinoid process. The caroticoclinoid foramen is a space through which the clinoidal segment of the internal carotid artery passes. It has an approximate diameter of 5.0–5.5 mm and causes morphological changes in the internal carotid artery in almost all cases, creating difficulty for neurosurgical techniques in the region (Freire et al. 2010) (Fig. 1.12).

Occasionally, ligaments near the foramen ovale – the pterygospinous (ligament of Civinini) and pterygoalar (ligament of Hyrtl) ligaments – ossify and form variant foramina. The pterygoalar bar is a bony bridge that stretches between the lateral pterygoid lamina and the greater wing of the sphenoid bone; the space under this bar is termed the pterygoalar foramen (Skrzat et al. 2005). Pterygospinous foramina occur in about 5% of cases. In another study, the pterygospinous foramen was found in 6.28% of 1544 skulls and in 5.46% of a second series of 2745 skulls in American whites and blacks; it was more frequent in the whites and in males (Bergman et al. 1996). Tubbs et al. (2009) analyzed 154 adult dry human skulls and reported one pterygospinous foramen (foramen of Civinini) and one pterygoalar foramen (foramen of Hyrtl). A study of 160 skulls revealed complete and incomplete pterygospinous foramina in 1.25% and 7.5%, respectively (Saran et al. 2013).

The foramen rotundum is 1–5 mm from the superior orbital fissure and has a lateral angulation of 3–20° (Sondheimer 1971).

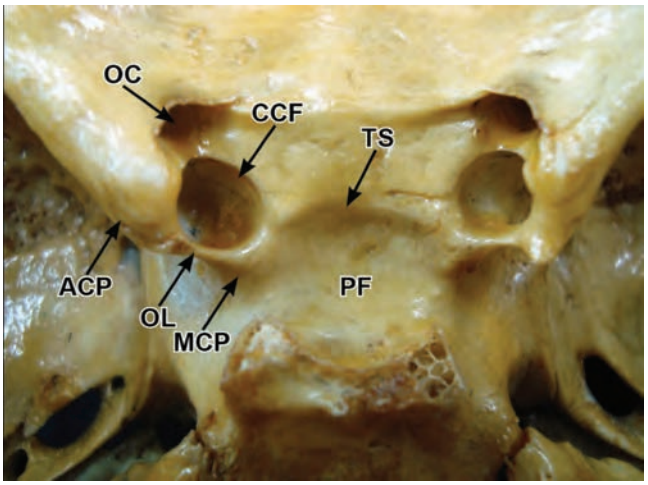

Figure 1.12 Internal view of skull with the caroticoclinoid foramen and adjacent structures. (CCF: caroticoclinoid foramen; ACP: anterior clinoid process; OL: ossified ligament; MCP: middle clinoid process; OC: optic canal; TS: tuberculum sellae; PF: pituitary fossa).

Source: Freire et al. (2010). Reproduced with permission from International Journal of Anatomical Variations.

Its length falls within the range 1–5 mm and average width is 1.5–4 mm. A small foramen within the foramen rotundum can sometimes be found in its inferomedial wall and might transmit an emissary vein (Sonheimer 1971). The foramen may be narrowed or missing.

Among several foramina on the greater wing of the sphenoid bone, the inconstant foramen of Vesalius connects the pterygoid plexus with the cavernous sinus and transmits a small emissary vein that drains the cavernous sinus. The importance of this foramen is that it offers a pathway for the spread of infection from an extracranial source to the cavernous sinus. The small foramen of Vesalius, if present, is generally situated posteromedially from the foramen rotundum and anteromedially from the foramen ovale, foramen spinosum, and carotid canal. In a study of 377 dry skulls, the foramen of Vesalius was present in 11.9% unilaterally and 4.2% bilaterally (Chaisuksunt et al. 2012). Vesalius was the first to describe and illustrate the foramen that bears his name (foramen Vesalii), which is 1–4 mm in diameter. It is also known as the sphenoid emissary foramen, foramen venosum (of Vesalius) and canaliculus sphenoidalis. When present, it is located between the foramen rotundum and the foramen ovale on its medial side. It is traversed by a vein (vein of Vesalius), a small emissary from the cavernous sinus to the pterygoid plexus. It is not uncommon: in 157 skulls it was found 26 times bilaterally (17%) and 20 times unilaterally (13%). One report suggests a frequency as high as 40% (unilateral or bilateral) (Bergman et al. 1996). In another study of 400 skulls, the foramen of Vesalius was identified in 135 (33.75%) and absent on both sides in 265 (66.25%). It was present bilaterally in 15.5%. Its incidence was 18.25%, 7.75% on the right side and 10.5% on the left (Shinohara et al. 2010). It is also variable in size, shape, and position.

An innominate canal of Arnold is sometimes found a few millimeters posterior to the foramen ovale and medial to the foramen spinosum. It is seen in about 20% of skulls. When present, the lesser petrosal nerve travels through this defect.

The foramen ovale occasionally exhibits variations. Its length ranges from 1 to 10 mm and the width from 3 to 10 mm (Sondheimer 1971). Ray et al. (2005) observed variant foramina ovale in 24.2% of the skulls they studied. Its venous segment can be separated from the remainder of its contents by a bony spur, resulting in a so-called doubled foramen ovale. Such spurs are present in 0.5% of subjects studied (Bergman et al. 1996). Reymond et al. (2005) found that the foramen ovale is divided into two or three components in 4.5% of cases. Moreover, the borders of the foramen ovale in some skulls were irregular and rough. On radiological images this could suggest morbid changes, possibly the sole anatomical variation. An accessory process behind the foramen ovale is termed the process of Weber. When the innominate foramen is not present, the lesser petrosal nerve exits the skull through the foramen ovale. The foramen ovale can be confluent with the foramen lacerum and/or the foramina spinosum and Vesalius.

The foramen spinosum is 2–4 mm long and may communicate with the innominate foramen. Bergman et al. (1996) reported the absence of the foramen spinosum in 0.64–4.57% of cases. Nikolova et al. (2012) reported its absence as 0.72% on the right side and 2.13% on the left in medieval female skulls. The absence of the foramen spinosum involves an unusual development and course of the middle meningeal artery and is usually accompanied by replacement of the conventional middle meningeal artery with one arising from the ophthalmic artery system. In these cases, the middle meningeal artery most often enters the middle cranial fossa through the superior orbital fissure and rarely through the meningo-orbital foramen (Nikolova et al. 2012). If the middle meningeal artery has its usual origin, it enters the cranial cavity via the foramen ovale in the absence of a foramen spinosum (Bergman et al. 1996). When the lacrimal artery arises from the middle meningeal artery, it enters the middle fossa through an accessory foramen in the floor of the sphenoid bone known as the foramen of Hyrtl.

The superior orbital fissure can be divided into three anatomical regions by the annulus of Zinn: lateral, central, and inferior regions. The lateral wall of the superior orbital fissure can also be divided into upper and lower segments; and the angle between them was found to be 144.27±20.03° (Shi et al. 2007). According to Govsa et al. (1999), nine different types of shape of the superior orbital fissure were observed based on the classification of Sharma et al. (1988) (Fig. 1.13, Table 1.1). The shape of the superior orbital fissure was first classified into six different types by Shapiro and Janzen (1960). Sharma et al. (1988) added three new types to this classification and Magden et al. (1995) added eight original types to Sharma's classification. Natori and Rhoton (1994) measured the distance from the superomedial to the superolateral edges of the superior orbital fissure as 15.9 mm (7.7–22.1 mm), the distance from the superolateral to the inferior edge as 17.6 mm (10–24.3 mm), and the distance from the superomedial to the inferior edge as 7.0 mm (5.6–8.2 mm) (Natori and Rhoton 1995). Govsa et al. (1999) found the distance from the superomedial edge to the superolateral edge to be 17.3±3.4 mm on the right side and

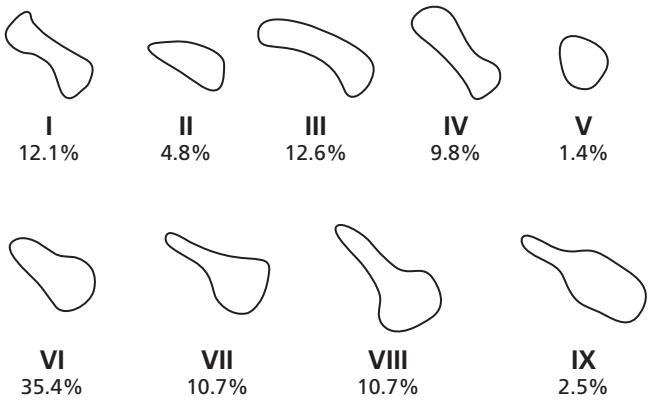

Figure 1.13 Variations in the shapes of the superior orbital fissure.

Source: Sharma et al. (1988).

Table 1.1 Comparative study of the types of shapes of the superior orbital fissure (percent).

Type	I	II	III	IV	V	VI	VII	VIII	IX	Other
Shapiro	40	16	12	12	11	9	—	—	—	—
Sharma	14	13	6.65	2.8	1.86	48.6	7.47	3.73	1.86	—
Magden	1.5	2.4	9.9	3.4	0.7	4.6	6	17.6	38.8	15.2
Govsa	12.1	4.8	12.6	9.8	1.4	35.4	10.7	10.7	2.5	—

Source: Govsa et al. (1999). Reproduced with permission from Wolters Kluwer Health.

16.9±2.9 mm on the left side, the distance from the superolateral to the inferior edge to be 20.8 ±3.9 mm on the right and 20.1±3.8 mm on the left side, and the distance from the superomedial to the inferior edge to be 9.5±2.2 mm on the right and 9.0±2.4 mm on the left side. Another study by Reymond et al. (2008) classified the morphology of the superior orbital fissure into nine types. Fissures A–E were grouped into one type and named type "a"; fissures F–I were grouped as morphological types "b." Type a occurred in 63% and type b in the remaining 37%. Type a had a mean length of 17.47 mm (SD=2.26) and a mean width of 7.31 mm (SD=2.34). Type b had a mean length of 12.48 mm (SD=3.15) and mean width of 7.86 mm (SD=2.45).

The inferior orbital fissure is medially narrower and laterally wider. Its anterolateral border in about 50% of individuals is formed by the zygomatic bone, while in the remaining 50% it is formed by the sphenoid and maxillary bones (Lang 2001). In rare cases, mainly in the older population, this part of the fissure may be thinned and orbital fat may protrude into the temporal fossa. Its length is approximately 20 mm long (Lang 2001). According to De Battista et al. (2012), the inferior orbital fissure length ranges from 25 to 35 mm (mean 29 mm). The length/width of the individual anterolateral, middle, and posteromedial segments averaged 6.46/5, 4.95/3.2, and 17.6/2.4 mm, respectively.

A study by Xu et al. (2004) classified the morphology of the inferior orbital fissure as either: (1) baseball bat shaped; or (2) V shaped.

The vomerobasilar canal lies between the sphenoid bone and the wings of the vomer. It is present in the majority of the cases. The palatovaginal canal is also present in the majority of the cases. The palatovaginal canal is formed by a longitudinal groove on the inferior surface of the vaginal process, which is converted into a canal anteriorly by the sphenoidal process of the palatine bone. Its anterior opening lies in the posterior wall of the pterygopalatine fossa. The posterior opening of the palatovaginal canal lies on the inferior surface of the vaginal process of the sphenoid bone. On that surface and posterior to the opening, a small groove is present in most cases. The vomerovaginal canal is bounded by the inferior surface of the sphenoid bone, the upper surface of the vaginal process of the pterygoid process. In 60% of the cases, the vomerovaginal canal originates posterior to the anterior opening of the pterygoid canal, with an average distance of 4.4 mm (Lang 1995). In the remaining 40%, the vomerovaginal canal originates within the pterygopalatine fossa medial to the anterior opening of the pterygoid canal. Tanaka (1932) found it arising from the anterior part of the pterygoid canal in 18.3% of his Japanese specimens. The overall mean length of the vomerovaginal canal was 7 mm.

Within the vomerovaginal canal there are on average three nerve fiber bundles with a thickness of 136 μm (55–370 μm) and also 1–3 arteries with an average lumen of 38 μm (74–814 μm). The median craniopharyngeal canal is present in 0.5% of the adult population. The lateral craniopharyngeal canal lies between the medial border of the superior orbital fissure and the vomerovaginal canal. It is usually seen in children of 6 years in age or less (Lang 2001).

The pterygoid canal travels below the level of the floor of the sphenoidal sinus in 38% of individuals (Lang 1989). The roof of the canal is dehiscent in 10% and the nerve runs at the same level in 18% (Lang 1989). The pterygoid canal (Vidian canal) is 11.5–23 mm long and, in 44% of cases, runs anteromedially. The posterior opening of the canal is 12.4–19.2 mm from the midline and the anterior opening is 5.5–17.5 mm from the midline (Lang 1989). In about one-third of skulls, the canal protrudes into the floor of the sphenoid sinus. In about 3% it is entirely within this sinus, and in 6% the roof of the canal is dehiscent (Sondheimer 1971).

The carotid canal is in the inferior aspect of the petrous part of the temporal bone; and is 5–6.5 mm wide and 3–4 cm long. It can be absent with associated agenesis of the internal carotid artery.

The basi-sphenoid can have a retro-orbital pseudoforamen.

The optic canal has variable dimensions as described by Maniscalco and Habal (1978) in their study of 83 cadavers, with a mean length of 9.22 mm (5.5–11.5 mm), mean horizontal canal width 7.18 mm (5–9.5 mm), mean medial canal wall proximal thickness 0.21 mm (0.1–0.31 mm), and mean optic ring thickness 0.57 mm (0.4–0.74 mm). In a study by Choudhry et al. (2005), the cranial openings of the optic canal viewed from the cranial aspect revealed a large number of recesses, fissures, and notches. In 229 sides (61.5%) of the 372 examined, the cranial opening of the optic canal was found to be associated with recesses on its lateral wall. These were bilateral in 224 sides (112 skulls) and unilateral in 7 sides. The recess was mostly accompanied by a fissure (42.4%) in the superior root of the lesser wing of the sphenoid bone. The upper slightly concave border of the roof had a small notch on 66 sides (17.7%).

A duplicated optic canal is a rare variation. Typically, the larger canal contains the optic nerve and the meninges and the smaller canal transmits the ophthalmic artery (Choudhry et al. 1988). Duplicated optic canals are separated by a septum of variable thickness dividing the posterior part of the canal into a large canal in the usual position and a smaller canal inferior to it or a bar forming the caroticoclinoid canal. Other duplicated canals may be divided by thin septae having a small slit (Choudhry et al. 1999). White (1923), Whitnall (1932),

Keyes (1935), and Choudhry et al. (1988, 1999) have reported duplicated optic canals. Bilaterally duplicated canals are very rare variations and are seldom reported in the literature (Zoja 1885; Le Double 1903; Warwick 1951; Choudhry et al. 1988; Magden and Kaynak 1996; Singh 2005).

Temporal bone

The styloid processes vary markedly in length and can comprise two–five osselets, articulating by synchondroses (Bergman et al. 1996); the stylohyoid ligament can calcify to make a rigid connection with the hyoid bone. A 75-mm-long styloid process has been reported but the usual length is 2–3 cm. When it is more than 3 cm it is called an elongated styloid process; and can cause pain in the throat, difficulty in swallowing, foreign body sensation, carotid artery compression syndrome, etc. This elongation was first described in 1652 by the Italian surgeon Pietro Marchetti. In 1937, Watt W. Eagle coined the term "stylalgia" to describe the pain associated with elongation of the styloid process. Kolagi et al. (2010) reported a case of bilaterally elongated styloid process with ossified stylohyoid ligament. The total length of the process was 8 cm and it was 1 cm thick at the base which is extremely rare. The styloid process proper was 5 cm long and the remaining 3 cm was ossified stylohyoid ligament, the junction between the two being marked by a bulge of bony mass (Fig. 1.14).

Mukherjee et al. (2011) reported a 24-year-old female who presented with a two-year history of foreign body sensation in her throat, more to the left side, along with dysphagia, excessive salivation, and vague pharyngeal pain radiating to the mastoid region aggravated by rotation of the head. Palpation of the tonsillar fossa revealed elongated styloid processes on both sides. Digital X-ray of the skull revealed asymmetrical ossification of bilateral stylohyoid chains. On the left side it comprised two components, with the long styloid process as proximal and calcified stylohyoid ligament as distal part, total length (approximately) 4.7 cm with prominent "pseudoarticulation." On the right side it was (approximately) 4.5 cm long, the distal portion being calcified stylohyoid ligament, but the proximal elongated styloid process was again divided into two parts representing its tympanohyal and stylohyal components (Fig. 1.15).

About 4% of the population has styloid processes more than 3 cm long; however, only 4.0–10.3% of these are symptomatic. Sasani et al. (2013) reported a case of bilateral elongated styloid processes that extended to the C3 vertebral level on the right side (78 mm) and C2 on the left (50 mm) (Fig. 1.16).

Embryologically, four different segments are present in the stylohyoid apparatus: the tympanohyal, stylohyal, ceratohyal, and hypohyal segments. The ligamentous part has its origin from the ceratohyal cartilage and extends from the stylohyal segment to the lesser horn of hyoid bone. There is a potential for ossification of the ligament, and when it is ossified there can be segmentation and pseudoarticulation (Sasani et al. 2013).

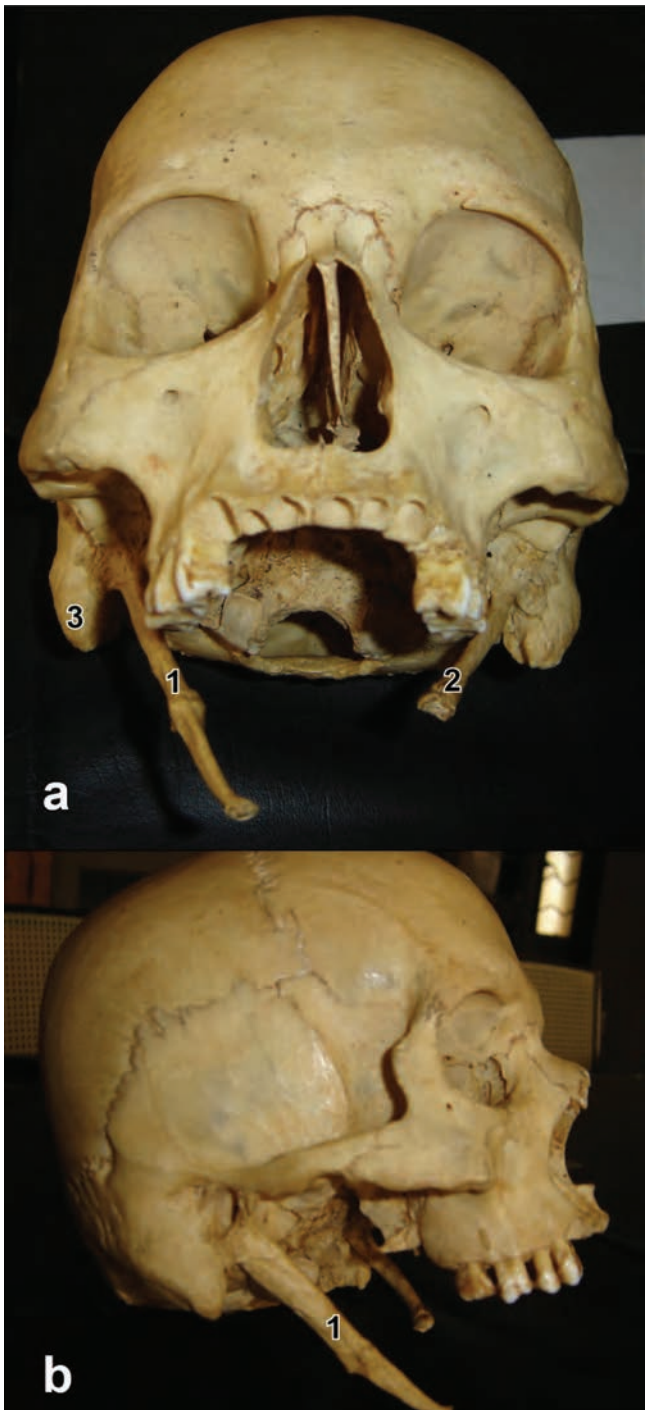

Figure 1.14 (a) Frontal view of skull showing bilateral elongated styloid processes. (b) Right elongated styloid process. 1: right styloid process; 2: left styloid process; 3: mastoid process.

Source: Kolagi et al. (2010). Reproduced with permission from International Journal of Anatomical Variations.

A canal or foramen (foramen of Hüschke) is found in the floor of the bony part of the external auditory meatus, near

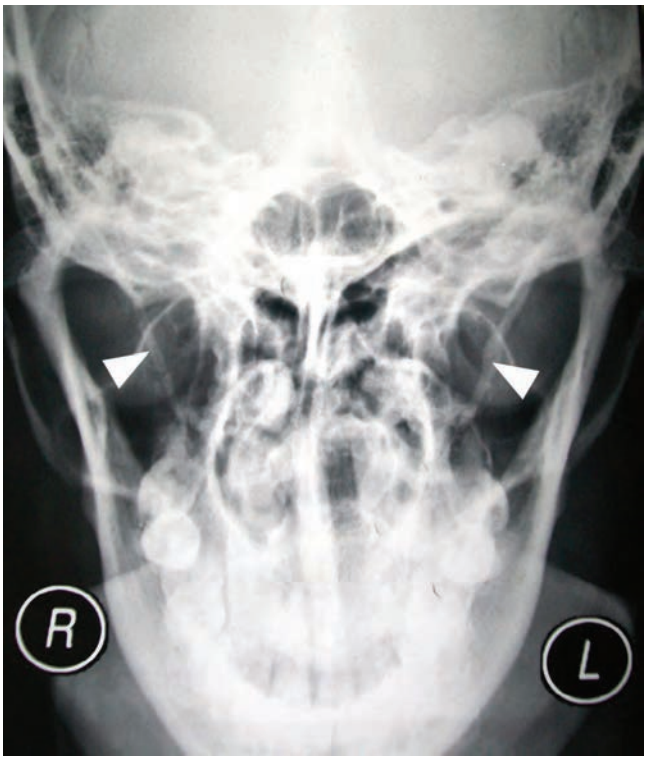

Figure 1.15 Photograph shows the bilateral asymmetrical ossification of the stylohyoid chain (white arrowheads).

Source: Mukherjee et al. (2011). Reproduced with permission from International Journal of Anatomical Variations.

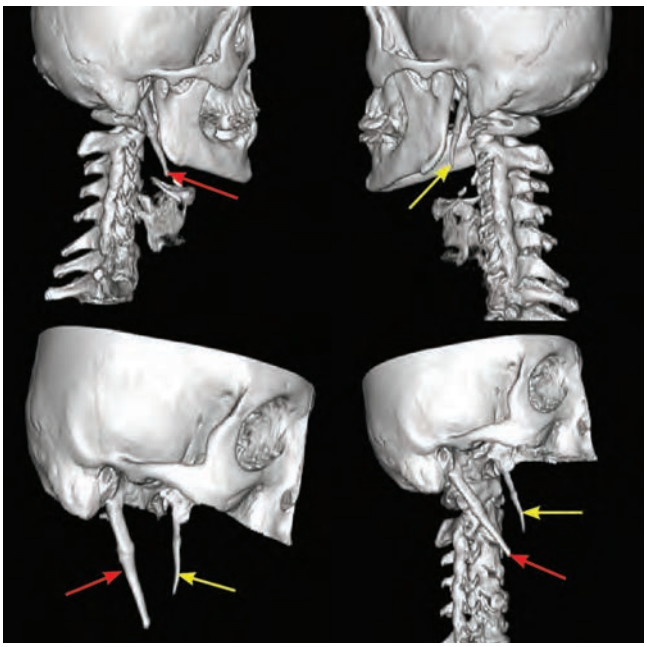

Figure 1.16 Bilateral elongated styloid processes are more prominent on the right side (red arrows) than the left side (yellow arrows), and extended to C3 vertebral level.

Source: Sasani et al. (2013). Reproduced with permission from International Journal of Anatomical Variations.

the tympanic ring, during the first five years of life. It can persist throughout life (Bergman et al. 1996). The German anatomist Hüschke (1797–1858) first described the probability of a deficiency in the development of the tympanic plate of the temporal bone, named the "foramen of Hüschke" or foramen tympanicum, which usually becomes apposed in adulthood. If it persists in adult life, complications can ensue such as herniation of the temporomandibular joint (TMJ), formation of salivary otorrhea, and spread of infection or tumor from the external acoustic meatus to the infratemporal fossa and vice versa. Srimani et al. (2013) identified seven cases of foramen of Hüschke among 53 skulls studied. The diameter of the foramen was 1–3 mm (Srimani et al. 2013) (Fig. 1.17). The external auditory meatus is sometimes duplicated (Vokurka 1989).

The mastoid process can have a doubled apex, the medial portion being divided from the lateral by a fissure. Usually, the medial lip of the groove forms a distinct ridge and provides the point of attachment of the digastric muscle; an enlarged paramastoid process can result from the development of air cells within the medial portion of the process. Air cells, usually confined to the mastoid process, can invade the horizontal or vertical part of the squama or even the pars petrosa (Bergman et al. 1996). In a study of 298 temporal bones, 6% of the mastoid processes exhibited variations. There was no statistically significant difference between genders (Manolis et al. 2008).

The petrosphenoid ligament may be ossified and result in a bony foramen for the abducens nerve to travel through. Accessory ossicles can be present in the foramen lacerum and are known as ossicles of Cortese and Riolan. An accessory tubercle

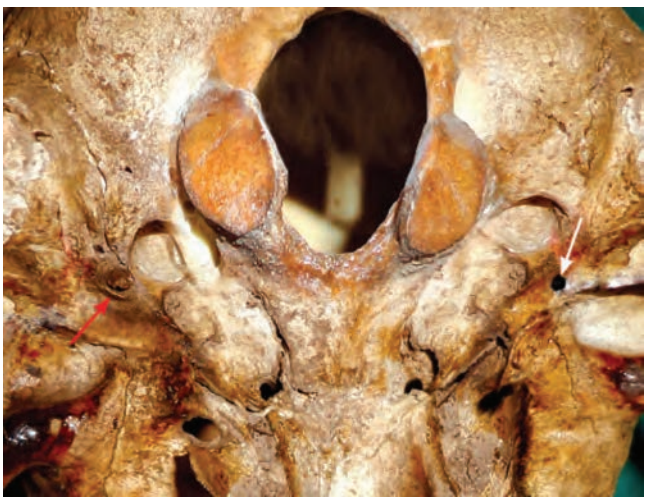

Figure 1.17 Figure showing a single oval-shaped foramen (red arrow) having transverse diameter of 0.2 cm and longitudinal diameter of 0.1 cm was noted on the left tympanic plate, and a single rounded foramen (white arrow) of 0.1 cm in diameter is present on the right side.

Source: Srimani et al. (2013). Reproduced with permission from International Journal of Anatomical Variations.

of the supramastoid crest is known as the tubercle of Waldeyer. The internal acoustic meatus can be narrowed, dehiscent, doubled, or tripled.

Ethmoid bone

The crista galli can be pneumatized (Bergman et al. 1996). Hajiioannou et al. (2010) reviewed computed tomography findings of the morphology of the crista galli in 99 patients. Pneumatization of the crista galli was noticed in 14.1% of the scans.

The superior nasal conchae can also be pneumatized. Ariyürek et al. (1996) evaluated CT scans of 52 patients who underwent CT examination prior to endoscopic sinus surgery and had normally aerated posterior ethmoidal cells and an unobscured nasal cavity. Pneumatization was evident in 48% of these patients. The superior turbinates seemed to be aerated through the posterior ethmoid cells.

There are sometimes accessory ethmoidal foramina. Takahashi et al. (2011) studied 54 orbits from 27 Japanese cadavers. Accessory ethmoidal foramina were detected in 18 orbits (33.3%) from 11 cadavers; one accessory foramen (middle ethmoidal foramen) was identified in 17 orbits, and two foramina (additional deep middle ethmoidal foramina) in one orbit (Takahashi et al. 2011). The textbook number of ethmoid foramina is two; Lang (1983) found them on the left side in 68.3% of skulls and on the right side in 67.4%. In the remainder there were three–five; there were three foramina in about 40% of skulls (Bergman et al. 1996).

The perpendicular plate may protrude outward between the nasal bones (Lang 1989).

Lacrimal bone

The lacrimal bone can be divided into two or more parts or fused with neighboring bones. This bone sometimes exhibits so many minute foramina that it takes the appearance of a bony net (Bergman et al. 1996). Its thickness is variable. Hartikainen et al. (1996) reported the mean thickness of the bone as 106 μm. In 67% of patients the mean thickness of individual lacrimal bones was less than 100 μm and in 4% it was more than 300 μm. The thinnest measured cross-section of the lacrimal bone sample was 11 μm and the thickest was 722 μm. The lacrimal bone is composed of a thin plate of lamellar bone. An accessory ossicle located deep to the lacrimal bone has been termed the ossicle of the lacrimal canal or the ossicle of Gruber.

Vomer

Isolated vomer aplasia is rarely reported in the literature. It is a genetic variant presenting with no significant medical problems (Verim et al. 2012). Recently, absence of the vomer during the first two trimesters of pregnancy was identified as a marker of trisomy 21 and trisomy 13. There was no single case of trisomy in which the vomer could be identified during the first or early second trimester. The diagnostic accuracy of the vomer as a marker for trisomy was 0.985 (Mihailovic et al. 2012).

The vomer can be separated from the perpendicular plate of the ethmoid by a strip of cartilage from the nasal septum (Bergman et al. 1996). Rarely, a recess of the sphenoid sinus can extend into the vomer (Lang 1989).

Inferior nasal concha

Lang and Kley (1981) reported absence of the conchae, the vomer, and perpendicular plate. Bony bridges may exist between the inferior and middle nasal conchae. The inferior concha may be notched or have a curved convex surface.

Maxilla

Two or more infraorbital foramina have been described. Gruber reported that the number can range from one to five. In 1970, Kadanoff, Mutafov and Jordanov tabulated and illustrated the variety of infraorbital foramina found in over 1400 skulls; they found it doubled in 9%, tripled in 0.5%, and more than tripled in 0.3% (Bergman et al. 1996). Boopathi et al. (2010) examined 80 dry adult South Indian human skulls of unknown age and gender. Accessory infraorbital foramina were found in 16.25%. Saylam et al. (1999) examined 119 crania and 229 maxillae (a total of 467 infraorbital foramina); they found a single accessory foramen in 11.5% of specimens and double accessory foramina in 1.28%. In 79.6% of those with a single accessory foramen, the accessory foramen was superior and medial to the main opening.

The infraorbital canal issues a small branch on its lateral face close to its midpoint to allow the anterior superior alveolar nerve to pass. This small canal, sometimes called the canalis sinuosus, runs forward and downward to the inferior wall of the orbit, lateral to the infraorbital canal and bent medially to the anterior wall of the maxillary sinus, passing below the infraorbital foramen (Neves et al. 2012).

Maxillary sinus hypoplasia is an uncommon condition. It can be misdiagnosed as an infection or a neoplasm of the maxillary sinuses. Variations of the other paranasal structures, especially the uncinate process associated with maxillary sinus hypoplasia, have been defined. Maxillary sinus hypoplasia shows three distinct patterns: type I, mild hypoplasia of the maxillary sinus, normal uncinate process and a well-developed infundibular passage; type II, significant hypoplasia of the maxillary sinus, hypoplastic or absent uncinate process and absent or pathological infundibular passage; and type III, absence of an uncinate process and cleft-like maxillary sinus hypoplasia (Erdem et al. 2002).

Bilateral maxillary sinus aplasia or severe hypoplasia with associated paranasal sinus variations is extremely rare. Tasar et al. (2007) reported two cases with severe maxillary sinus hypoplasia/aplasia, one of them associated with other paranasal sinus variants. Aydinlioğlu and Erdem (2004) examined CT scans in the axial and coronal planes of the paranasal sinuses of 1526 patients. They reported only one case of bilateral and only one case of unilateral maxillary sinus aplasia.

The maxillary sinus can be septated. These septa are barriers of cortical bone that arise from the floor or the walls of the sinus, and can even divide the sinus into two or more cavities. They can originate during maxillary development and tooth growth, in which case they are known as primary septa, or can be acquired structures resulting from the pneumatization of the maxillary sinus after tooth loss, in which case they are called secondary septa. Between 13% and 35.3% of maxillary sinuses have septa (Maestre-Ferrín et al. 2010).

Accessory ostia of the maxillary sinus are found in about 30% of skulls; as many as three in one skull have been reported (Bergman et al. 1996).

The incisive part of the alveolar process can be an independent bone, the os incisivum (Bergman et al. 1996). The discovery of the premaxillary bone (os incisivum, os intermaxillare, or premaxilla) in humans has been attributed to Goethe, so it has also been named "os Goethei". However, Broussonet and Vicq d'Azyr obtained the same result in 1779 and 1780, respectively, using different methods. Early anatomists described this medial part of the upper jaw as a separate bone in the vertebrate skull; Coiter was the first in 1573 to present an illustration of the sutura incisiva in the human (Barteczko and Jacob 2004). Sutural bones can sometimes be seen in the sutures of the hard palate.

Palatine bone

One study demonstrated that the sphenopalatine foramen can be single (61.5–87%), double (11.1–32.5%), triple (1.9–5.5%), or quadrupled (0.05%) (Lang 1995). It is located at the superior nasal meatus in 81.5% of cases, between the middle and superior nasal meatus in 14.8%, and in the middle nasal meatus in 1.9% (Scanavine et al. 2009).

The lesser palatine canal is frequently absent. It can also be located between the palatine bone and maxilla (Bergman et al. 1996).

The torus palatinus is an overgrowth of bone in the palatal region and represents an anatomical variation. Its prevalence varies with the population studied and its etiology is still unclear; however, it seems to be a multifactorial disorder with genetic and environmental involvement. Surgical removal of the torus palatinus is indicated under the following circumstances: (1) deglutition and speech impairment; (2) cancer phobia; (3) traumatized mucosa over the torus; and (4) prosthetic reasons (Nogueira et al. 2013). Palatal tori are seen in approximately 20–30% of the population and are more common in females than in males. Frequently, these bony outgrowths are incidental findings on routine oral examinations, and there is often considerable variation in clinical appearance (Bennet 2013). Simunković et al. (2011) studied 1679 subjects, 985 females and 694 males in the age range 9–99 years, who were subjected to clinical examination and analysis of plaster casts. The torus palatinus was found in 42.9%, 40.1% of females and 46.8% of males, indicating a significantly higher prevalence in the male population (P=0.006). Interestingly, Sisman et al. (2008) studied 2660 patients and reported the prevalence of the torus palatinus as low as 4.1%. Yildiz et al. (2005) examined a total of 1943 schoolchildren, 1056 males and 887 females ranging in age from 5 to 15 years. The prevalence of the torus palatinus in the study population was 30.9%, and was significantly more frequent in females than males (34.3 vs 28.1%, P<0.005). Most of the palatine tori were smaller than 2 cm (91.5%) and in molar location (62.9%).

The hard palate has been reported to be duplicated by Bruns (1947) and can have a cleft. Wormian bones can be seen in between the palatine bones or between this bone and the maxillary part of the hard palate.

Zygomatic bone

The zygomatic bone is sometimes divided into two parts by either a horizontal or a vertical suture. Such a bipartite bone has been called os Japonicum (os Ainoicum) as it has mostly been observed in Japanese subjects. A sutural bone may be seen between the zygomatic bone and temporal bones where they join to form the zygomatic arch. Anil et al. (2000) studied 1266 zygomatic bones in 633 dry Anatolian skulls and 1348 zygomatic bones in 674 plain cranium radiographs of adult patients. The os Japonicum was present in 2.2% of female and 1.7% of male specimens. All 24 multipartite bones observed in the study were bipartite except for one. In addition, 15 of 690 female (2.2%) and 12 of 658 male (1.8%) zygomatic bones examined radiologically were bipartite or tripartite; there was a total of 674 plain cranium radiographs. Jeyasingh et al. (1982) studied 500 crania in Uttar Pradesh and found the prevalence of os Japonicum to be 4%. Typical bipartite zygomatic bone was present in 40 instances. In only 6 bones, a horizontal groove was seen on the temporal surface. In one skull the zygomatic process of the maxilla and the zygomatic process of the temporal bone articulated directly on the temporal surface of the zygomatic bone. In another skull the maxilla and the temporal bone articulated with each other along the lower border of the zygomatic bone, giving the appearance of a tripartite condition.

Multiple zygomaticofacial and zygomaticotemporal canals can be observed; their detailed intrabony courses are unknown. Kim et al. (2013) scanned 14 sides of the zygomatic bones with micro-computed tomography, with 32 μm slice thickness. They

found that some zygomaticotemporal canals originated from the zygomaticofacial canal. In 71.4% of specimens the zygomaticotemporal canals divided from the intrabony canal along the course of the zygomaticofacial canals; 28.6% of zygomaticotemporal canals were opened through each corresponding zygomaticotemporal foramen. The zygomaticofacial canal originated from the zygomaticoorbital foramen, divided into some of the zygomaticotemporal canals, and finally opened as the zygomaticofacial foramen. Aksu et al. (2009) evaluated the number of foramina on the facial aspects of zygomatic bones. There were none in 15.6%, one in 44.4%, two in 28.1%, three in 6.3%, four in 4.4%, and five in 1.3% of sides. Loukas et al. (2008) studied 200 dry human skulls for zygomaticofacial (ZF), zygomaticoorbital (ZO) and zygomaticotemporal (ZT) foramina. All three foramina varied from absence to as many as four small openings. The authors classified each of these foramina as types I–V for single, double, triple, quadruple, and absent foramina, respectively. The relative frequencies were as follows: type I, ZO 50%, ZF 40%, ZT 30%; type II, ZO 20%, ZF 15%, ZT 15%; type III, ZO 10%, ZF 5%, ZT 5%; type IV, ZO 3%, ZF 1%, ZT 0%; and type V, ZO 17%, ZF 39%, ZT 50%.

Similarly, Mangal et al. (2004) studied these foramina in 165 dry human skulls. A single ZF foramen was seen in 148 (44.9%) sides. Two ZF foramina were found in 92 (27.9%) sides, out of which 29 (8.8%) sides had one ZO foramen, while 63 (19.1%) sides had two ZO foramina. Three ZF foramina, a relatively uncommon occurrence, were found in 17 (5.1%) sides, which included eight (2.4%) sides with one less and nine (2.7%) sides with the same number of ZO foramina. Four ZF foramina were seen in one (0.3%) side with three on the orbital aspect, a feature not reported before.

Govsa et al. (2009) reported that the angle between the ZT nerve and the ZF nerve within the orbit was approximately 42.21 degrees. The mean (SD) distance between the orbital opening of the ZT nerve and the meeting point of the ZT nerve was measured as 9.21 (5.18) mm. The mean (SD) distance between the orbital opening of the ZF nerve and the meeting point of the ZT nerve was calculated as 11.22 (4.25) mm. The mean (SD) distance between the orbital opening of the ZFN and the infraorbital margin of the orbit was 13.04 (3.21) mm. According to Tubbs et al. (2012), the zygomaticotemporal nerve penetrated the facial muscles at a mean of 2.3 cm superior to the zygomatic arch.

The orbital eminence (eminentia orbitalis) or marginal tubercle (of Whitnall) is located on the orbital surface of the frontal process of the zygomatic bone just within the orbital margin and about 1 cm inferior to the frontozygomatic suture (Didio 1962). The marginal tubercle serves as an attachment point for the lateral check ligament. According to Lang (1989), the marginal tubercle is present in 20% of the cases before puberty and in 95% of adults. The marginal process was present in 4% of the cases.

Other authors have also studied the incidence of the marginal tubercle and are presented in Table 1.2.

Table 1.2 Incidence of marginal tubercle.

Reference	No. samples	Incidence (%)
Whitnall (1911)	2000 skulls	>95
Buschkowitsch (1927)	419 skulls	63
Kangas (1928)	1,350 skulls	80.1
Ono (1928)	164 skulls	80
Tomita (1935)	476 skulls	49.15
Didio (1942)	285 skulls and 100 living	89.56
Didio (1962)	163 skulls	96.3

Mandible

The mandible varies extensively in size and weight during an individual's lifetime. The chin can protrude or recede, and there can be one rather than two mental tubercles (Bergman et al. 1996). A torus mandibularis can be present on one or both sides of the lingual aspect of the mandible.

The mental foramen is sometimes doubled or tripled. It can be located as far forward as the first premolar or as far back as the second. In very rare cases a median mental foramen is present, comparable with an arterial canal normally found in certain apes (Bergman et al. 1996). Sahin et al. (2010) reported a case with double mental nerve and foramina in a 44-year-old trauma patient. On the left side, below the level of the premolar teeth, two mental nerves emerged from two different mental foramina. The nerves had almost the same diameter. One of the mental foramina was located more anterior and superiorly (Fig. 1.18).

In contrast to other primates the mental foramen is usually single in humans, but accessory foramina have been recorded. It has been suggested that separation of the mental nerve into several fasciculi earlier than the formation of the mental foramen up to the 12th gestational week could explain why accessory mental foramina are formed (Hasan et al. 2010). Naitoh et al. (2011) analyzed

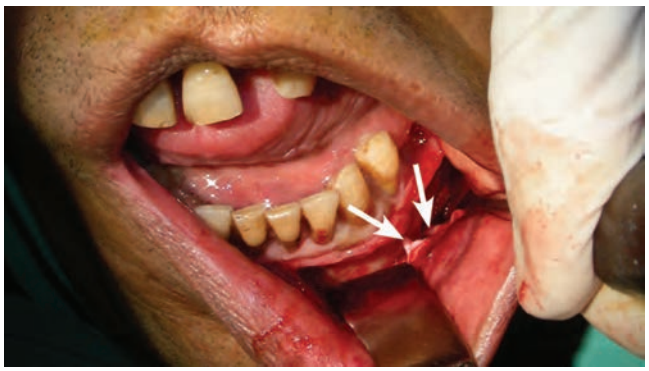

Figure 1.18 Intraoperative view of two mental nerves. (Arrows: mental nerves).

Source: Sahin et al. (2010). Reproduced with permission from International Journal of Anatomical Variations.

365 patients (130 males and 235 females). Para-panoramic images were reconstructed from cone-beam computed tomography (CBCT) images of the accessory mental foramen/foramina using 3D visualization and measurement software. A total of 37 accessory mental foramina were observed in 28 patients on CBCT images. Naitoh et al. (2009) studied CBCT images of 157 patients and found accessory mental foramina in 7%. The presence or absence of the accessory structure had no significant effect on the size of the mental foramen. The mean distance between the mental and accessory mental foramina was 6.3 mm (SD 1.5 mm). Toh et al. (1992) reported three cases with accessory mental foramina in which the distribution of the accessory mental nerve was different. These nerves communicated with the branches of the facial and buccal nerves.

In very rare cases the mental foramen is absent. The foramen was absent twice on the right side (0.06%) and once on the left side (0.03%) in a study of 1435 dry human mandibles (2870 sides) (de Freitas et al. 1979). The frequency of unilateral absence of the mental foramen ranges from less than 0.02% to 0.47%. No sexual or ethnic differences in absence of the mental foramen have been found (Hasan et al. 2010). Hasan et al. (2010) reported one case with bilateral absence of the mental foramina. The dry mandible (unspecified age and sex, and unknown ethnic background, average sized, and partially edentulous) was normal in all other aspects of gross morphology. The mandibular foramen was bilaterally symmetrical and the mandibular canal was patent to a distance of 3 cm on the right and 4.7 cm on the left side using a steel wire probe. Radiography established normal bone density with no evidence of age-related bone resorption or previous surgical or mechanical trauma, establishing that the case was one of congenital absence of the mental foramen (Fig. 1.19). An accessory foramen (of Dubreuil–Chambardel) has been described in the mandibular symphysis.

Figure 1.19 Dry human mandible with bilateral absence of mental foramen.

Source: Hasan et al. (2010). Reproduced with permission from International Journal of Anatomical Variations.

Figure 1.20 Mandible showing elongated coronoid processes, lateral view.

Source: Chauhan and Dixit (2011). Reproduced with permission from International Journal of Anatomical Variations.

Chauhan and Dixit (2011) reported a mandible with unusually long coronoid processes on both sides. It proved to be that of male in late adulthood. The length of the coronoid was taken from the line tangent to the deepest part of the mandibular notch to the apex; it measured 2.4 cm on the right and 2.6 cm on the left side (Fig. 1.20).

Coronoid processes project above the level of the condyles at the time of birth. As the neck of the mandible grows, it comes to lie at a lower level in adults. Unusual elongation of the coronoid process, formed of histologically normal bone with no synovial tissue around it, suggests hyperplasia. Bilateral hyperplasia of the coronoid processes of the mandible is quite infrequent and affects mostly males (male to female ratio 5:1) between the ages of 14 and 16. It leads to restricted mouth opening caused by impingement of the process on the medial and anterior surfaces of the zygomatic arch (Chauhan and Dixit 2011). Huang et al. (2013) studied mandibular morphology and dental anomalies to propose a relationship between mandibular/dental phenotypes and deficiency of CCAAT/enhancer-binding protein beta in mice. They concluded that CCAAT/enhancer-binding protein beta deficiency was related to elongation of the coronoid process and formation of supernumerary teeth.

A small accessory tubercle on the posterior border of the coronoid process is known as Delachapelle's tubercle. An accessory tubercle between the oblique line and anterior margin of the ramus of the mandible is termed the proeminentia lateralis of Rasche.

Nasal bone

There can be several nasal bones or only one (unpaired). Internasal bones have been found at the edges of the nasal bones in the upper corner of the piriform aperture, lying on the anterior tip of the perpendicular plate of the ethmoid (Fig. 1.21) (Bergman et al. 1996).

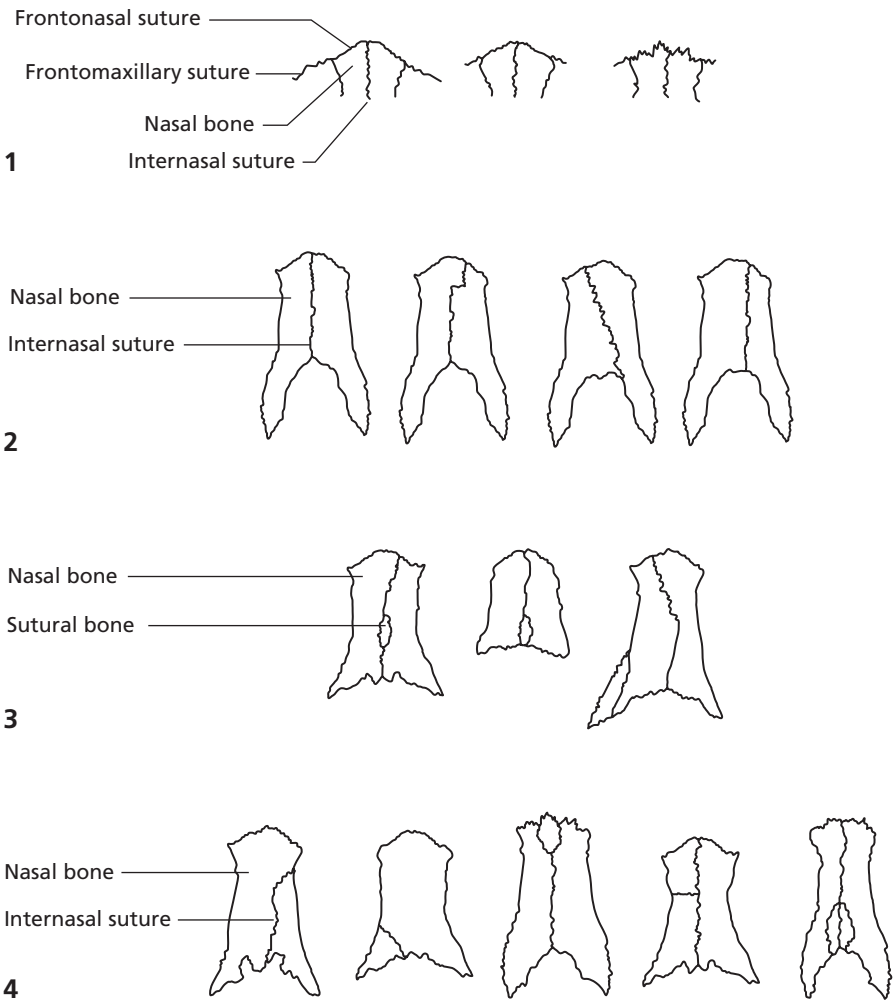

Figure 1.21 Variations in the sutures of the nasal bones. Redrawn after Krmpotić-Nemanić et al. (1988).

Teeth

It is common to find fewer (partial anodontia) than the normal complement of teeth, although complete absence (true anodontia) of the teeth has been reported (Woelfel and Scheid 1997). The upper lateral incisors are most often absent, then the second lower premolars, the wisdom teeth, and the medial incisors, in that order. The upper canines are rarely missing, the upper premolars and second molars even more rarely, and most rarely the first permanent molars (Bergman et al. 1996). The mandibular canine tooth and root can divide into labial and lingual parts or its lingual surface can be shovel-shaped. This rarely occurs with the maxillary canine (Woelfel and Scheid 1997).

Supernumerary teeth can appear in both deciduous and permanent dentitions, but usually in the permanent dentition, and occur in 0.3–3.8% of the population (Woelfel and Scheid 1997). The most common supernumerary tooth is a mesiodens, which is usually small and conical, between the maxillary incisors. This is generally followed by maxillary lateral incisor, maxillary fourth molar, and mandibular third premolar supernumeraries. Supernumerary maxillary premolar, canine, and mandibular fourth molar are the least common. The incidence in the mandibular anterior tooth area is about 0.01% (Rossi et al. 2010). Rossi et al. (2010) reported a supernumerary permanent lower incisor in the dry mandible of an adult Brazilian male. Owing to its location and morphology, the supernumerary tooth presented as a lower lateral incisor joined to the lower lateral incisor normal in the mandibular arch through their distal and mesial contact faces, respectively (Figs 1.22, 1.23).

Ozgul et al. (2013) evaluated 7551 non-syndromic patients aged 3–16 years who applied for routine check-up. Supernumerary teeth were detected in 74 (0.98%). Of these, 48 were male and 26 were female (male-to-female ratio: 1.84:1). A total of 84 supernumerary teeth were detected, 80 (95.2%) permanent and four (4.8%) deciduous (n=4). Most supernumerary teeth (n=59, 70.2%) were located in the maxillary arch. The most common supernumerary teeth were mesiodens (36.9%), followed by those located in the maxillary incisor region (33.3%), the mandibular

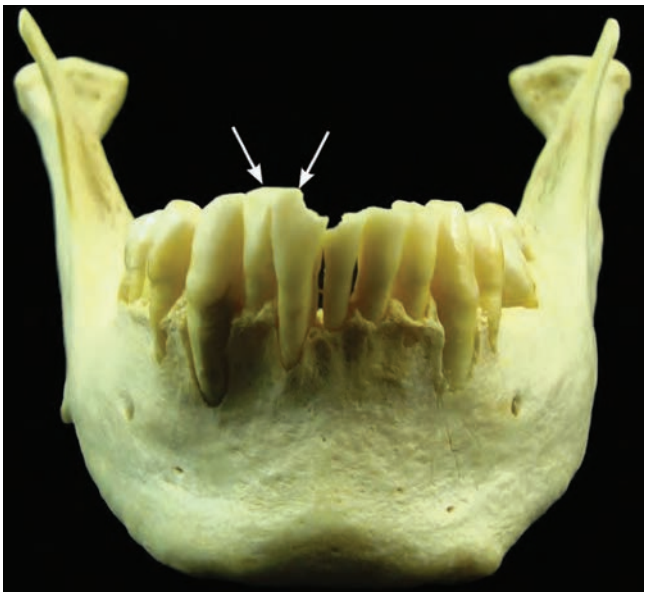

Figure 1.22 Frontal view of the mandible showing the two lateral incisors (arrows: lateral incisors).

Source: Rossi et al. (2010). Reproduced with permission from International Journal of Anatomical Variations.

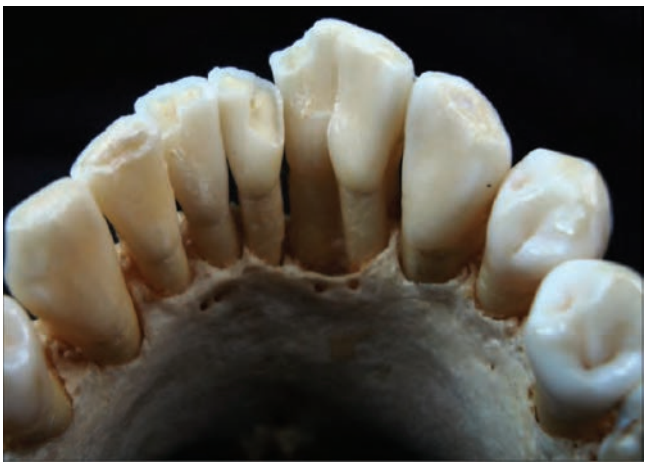

Figure 1.23 Occlusal view showing the union of the lateral incisors on the mesial surface.

Source: Rossi et al. (2010). Reproduced with permission from International Journal of Anatomical Variations.

premolar region (17.9%), the mandibular molar region (5.9%), the mandibular incisor region (4.8%), and the mandibular canine region (1.2%). Overall, the prevalence of supernumerary teeth was 0.98% and the mesiodens was the most common type. Mossaz et al. (2014) studied 82 patients with supernumerary teeth in the maxilla and mandible using cone-beam computed tomography. The study comprised a total of 101 supernumerary teeth. Most of the patients (80.5%) exhibited a single supernumerary tooth, while 15.8% had two and 3.7% had three. Males were affected more than females with a ratio of 1.65:1. Mesiodentes were the most frequently diagnosed type of supernumerary teeth (48.52%), followed by supernumerary premolars (23.76%) and lateral incisors (18.81%). Supernumeraries were most commonly conical in shape (42.6%) with a normal or inclined vertical position (61.4%).

Other oddities of the teeth include variable sizes, crown shape, peg-shaped lateral incisor or notched incisor or maxillary central incisors, fused teeth, multiple roots, accessory cusps or tubercles (e.g., cusp of Carabelli of the mesiopalatal upper first molar), shovel-shaped maxillary incisors, angled root, root fusion, segmented root, dwarfed (short) roots, unerupted teeth, transposition of the teeth, rotation of a tooth, and ectopic teeth (e.g., nasal septum) (Woelfel and Scheid 1997).

Middle ear bones

Stapes

The stapes exhibits marked variations. The head differs in the prominence of its margins, shape of the articular facet, and degree of inclination in relation to the crural arches. There is no correlation between the length of the stapes and its weight; the breadth and weight of the ossicle could be more closely related. In most cases the posterior crus was found to be thicker, larger, and more curved than the anterior crus. The junction of the anterior crus with the base is usually thinner than the junction of the posterior crus (Bergman et al. 1996).

Van de Maele et al. (1989) reported a columellaform stapes in an 18-year-old male patient with a conductive hearing loss. SEM and light microscopy demonstrated that the ossicle was smaller than normal. The head was linked to the base by a crural plate, probably formed by fusion of the material of the two crura. Microscopy demonstrated a slightly less interwoven structure of the fibrillar bone, mainly at the cranial aspect of the crural plate. Honeycomb-like bone was confined to the caudal part of the crural plate. Microscopy revealed a cavity in the center of the stapes at the transition between the base and the plate. During surgery, a bony structure was found to link the posterior side of the head of the stapes to the pyramidal eminence. The authors concluded that a columellaform stapes can occur without forming part of a syndrome.

Malleus

Arviso and Todd (2010) studied a total of 41 adult crania without clinical otitis. They measured: (1) the distance from the lateral process of the malleus to the umbo and to the annulus; and (2) the angles formed anteriorly and posteriorly at the umbo. The two metrics of malleus foreshortening did not correlate with one another; that is, the manubrium-length/tympanic-diameter ratio did not correlate with the posterior/anterior umbo angle ratio. Mastoid size did not correlate with either metric of malleus foreshortening. The authors concluded that a foreshortened malleus is an anatomical variant, not a sign of pathology.

Incus

Chien et al. (2009) studied the anatomy of the distal incus, including the lenticular process, in histological sections from 270 normal cadaveric human temporal bones covering an age range from less than 1 month to 100 years. All but nine of the sections exhibited signs of a bony connection between the long process of the incus and the flattened plate of the lenticular process, and in 108 specimens a complete bony attachment was observed in a single 20 μm section. In these 108 ears, the bony lenticular process consisted of a proximal narrow "pedicle" connected to a distal flattened "plate" that formed the incudal component of the incudo-stapedial joint. A fibrous joint capsule extended from the stapes head to the pedicle of the lenticular process on all sides, where it was considerably thickened.

References

Agarwal SK, Malhotra VK, Tewari SP. 1979. Incidence of the metopic suture in adult Indian crania. *Acta Anat (Basel)* 105: 469–474.

Aksu F, Ceri NG, Arman C, Zeybek FG, Tetik S. 2009. Location and incidence of the zygomaticofacial foramen: An anatomic study. *Clin Anat* 22: 559–562.

Anil A, Peker T, Turgut HB, Pelin C, Gülekon N. 2000. Incidence of os japonicum in Anatolian dry skulls and plain cranium radiographs of modern Anatolian population. *J Craniomaxillofac Surg* 28: 217–223.

Aragão JA, Fontes LM, Aragão JMR, Reis FP. 2013. Ossification of interclinoid ligaments and their clinical importance. *Int J Anat Var (IJAV)* 6: 201–202.

Ariyürek OM, Balkanci F, Aydingöz U, Onerci M. 1996. Pneumatised superior turbinate: a common anatomic variation? *Surg Radiol Anat* 18: 137–139.

Arviso LC, Todd NW Jr. 2010. The foreshortened malleus: Anatomic variant, not pathologic sign. *Otolaryngol Head Neck Surg* 143: 561–566.

Athavale SA. 2010. Morphology and compartmentation of the jugular foramen in adult Indian skulls. *Surg Radiol Anat* 32: 447–453.

Aydinlioğlu A, Erdem S. 2004. Maxillary and sphenoid sinus aplasia in Turkish individuals: a retrospective review using computed tomography. *Clin Anat* 17: 618–622.

Aydinlioğlu A, Kavakli A, Erdem S. 2003. Absence of frontal sinus in Turkish individuals. *Yonsei Med J* 44: 215–218.

Bademci G, Kendi T, Agalar F. 2007. Persistent metopic suture can mimic the skull fractures in the emergency setting? *Neurocirugia (Astur)* 18: 238–240.

Bajwa M, Srinivasan D, Nishikawa H, Rodrigues D, Solanki G, White N. 2013. Normal fusion of the metopic suture. *J Craniofac Surg* 24: 1201–1205.

Barteczko K, Jacob M. 2004. A re-evaluation of the premaxillary bone in humans. *Anat Embryol (Berl)* 207: 417–437.

Bennett WM. 2013. Images in clinical medicine. Torus palatinus. *N Engl J Med* 368: 1434.

Bergman RA, Afifi AK, Miyauchi R. 1996. Illustrated Encyclopedia of Human Anatomic Variation: Opus V: Skeletal Systems: Cranium. Available at http://www.anatomyatlases.org/AnatomicVariants/SkeletalSystem/Regions/Cranium.shtml (accessed 12 October 2015).

Berry AC, Berry RJ. 1967. Epigenetic variation in the human cranium. *J Anat* 101: 361–380.

Boopathi S, Chakravarthy Marx S, Dhalapathy SL, Anupa S. 2010. Anthropometric analysis of the infraorbital foramen in a South Indian population. *Singapore Med J* 51: 730–735.

Bose A, Shrivastava S. Partial occipitalization of atlas. 2013. *Int J Anat Var (IJAV)* 6: 81–84.

Bruns G. 1947. Über einen polygnathen Epignathus. *Virch Arch* 314: 125–136.

Burdan F, Szumiło J, Walocha J, Klepacz L, Madej B, Dworzański W, Klepacz R, Dworzańska A, Czekajska-Chehab E, Drop A. 2012. Morphology of the foramen magnum in young Eastern European adults. *Folia Morphol (Warsz)* 71: 205–216.

Buschkowitsch WJ. 1927. Ueber das "Tuberculum orbitale" des Jochbeins des Menschen. *Anat Anz* 63: 353–357.

Çakur B, Sumbullu MA, Durna NB. 2011a. Aplasia and agenesis of the frontal sinus in Turkish individuals: a retrospective study using dental volumetric tomography. *Int J Med Sci* 8: 278–282.

Çakur B, Sümbüllü MA, Yılmaz AB. 2011b. A retrospective analysis of sphenoid sinus hypoplasia and agenesis using dental volumetric CT in Turkish individuals. *Diagn Interv Radiol* 17: 205–208.

Chaisuksunt V, Kwathai L, Namonta K, Rungruang T, Apinhasmit W, Chompoopong S. 2012. Occurrence of the foramen of Vesalius and its morphometry relevant to clinical consideration. *Scientific World Journal* 2012: 817454.

Champion T, Cope JM. 2012. A severe case of hyperostosis frontalis interna and multiple comorbidities. *Int J Anat Var (IJAV)* 5: 76–78.

Chauhan NK, Chopra J, Rani A, Rani A, Srivastava AK. 2010. A bony canal in the basilar part of occipital bone. *Int J Anat Var (IJAV)* 3: 112–113.

Chauhan P, Dixit SG. 2011. Bilateral elongated coronoid processes of mandible. *Int J Anat Var (IJAV)* 4: 25–27.

Chethan P, Prakash KG, Murlimanju BV, Prashanth KU, Prabhu LV, Saralaya VV, Krishnamurthy A, Somesh MS, Kumar CG. 2012. Morphological analysis and morphometry of the foramen magnum: an anatomical investigation. *Turk Neurosurg* 22: 416–419.

Chien W, Northrop C, Levine S, Pilch BZ, Peake WT, Rosowski JJ, Merchant SN. 2009. Anatomy of the distal incus in humans. *J Assoc Res Otolaryngol* 10: 485–496.

Choudhry R, Choudhry S, Anand C. 1988. Duplication of optic canals in human skulls. *J Anat* 159: 113–116.

Choudhry R, Anand M, Choudhry S, Tuli A, Meenakshi A, Kalra A. 1999. Morphologic and imaging studies of duplicate optic canals in dry adult human skulls. *Surg Radiol Anat* 21: 201–205.

Choudhry S, Kalra S, Choudhry R, Choudhry R, Tuli A, Kalra N. 2005. Unusual features associated with cranial openings of optic canal in dry adult human skulls. *Surg Radiol Anat* 27: 455–458.

Comer BT, Kincaid NW, Smith NJ, Wallace JH, Kountakis SE. 2013. Frontal sinus septations predict the presence of supraorbital ethmoid cells. *Laryngoscope* 123: 2090–2093.

Danesh-Sani SA, Bavandi R, Esmaili M. 2011. Frontal sinus agenesis using computed tomography. *J Craniofac Surg* 22: e48–e51.

De Battista JC, Zimmer LA, Theodosopoulos PV, Froelich SC, Keller JT. 2012. Anatomy of the inferior orbital fissure: implications for endoscopic cranial base surgery. *J Neurol Surg B Skull Base* 73: 132–138.

de Freitas V, Madeira MC, Toledo Filho JL, Chagas CF. 1979. Absence of the mental foramen in dry human mandibles. *Acta Anat (Basel)* 104: 353–355.

Didio LJ. 1942. Observacoes sobre o "tuberculo orbitario" de Whitnall no osso zigomatico de homem (com pesquisas no vivo). *Anais Fac Med S Paulo* 18: 43–63.

Didio LJ. 1962. The presence of the eminentia orbitalis in the os zygomaticum of Hindu skulls. *Anat Rec* 142: 31–39.

Erdem T, Aktas D, Erdem G, Miman MC, Ozturan O. 2002. Maxillary sinus hypoplasia. *Rhinology* 40: 150–153.

Figueiredo N, Moraes LB, Serra A, Castelo S, Gonsales D, Medeiros RR. 2008. Median (third) occipital condyle causing atlantoaxial instability and myelopathy. *Arq Neuropsiquiatr* 66: 90–92.

Freire AR, Rossi AC, Prado FB, Caria PHF, Botacin PR. 2010. The caroticoclinoid foramen formation in the human skull and its clinical correlations. *Int J Anat Var (IJAV)* 3: 149–150.

Göçmez C, Göya C, Hamidi C, Kamaşak K, Yilmaz T, Turan Y, Uzar E, Ceviz A. 2014. Three-dimensional analysis of foramen magnum and its adjacent structures. *J Craniofac Surg* 25: 93–97.

Govsa F, Kayalioglu G, Erturk M, Ozgur T. 1999. The superior orbital fissure and its contents. *Surg Radiol Anat* 21: 181–185.

Govsa F, Celik S, Ozer MA. 2009. Orbital restoration surgery in the zygomaticotemporal and zygomaticofacial nerves and important anatomic landmarks. *J Craniofac Surg* 20: 540–544.

Hajiioannou J, Owens D, Whittet HB. 2010. Evaluation of anatomical variation of the crista galli using computed tomography. *Clin Anat* 23: 370–373.

Hartikainen J, Aho HJ, Seppä H, Grenman R. 1996. Lacrimal bone thickness at the lacrimal sac fossa. *Ophthalmic Surg Lasers* 27: 679–684.

Hasan T, Fauzi M, Hasan D. 2010. Bilateral absence of mental foramen — a rare variation. *Int J Anat Var (IJAV)* 3: 167–169.

Huang B, Takahashi K, Sakata-Goto T, Kiso H, Togo Y, Saito K, Tsukamoto H, Sugai M, Akira S, Shimizu A, Bessho K. 2013. Phenotypes of CCAAT/enhancer-binding protein beta deficiency: hyperdontia and elongated coronoid process. *Oral Dis* 19: 144–150.

Idowu OE, Balogun BO, Okoli CA. 2009. Dimensions, septation, and pattern of pneumatization of the sphenoidal sinus. *Folia Morphol (Warsz)* 68: 228–232.

Jeyasingh P, Gupta CD, Arora AK, Saxena SK. 1982. Study of Os japonicum in Uttar Pradesh crania. *Anat Anz* 152: 27–30.

Kadanoff D, Mutafov S, Jordanov J. 1970. The principle openings and incisures of the facial bones (incisura frontalis seu foramen frontale, foramen supraoriitale seu incisura supraorbitalis, foramen infraorbitale, foramen mentale). *Gegenbaurs Morphol Jahrb* 115(1): 102–118.

Kangas T. 1928. Das Vorkommen des "Tuberculum orbitale" in menschlichen Schaedel, insbesondere bei Finnen und Lappen. *Helsinki: Duodecim*, 68–74.

Keyes JEL. 1935. Observations on four thousand optic foramina. Albrecht v. *Graefes Archiv fur Ophthalmologie* 13: 538–568.

Kim HS, Oh JH, Choi DY, Lee JG, Choi JH, Hu KS, Kim HJ, Yang HM. 2013. Three-dimensional courses of zygomaticofacial and zygomaticotemporal canals using micro-computed tomography in Korean. *J Craniofac Surg* 24: 1565–1568.

Kolagi SI, Herur A, Mutalik A. 2010. Elongated styloid process – report of two rare cases. *Int J Anat Var (IJAV)* 3: 100–102.

Krmpotić-Nemanić J, Draf W, Helms J. 1988. *Surgical Anatomy of Head and Neck*. Berlin, Heidelberg: Springer-Verlag.

Lang J. 1983. *Clinical Anatomy of the Head, Neurocranium, Orbit and Craniocervical Region*. Berlin: Springer-Verlag.

Lang J. 1989. *Clinical Anatomy of the Nose, Nasal Cavity and Paranasal Sinuses*. New York: Thieme.

Lang J. 1990. *Clinical Anatomy of the Posterior Cranial Fossa and its Foramina*. Stuttgart, New York: Georg Thieme Verlag.

Lang J. 1995. *Clinical Anatomy of the Masticatory Apparatus and Peripharyngeal Spaces*. New York: Theime.

Lang J. 2001. *Skull Base and Related Structures, second edition*. New York: Thieme.

Lang J, Kley W. 1981. Über die agnesis und hypoplasie der concahe nasals und des septum nasi. *HNO* 29: 200–207.

Le Double AF. 1903. *Traite des Variations des Os du Crane de l'Homme p. 372*. Paris: Vigot Freres.

Loukas M, Owens DG, Tubbs RS, Spentzouris G, Elochukwu A, Jordan R. 2008. Zygomaticofacial, zygomaticoorbital and zygomaticotemporal foramina: anatomical study. *Anat Sci Int* 83: 77–82.

Maestre-Ferrín L, Galán-Gil S, Rubio-Serrano M, Peñarrocha-Diago M, Peñarrocha-Oltra D. 2010. Maxillary sinus septa: a systematic review. *Med Oral Patol Oral Cir Bucal* 15: e383–e386.

Magden AO, Kaynak S. 1996. Bilateral duplication of optic canals. *Ann Anat* 178: 61–64.

Magden O, Icke C, Arman C, Ozyurt D, Kaynak S. 1995. Fissura orbitalis superior: un original tipleri. *MN Oftalmoloji* 2: 130–135.

Mangal A, Choudhry R, Tuli A, Choudhry S, Choudhry R, Khera V. 2004. Incidence and morphological study of zygomaticofacial and zygomatico-orbital foramina in dry adult human skulls: the non-metrical variants. *Surg Radiol Anat* 26: 96–99.

Maniscalco JE, Habal MB. 1978. Microanatomy of the optic canal. *J Neurosurg* 48: 402–406.

Manolis E, Filippou D, Papadopoulos PV, Tsoumakas K, Katostaras T, Christianakis E, Fildisis G, Mompheratou E. 2008. Temporal bone and mastoid process morphology in Mediterranean population. *Ital J Anat Embryol* 113: 117–128.

May H, Peled N, Dar G, Abbas J, Hershkovitz I. 2011. Hyperostosis frontalis interna: what does it tell us about our health? *Am J Hum Biol* 23: 392–397.

Mihailovic T, Stimec BV, Terzic M, Dmitrovic A, Micic J. 2012. The absence of the vomer in the first and early second trimester of pregnancy – a new marker of trisomy 21 and trisomy 13. *Ultraschall Med* 33: E68–E74.

Mossaz J, Kloukos D, Pandis N, Suter VG, Katsaros C, Bornstein MM. 2014. Morphologic characteristics, location, and associated complications of maxillary and mandibular supernumerary teeth as evaluated using cone beam computed tomography. *Eur J Orthod* 36(6): 708–718.

Mukherjee P, Palit S, Tapadar A, Roy H. 2011. Asymmetrical bilateral ossification of stylohyoid chains — a case report with embryological review. *Int J Anat Var (IJAV)* 4: 134–136.

Naderi S, Korman E, Citak G, Güvençer M, Arman C, Senoğlu M, Tetik S, Arda MN. 2005. Morphometric analysis of human occipital condyle. *Clin Neurol Neurosurg* 107: 191–199.

Naitoh M, Hiraiwa Y, Aimiya H, Gotoh K, Ariji E. 2009. Accessory mental foramen assessment using cone-beam computed tomography. *Oral Surg Oral Med Oral Pathol Oral Radiol Endod* 107: 289–294.

Naitoh M, Yoshida K, Nakahara K, Gotoh K, Ariji E. 2011. Demonstration of the accessory mental foramen using rotational panoramic radiography compared with cone-beam computed tomography. *Clin Oral Implants Res* 22: 1415–1419.

Nakatani T, Tanaka S, Mizukami S. 1998. A metopic suture observed in a 91-year-old Japanese male. *Kaibogaku Zasshi* 73: 265–267.

Natori Y, Rhoton AL Jr. 1994. Transcranial approach to orbit: microsurgical anatomy. *J Neurosurg* 81: 78–86.

Natori Y, Rhoton AL Jr. 1995. Microsurgical anatomy of the superior orbital fissure. *Neurosurgery* 36: 762–775.

Nayak SB, Soumya KV. 2008. Unusual sutural bones at pterion. *Int J Anat Var (IJAV)* 1: 19–20.

Neves FS, Crusoé-Souza M, Franco LC, Caria PH, Bonfim-Almeida P, Crusoé-Rebello I. 2012. Canalis sinuosus: a rare anatomical variation. *Surg Radiol Anat* 34: 563–566.

Nikolić S, Djonić D, Zivković V, Babić D, Juković F, Djurić M. 2010. Rate of occurrence, gross appearance, and age relation of hyperostosis frontalis interna in females: a prospective autopsy study. *Am J Forensic Med Pathol* 31: 205–207.

Nikolova SY, Toneva DH, Yordanov YA, Lazarov NE. 2012. Absence of foramen spinosum and abnormal middle meningeal artery in cranial series. *Anthropol Anz* 69: 351–366.

Nogueira AS, Gonçales ES, Santos PS, Damante JH, Alencar PN, Sampaio FA, Garcia AS. 2013. Clinical, tomographic aspects and relevance of torus palatinus: case report of two sisters. *Surg Radiol Anat* 35: 867–871.

Ono R. 1928. Untersuchungen ueber die Orbita von Japaner. *Jap J Med Shi 1 Anatomy* 1: 307–308.

Ozer MA, Celik S, Govsa F, Ulusoy MO. 2011. Anatomical determination of a safe entry point for occipital condyle screw using three-dimensional landmarks. *Eur Spine J* 20: 1510–1517.

Ozgul BM, Arikan V, Oz FT. 2013. Prevalence and characterıstıcs of supernumerary teeth in a child population from central anatolıa — Turkey. *Oral Health Dent Manag* 12: 269–272.

Ozgursoy OB, Comert A, Yorulmaz I, Tekdemir I, Elhan A, Kucuk B. 2010. Hidden unilateral agenesis of the frontal sinus: human cadaver study of a potential surgical pitfall. *Am J Otolaryngol* 31: 231–234.

Paraskevas GK, Tsitsopoulos PP, Papaziogas B, Kitsoulis P, Spanidou S, Tsitsopoulos P. 2009. Osseous variations of the hypoglossal canal area. *Med Sci Monit* 15: BR75–BR83.

Poirier J, Duggal N, Lee D, Rotenberg B. 2011. Sphenoid sinus septations: unpredictable anatomic landmarks in endoscopic pituitary surgery. *J Otolaryngol Head Neck Surg* 40: 489–492.

Prakash BS, Latha PK, Menda JL, Ramesh BR. 2011. A tubercle at the anterior margin of foramen magnum. *Int J Anat Var (IJAV)* 4: 118–119.

Rao PV. 2002. Median (third) occipital condyle. *Clin Anat* 15: 148–151.

Rastogi R, Budhiraja V. 2010. Slit-like jugular foramen due to abnormal bone growth at jugular fossa. *Int J Anat Var (IJAV)* 3: 74–75.

Ray B, Gupta N, Ghose S. 2005. Anatomic variations of foramen ovale. *Kathmandu Univ Med J (KUMJ)* 3: 64–68.

Reymond J, Charuta A, Wysocki J. 2005. The morphology and morphometry of the foramina of the greater wing of the human sphenoid bone. *Folia Morphol (Warsz)* 64: 188–193.

Reymond J, Kwiatkowski J, Wysocki J. 2008. Clinical anatomy of the superior orbital fissure and the orbital apex. *J Craniomaxillofac Surg* 36: 346–353.

Rossi AC, Freire AR, Prado FB, Caria PHF, Botacin PR. 2010. Anatomical variation in a Brazilian human mandible: case report of a supernumerary permanent lower incisor. *Int J Anat Var (IJAV)* 3: 151–152.

Sahin B, Ozkan HS, Gorgu M. 2010. An anatomical variation of mental nerve and foramen in a trauma patient. *Int J Anat Var (IJAV)* 3: 165–166.

Saini V, Singh R, Bandopadhyay M, Tripathi SK, Shamal SN. 2009. Occipitalization of the atlas: its occurrence and embryological basis. *Int J Anat Var (IJAV)* 2: 65–68.

Sanchez T, Stewart D, Walvick M, Swischuk L. 2010. Skull fracture vs. accessory sutures: how can we tell the difference? *Emerg Radiol* 17: 413–418.

Saran RS, Ananthi KS, Subramaniam A, Balaji MT, Vinaitha D, Vaithianathan G. 2013. Foramen of civinini: a new anatomical guide for maxillofacial surgeons. *J Clin Diagn Res* 7: 1271–1275.

Sasani H, Ceyhan O, Sencer S, Sasani M. 2013. 3D reconstruction computerized tomography findings of an asymptomatic Eagle's Syndrome patient: a case report. *Int J Anat Var (IJAV)* 6: 176–178.

Saylam C, Özer MA, Bilge O, Ozek C, Alper M. 1999. Anatomic variations of the infraorbital foramen. *Ann Plast Surg* 43: 613–617.

Scanavine AB, Navarro JA, Megale SR, Anselmo-Lima WT. 2009. Anatomical study of the sphenopalatine foramen. *Braz J Otorhinolaryngol* 75: 37–41.

Shapiro R, Janzen AH. 1960. The Normal Skull. New York: Medical Division of Harper and Brothers.

Sharma PK, Malhotra VK, Tewari SP. 1988. Variations in the shape of the superior orbital fissure. *Anat Anz I65*: 55–56.

Shi X, Han H, Zhao J, Zhou C. 2007. Microsurgical anatomy of the superior orbital fissure. *Clin Anat* 20: 362–366.

Shinohara AL, de Souza Melo CG, Silveira EM, Lauris JR, Andreo JC, de Castro Rodrigues A. 2010. Incidence, morphology and morphometry of the foramen of Vesalius: complementary study for a safer planning and execution of the trigeminal rhizotomy technique. *Surg Radiol Anat* 32: 159–164.

Simunković SK, Bozić M, Alajbeg IZ, Dulcić N, Boras VV. 2011. Prevalence of torus palatinus and torus mandibularis in the Split-Dalmatian County, Croatia. *Coll Antropol* 35: 637–641.

Singh M. 2005. Duplication of optic canal in adult Japanese human skulls. *J Anat Soc India* 54(2): 1–9.

Sisman Y, Ertas ET, Gokce C, Akgunlu F. 2008. Prevalence of torus palatinus in cappadocia region population of Turkey. *Eur J Dent* 2: 269–275.

Skrzat J, Walocha J, Srodek R. 2005. An anatomical study of the pterygoalar bar and the pterygoalar foramen. *Folia Morphol (Warsz)* 64: 92–96.

Sondheimer FK.1971. Basal foramina and canals in Radiology of the Skull and Brain. *The Skull Vol 1*, Book 1 (Newton TH, Potts DG eds). Saint Louis: CV Mosby Co.

Srimani P, Mukherjee P, Ghosh E, Roy H. 2013. Variant presentations of "Foramen of Hüschke" in seven adult human crania. *Int J Anat Var (IJAV)* 6: 120–123.

Srivastava HC. 1992. Ossification of the membranous portion of the squamous part of the occipital bone in man. *J Anat* 180: 219–224.

Stotland MA, Do NK, Knapik TJ. 2012. Bregmatic wormian bone and metopic synostosis. *J Craniofac Surg* 23: 2015–2018.

Takahashi Y, Kakizaki H, Nakano T. 2011. Accessory ethmoidal foramina: an anatomical study. *Ophthal Plast Reconstr Surg* 27: 125–127.

Tanaka T. 1932. Ganglion sphenopalatinum des Menschen. *Arb. 3 Abt Anat Inst Kyoto* 3: 91–115.

Tasar M, Cankal F, Bozlar U, Hidir Y, Saglam M, Ors F. 2007. Bilateral maxillary sinus hypoplasia and aplasia: radiological and clinical findings. *Dentomaxillofac Radiol* 36: 412–415.

Toh H, Kodama J, Yanagisako M, Ohmori T. 1992. Anatomical study of the accessory mental foramen and the distribution of its nerve. *Okajimas Folia Anat Jpn* 69: 85–88.

Tomita S. 1935. On the tuberculum orbitale of the zygomatic bone in the Japanese (in Japanese). *Kanazawa daigaku igakubu kaibogaku kyoshitsu gyoseki* 20: 149–154.

Tubbs RS, May WR Jr, Apaydin N, Shoja MM, Shokouhi G, Loukas M, Cohen-Gadol AA. 2009. Ossification of ligaments near the foramen ovale: an anatomic study with potential clinical significance regarding transcutaneous approaches to the skull base. *Neurosurgery* 65: 60–64.

Tubbs RS, Mortazavi MM, Shoja MM, Loukas M, Cohen-Gadol AA. 2012. The zygomaticotemporal nerve and its relevance to neurosurgery. *World Neurosurg* 78: 515–518.

Tunnessen WW. 1990. Persistent open anterior fontanelle. *JAMA* 14: 2450.

Udare AS, Bansal D, Patel B, Mondel PK, Aiyer S. 2014. Condylus tertius with atlanto-axial rotatory fixation: an unreported association. *Skeletal Radiol* 43(4): 535–539.

Udupi S, Srinivasan JK. 2011. Interparietal (Inca) bone: a case report. *Int J Anat Var (IJAV)* 4: 90–92.

van de Maele C, Van Cauwenberge P, Kluyskens P, Vakaet L. 1989. Morphology of a columellaform stapes. *J Laryngol Otol* 103: 79–82.

Verim A, Faruk Çalım Ö, Yenigün A, Kocagöz GD, Kökten N, Özkul H. 2012. Hereditary characteristic of isolated congenital vomer aplasia. *J Craniomaxillofac Surg* 40: e392–e396.

Vokurka J. 1989. Congenital duplication of the external acoustic meatus. *Cesk Otolaryngol* 38: 314–317.

Warwick R. 1951. A juvenile skull exhibiting duplication of the optic canals and subdivision of the superior orbital fissure. *J Anat* 85: 289–291.

White LE. 1923. An anatomic and X-ray study of the optic canal in cases of optic nerve involvement. *Bos Med Surg J* 189: 741–748.

Whitnall SE. 1911. On a tubercle on the malar bone, and on the lateral attachments of the tarsal plaes. *Anat Physiol* 54: 426–432.

Whitnall SE. 1932. The Anatomy of the Hunan Orbit, second ed. London: Oxford University Press.

Woelfel JB, Scheid RC. 1997. Dental Anatomy: Its Relevance to Dentistry. Baltimore: Williams and Wilkins.

Xu LM, Zhang SZ, Xie XF. 2004. Inferior orbital fissure and groove: axial CT findings and their anatomic variation. *Fa Yi Xue Za Zhi* 20: 18–20.

Yildiz E, Deniz M, Ceyhan O. 2005. Prevalence of torus palatinus in Turkish schoolchildren. *Surg Radiol Anat* 27: 368–371.

Zoja G. 1885. Spora il foro ottico doppio. *Bollettino scientifico, Pavia*, 7, 65–69.

Further reading

Hauser G, De Stefano GF. 1989. Epigenetic Variants of the Human Skull. Stuttgart: E. Schweizerbart'sche Verlagsbuchhandlung.

Patil GV, Kolagi S, Padmavathi G, Rairam GB. 2011. The duplication of the optic canals in human skulls. J Clin Diag Res 5: 536–537.

Wolff E. 1976. Anatomy of the Eye and Orbit, seventh edition, vol. 15. London: HK Lewis.

2 Hyoid bone

R. Shane Tubbs[1] and Koichi Watanabe[2]
[1]Seattle Science Foundation, Seattle, Washington, USA
St George's University, School of Medicine, St Georges, Grenada
University of Dundee, Dundee, UK
[2]Kurume University School of Medicine, Fukuoka, Japan

The hyoid bone ossifies from six centers. The two centers that give rise to the lateral parts of the body are the basihyal and the two parts that give rise to the two centers of the greater horns are termed the thyrohyals. The two centers that give rise to the lesser horns are the ceratohyals (Evans 1940). The hyoid may be absent (Mendis and Moss 2007) or positioned more inferiorly than normal (Rajion et al. 2006). It may be located anterior to the thyroid cartilage (Kainz et al. 1990). The lesser horns may articulate with the greater horns (Porrath 1969) or be absent unilaterally or bilaterally (Fig. 2.1) (Gok et al. 2012). Parsons (1909) identified a synovial joint between the greater and lesser horns in 35 of 77 hyoid bones. This author also found that the lesser horn may fuse with the body of the hyoid and may do this without fusing to the lesser horn. In a radiographic study, Evans (1940) found lesser horns in only 20 cases. The lesser horns may persist into adulthood as partially or completely cartilaginous (Porrath 1969). The lesser horns may be elongated, especially when attached to a stylohyoid ossicular chain. Evans (1940) found that the lesser horn may be up to 12 mm in length. Janczak et al. (2012) described an adult male with syncope due to the carotid artery compression from an enlarged lesser horn of the hyoid bone. The hyoid may be connected to the styloid via a stylohyoid ossicular chain or continuous piece of bone (Krennmair and Piehslinger 1989). The greater horns may not fuse to the body of the hyoid (Porrath 1969), even in old age (Miller 1941). The greater horn of the hyoid may fuse to the greater horn of the thyroid cartilage or form a joint with the body of the hyoid bone. Ilankovan (1987) reported a 47-year-old male patient with an abnormal bone that articulated with the superior horn of the thyroid cartilage and the greater horn of the hyoid bone. Klinfelter (1952) reported a 39-year-old male who had suffered with pain in the right neck for 25 years. The pain came on with sudden rotation of the head to the right. Radiography identified a hyoid bone described as being 50% larger than usual. The right greater horn was 1.5 cm longer that the left greater horn. The right greater horn also consisted of a horizontal and vertical segment, which formed a number 7 shape. Additionally, the vertical segment formed a joint with the superior horn of the thyroid cartilage. The distal centimeter of the left greater horn was angulated 40 degrees posteroinferior. Puchowski (1933) reported a case where the thyrohyoid ligament was ossified. Di Nunno et al. (2004) found total fusion of the body of the hyoid bone with the greater horns in 10 (25%), partial fusion in 4 (10%), and evident articular rima between the body and the greater horns of the hyoid bone in 14 (35%). The lesser horns of the hyoid bone were symmetrical in 29 cases (72.5%), asymmetric in 11 (27.5), and absent in 1 (2.5%). A ridge may be found on the superior surface of the greater horn and mark the attachment of the middle pharyngeal constrictor muscle. The upward traction of the digastric and stylohyoid muscles on the greater horn may result in a slight notch.

Kanetaka et al. (2011) studied the structure of the joint between the body and the greater horn in the human hyoid bone in 259 cadavers (16–98 years). Joints were classified into three grades based on histological observations. Grade I showed fibrocartilage without degenerative change in the marginal region of the joint. Grade II showed prominent calcification or ossification on the outer margin of the joint without fusion. Grade III showed bony fusion. Evans (1940) described epihyal bones or ossification of parts of the stylohyoid ligament between the styloid process and hyoid bone. The hyoid may be pierced by the thyroglossal duct (Nathanson and Gough 1989). Kindschuh et al. (2012) found that the hyoid was broader in European versus African hyoids while the African hyoid was generally longer. The normally U-shaped hyoid may be horseshoe-shaped and may present with a midline superiorly projecting tubercle from the body termed the lingula (Ito et al. 2012). Kawar and Siplovich (2008) described a child with a bridge extending from the hyoid to the sternal notch.

Measurements (mm) of the hyoid bone (mean, SD, and range) for length, breadth, transverse diameter, medial height, anteroposterior thickness, maximum anteroposterior thickness, depth of the posterior surface, length of the greater horn, and width of the greater horn have been found to be: 36±4.1 (27.8–42.4); 40.7±5.2 (30.7–50.6); 23.4±2.5 (17.1–29.9); 10.6±1.2 (8–13.7); 5.1±1 (3.1–7.4); 5.1±1 (3.4–7.6); 2±0.7 (0.9–3.8); 28.1±3.8 (19.2–35.5); and 7±1.1 (5.2–9.3), respectively (Arsenburg et al. 1989). Papadopoulos et al. (1989) classified the hyoid bone into five types, in the following order of frequency: D-type, 29%; B-type, 26.5%; H-type, 21%; U-type, 18.5%; and V-type 5.0%. In 60% of the cases,

Bergman's Comprehensive Encyclopedia of Human Anatomic Variation, First Edition. Edited by R. Shane Tubbs, Mohammadali M. Shoja and Marios Loukas.

Figure 2.1 Skeleton with absence of both lesser horns of the hyoid bone.

the shape of the hyoid bone did not belong to any of the shapes that are conventionally described. Almost half of the hyoid bones were asymmetric and/or anisometric. According to their width, the hyoid bones may be designated as narrow (45%), intermediate (34%), or wide (21%). There was no standard correlation of the distance between the tubercles of the greater horns to the distance between the lesser horns in the same hyoid bone.

The inferior aspect of the body of the hyoid may distinct knobs as identified in 6 of 108 hyoid specimens studied by Parsons (1909). He believed these to be outgrowths into the geniohyoid mucles. The mylohyoid often forms a slight ridge on the lower part of the anterior surface of the basihyal part of the hyoid (Parsons 1909).

References

Arensburg B, Tillier AM, Duday H, Schepartz LA, Rak Y.1989. A Middle Palaeolithic human hyoid bone. *Nature 338*: 758–760.

Di Nunno N, Lombardo S, Costantinides F, Di Nunno C. 2004. Anomalies and alterations of the hyoid-larynx complex in forensic radiographic studies. *Am J Forensic Med Pathol* 25: 14–19.

Evans WA. 1940. The epihyal bone; consideration of some small accessory bones of the neck. *Am J Roentgenol* 44: 714–715.

Gok E, Kafa IM, Fedakar R. 2012. Unusual variation of the hyoid bone: bilateral absence of lesser cornua and abnormal bone attachment to the corpus. *Surg Radiol Anat* 34: 567–579.

Ilankovan V. 1987. An anomaly of the thyro-hyoid articulation. *J Laryngol Otol* 101: 959–961.

Ito K, Ando S, Akiba N, Watanabe Y, Okuyama Y, Moriguchi H, Yoshikawa K, Takahashi T, Shimada M. 2012. Morphological study of the human hyoid bone with three-dimensional CT images: Gender difference and age-related changes. *Okajimas Folia Anat Jpn* 89: 83–92.

Janczak D, Skora J, Rucinski A, Szuba A. 2012. Recurrent syncope caused by compression of internal carotid artery by an anomalous hyoid bone. *Vasa* 41: 221–224.

Kainz J, Friedrich G, Anderhumber F. 1990. Two atavistic characteristics of the laryngeal skeleton. *Acta Anat (Basel)* 137: 103–108.

Kanetaka H, Shimizu Y, Kano M, Kikuchi M. 2011. Synostosis of the joint between the body and greater cornu of the hyoid bone. *Clin Anat* 24: 837–842.

Kawar B, Siplovich L. 2008. Congenital midline cervical skin bridge: a case report. *J Pediatr Surg* 43: 544–555.

Kindschuh SC, Dupras TL, Cowgill LW. 2012. Exploring ancestral variation of the hyoid. *J Forensic Sci* 57: 41–46.

Klinefelter EW.1952. The anomalous hyoid. Review of the literature and report of a case. *Radiology* 58: 224–227.

Krennmair G, Piehslinger E. 1999. The incidence and influence of abnormal styloid conditions on the etiology of craniomandibular functional disorders. *Cranio* 17: 247–253.

Mendis D, Moss AL. 2007. Case series: variations in the embryology of congenital midline cervical clefts. *Acta Chir Plast* 49: 71–74.

Miller RA. 1941. The laryngeal sacs of an infant and an adult gorilla. *Am J Anat* 69: 1–17.

Nathanson LK, Gough IR. 1989. Surgery for thyroglossal cysts: Sistrunk's operation remains the standard. *Aust N Z J Surg* 59: 873–875.

Papadopoulos N, Lykaki-Anastopoulou G, Alvanidou E. 1989. The shape and size of the human hyoid bone and a proposal for an alternative classification. *J Anat* 163: 249–260.

Parsons FG. 1909. Topography and morphology of the human hyoid bone. *J Anat Physiol* 43: 279–290.

Porrath S. 1969. Roentgenologic consideration of the hyoid apparatus. *AJR* 105: 63–73.

Puchowski B. 1933. Un cas d'anomalie de l'appareil hyoidien. *Acta-otolaryng* 18: 447–452.

Rajion ZA, Townsend GC, Netherway DJ, Anderson PJ, Hughes T, Shuaib IL, Halim AS, Samsudin AR, McLean NR, David DJ. 2006. The hyoid bone in Malay infants with cleft lip and palate. *Cleft Palate Craniofac J* 43: 532–538.

3 Cervical vertebrae

Joseph H. Miller, Michael C. Lysek and Mark N. Hadley
University of Alabama at Birmingham, Birmingham, Alabama, United States

The human cervical spine allows for a wide range of motion for the head while protecting the spinal cord, cervical nerve roots, and vertebral arteries. Variations in the bony anatomy of the cervical spinal column are common and fall on a continuum from near-normal to pathologic. The focus of this chapter is on variations of the cervical vertebrae and spinal column. These variants may have clinical significance and may present unique challenges in the operating room.

The cervical vertebrae are the most unique in the spine and exhibit a great deal of variability. The cervical spine supports the head and allows for a wide range of motion. The atlas (C1), axis (C2), and subaxial cervical spine are all unique bony structures with their own variations from what is seen in normal subjects.

Embryology

The developing fetal spine derives from the paraxial mesoderm that is located lateral to the neural tube. The paraxial mesoderm develops into paired somites that form the axial skeleton, associated ligaments, tendons, and paraspinal muscles (Dubrulle and Pourquié 2004; Mallo et al. 2009). The demarcation of individual vertebrae takes place through a process known as resegmentation in which the anterior and posterior portions of adjacent somites fuse (Bagnall et al. 1988; Christ et al. 1998; Dubrulle and Pourquié 2004). Each vertebral body is therefore formed from two sclerotomes. The intervertebral discs are formed at the boundary between the anterior and posterior sclerotomal portions of the somite (Mallo et al. 2009). The formation of the spine begins in utero and continues until early adulthood. Any variations in this process can result in congenital variants.

Ossification of the atlas and axis are unique compared with the remainder of the subaxial cervical vertebrae. The posterior atlantal arch ossifies by age 5 and the anterior arch of C1 is typically ossified by age 8 (Wang et al. 2001). The atlas achieves a normal adult radiographic appearance by the age of 7–8 (Fesmire and Luten 1989).

The axis is more complex in that there are a total of six ossification centers, unlike the typical four at other spinal levels. The two additional ossification centers are involved in the formation of the odontoid process. The odontoid process begins to fuse to the body of C2 between the ages of 3 and 6 (Fesmire and Luten 1989). This process is normally completed by age 11 (Fesmire and Luten 1989). The remaining four ossification centers are involved in the formation of the remainder of the vertebrae. During the tenth week of gestation, the four posterior vertebral arch chondrification centers unite to form paired ossification bilateral ossification centers. Each of the two ossification centers forms the ipsilateral pedicle, lateral mass, and half of the lamina. This process is normally completed by 2–3 years of age and any aberration in this process can produce a number of anatomic variants (Sakaura et al. 2013).

The subaxial cervical spine typically follows a similar ossification pattern from C3 inferiorly to C7. The ossification of the posterior arch follows the same pattern as C2 and is typically fused with the vertebral body by age 6. Complete ossification does not typically occur until age 25 (Fesmire and Luten 1989). Recognizing epiphyseal variants, incomplete ossification of synchondroses and apophyses, unique vertebral architecture, pseudosubluxation of C2 on C3, overriding of the anterior atlas in relation to the odontoid in extension, and varied atlantodental intervals (ADI) is central to understanding spinal radiographs, especially in children (Townsend and Rowe 1952; Dunlap et al. 1958; Cattell and Filtzer 1965; Shaw et al. 1999; Lustrin et al. 2003).

Atlas

The atlas of adults is a fused ring formed by multiple ossification centers (OC) (Junewick et al. 2011). These OC are quite varied. In a radiographic study of 298 children, Karwacki and Schnedier (2012) found singular (n=196, 66%), bipartite OC (n=86, 29%), and multiple OCs (n=16, 5%). The posterior arch

Bergman's Comprehensive Encyclopedia of Human Anatomic Variation, First Edition. Edited by R. Shane Tubbs, Mohammadali M. Shoja and Marios Loukas.

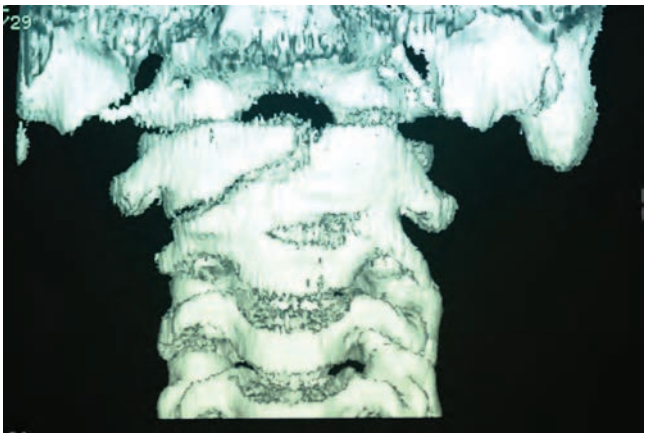

Figure 3.1 3D CT noting an oblique malfusion defect of the anterior arch of the atlas with simultaneous fusion anomaly.

usually fuses by 5 years of age and the anterior arch typically fuses before 8 years of age (Junewick et al. 2011). Incomplete fusion of the anterior or posterior part of the atlantal ring (Figs 3.1, 3.2) is considered a variant of normal when seen outside of the adolescent period. Both the anterior and posterior arches may have facets that articulate with the foramen magnum. Junewick's 13-part radiographic grading system of C1 ossification patterns is an indicator of the number of normal variants seen on routine imaging studies (Junewick et al. 2011) (Table 3.1). There are several cases in the literature that describe a congenital absence of the anterior portion of the ring of C1 (Thavarajah and McKenna 2012). This anomaly is quite rare and is estimated to occur in less than 0.1% of the population (Petraglia et al. 2012). The anterior arch may be enlarged and accessory ossicles may be found near it. Congenital malformation or non-union of the posterior ring is more common and is seen in approximately 4% of the population. Combined non-union of both the anterior and posterior rings is described as a bipartite atlas (Jans et al. 2009; Petraglia et al. 2012). A bipartite atlas is felt to be of little clinical significance, although there is a case report in the literature advocating cervical fusion in individuals with evidence of instability (Hu et al. 2009). The posterior arch may have two instead of one tubercle, which can also be bifid, and ossicles may be found in the posterior atlantooccipital membrane.

Table 3.1 Classification of C1 vertebra ossification patterns.

Classification	Description
Type 0	Completely cartilaginous anterior arch
Type 1	Single ossification center of the anterior arch; unfused neurocentral synchondroses
Type 2	Two symmetric ossification centers of the anterior arch; neurocentral synchondroses either unfused or fused
Type 3	Three ossification centers of the anterior arch; neurocentral synchondroses either unfused or fused
Type 3a	One large and one small ossification centers (type 3 morphology)
Type 4	Four symmetric ossification centers of the anterior arch; neurocentral synchondroses either unfused or fused
Type 4a	One large and two small ossification centers (type 4 morphology)
Type 5	Complete ossification of the anterior arch with fused neurocentral synchondroses
Type A	Unfused posterior synchondrosis
Type B	Bilateral paramedian clefts in posterior arch
Type C	Unilateral paramedian cleft in posterior arch
Type D	Posterior arch hypoplasia
Type E	Complete fusion of the posterior synchondrosis

Figure 3.2 Skull noting atlantooccipital fusion with simultaneous malfusion of the posterior arch of the atlas.

Spina bifida of the posterior arch of C1 is typically an incidental, asymptomatic variation of the atlas. However, Devi et al. (1997) described five male patients with symptomatic cervical stenosis secondary to C1 spina bifida. The pathologic distinction in these cases was that the bifid posterior arch was imbricated anteriorly. This latter pathologic variant should be differentiated from the more common congenital non-union of the posterior arch of the atlas.

The atlas articulates with the occipital condyles located at the base of the skull and there is considerable variation in this

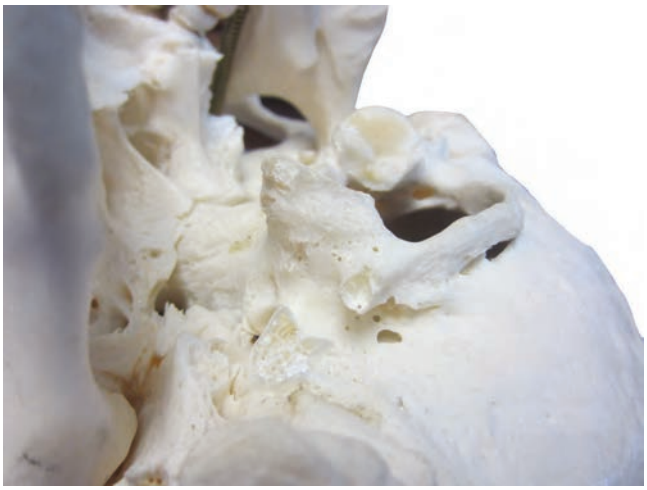

Figure 3.3 Lateral view of another skull with atlantooccipital fusion.

articulation. Interestingly, the atlas may rarely possess bipartite facets that articulate with projections from the occipital bone (Bergmann 1988; Billmann et al. 2007). The lateral mass of C1 where it articulates with the occipital condyles typically has a reniform or kidney-shaped appearance. Billmann et al. (2007) saw variation in the morphology of the lateral mass in 20.8% of specimens during a study of 500 atlases. Bipartition of the superior articular facets of C1 (foveae articulares craniales atlantis) were found both bilaterally (9.6%) and unilaterally (11.2%) (Billmann et al. 2007). The atlas may be fused with the skull base through the occipital condyles (assimilation of the atlas).

Assimilation of the atlas (Figs 3.2, 3.3) is felt to be a distinct variant from the presence of an occipital vertebrae. Another anomaly of the atlantooccipital region is the presence of paired ossicles within the atlantooccipital membrane that may represent a residual proatlas (Bergmann 1988).

The sulcus arteriae vertebralis is the sulcus created by the vertebral artery on the posterior arch of C1. These sulci may have varying levels of surrounding ossification. In as many as 13.8% of individuals there is a posterior bony spicule that projects from the superior articular process (Krishnamurthy et al. 2007). The atlas may even have a completely ossified arcuate foramen (Fig. 3.4a). In such cases, the vertebral artery exits the transverse foramen, passes through the arcuate foramen, and then travels through the foramen magnum (Fig. 3.4b). A laterally placed ponticulus may form a lateral arcuate foramen that can coexist with the more posteriorly located foramen resulting in a canal for the vertebral artery to travel through (Fig. 3.5).

An epitransverse process (Fig.3.6) can extend from the transverse process of the atlas superiorly and can even articulate with the paramastoid region of the occipital bone.

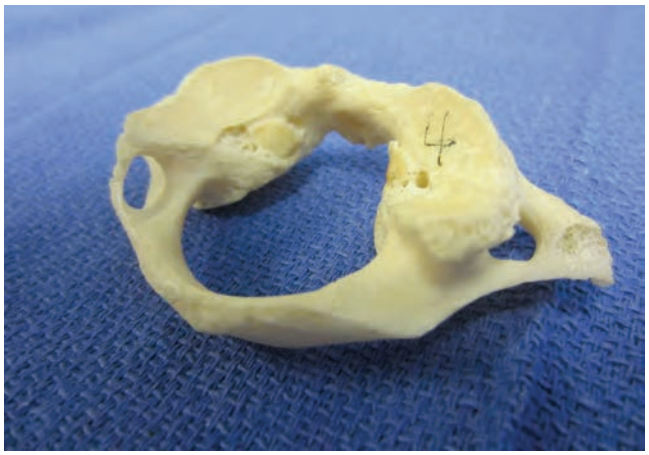

Figure 3.4 (a) Lateral view of the atlas with a left arcuate foramen; (b) 3D CT illustrating bilateral arcuate foramina with the vertebral artery traversing it. Courtesy of Dr Joel Curé.

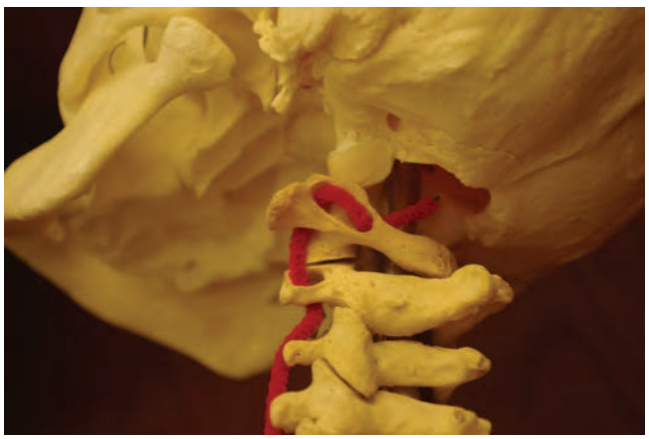

Figure 3.5 Lateral and posterior ponticles resulting in a bony canal for the vertebral artery.

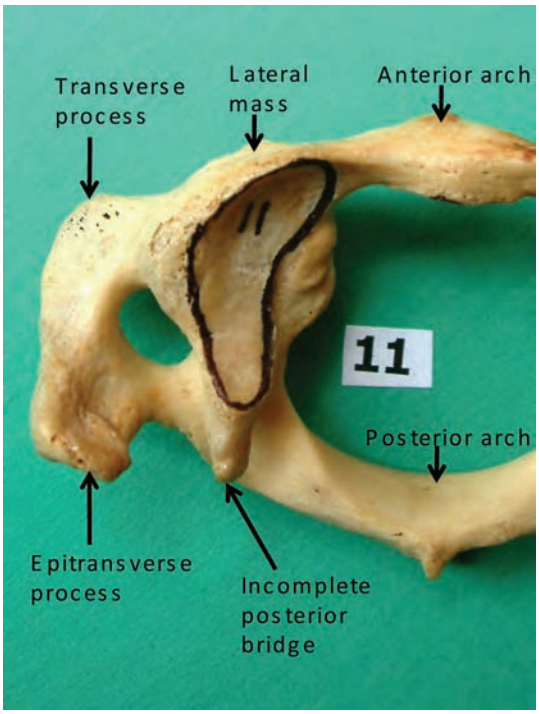

Figure 3.6 A left epitransverse process.

Source: Kaushal (2010). Reproduced with permission from International Journal of Anatomical Variations.

Axis

The axis (C2) is the most complex cervical vertebrae and allows for a tremendous degree of rotation. The odontoid process allows for this rotation and there is significant variation in this structure. Ossiculum terminale is a condition in which the secondary ossification center present at the apical portion of the odontoid does not fuse by the age of 12 (Gore et al. 2011). Ossiculum terminale is commonly identified on adult radiographs and usually carries no clinical significance. There are several case reports suggesting there may be an association with atlantoaxial instability (Liang et al. 2001).

Os odontoideum, a non-union of the synchrondosis of the odontoid process with pathologic instability, is a clinically distinct entity from ossiculum terminale. Radiographically the two can be differentiated by the location of non-union. The underlying etiology of non-union is likely embryologic as there is a known association between os odontoideum and failure of fusion of the atlas (Osti et al. 2006). Many authors consider os odontoideum to be inherently unstable regardless of findings on dynamic plain films. Klimo et al. (2008) described three patients with known os odontoideum that were followed non-operatively and experienced spinal cord injuries. Surgical management is often recommended in this pathologic variant to minimize risk of subsequent spinal cord injury.

Complete aplasia and hypoplasia of the odontoid process have been described (Clark and CSRSEC 2005). The most commonly described form of odontoid hypoplasia is a short, peg-like projection superior to the C1-2 facet articulation. The dens can be bifid, the so-called dens bicornis. A sulcus can sometimes be found at the base of the dens and represents the remnants of the synchondrosis found at this location. The length of the odontoid process ranges from 20 to 40 mm (Lang 1992). The odontoid process may be angulated posteriorly, referred to as a retroverted dens.

The C2 posterior arch fuses in the midline by the age of 3 years and with body of the axis between the ages of 3 and 6 (Gore et al. 2011). Failure of fusion of the posterior arch has been described. Additionally, there are case reports of laminar variants of the axis. Sakaura et al. (2013) described a bilaterally separated lamina that at age 68 resulted in cervical myelopathy (Fig. 3.2). Defects or spina bifida of the C2 is rare but may be clinically relevant.

An accessory bursa located above the odontoid process is known as the bursa of Trolard.

Uncinate process

The uncinate processes are superior projections from the C3 to C7 vertebral bodies that articulate with the superior vertebral body at its echancrure (anvil) (Tubbs et al. 2012). Tubbs et al. (2012) performed a morphometric analysis of 40 adult skeletons and classified the uncinate process based on three types of variants. A Type I uncinate process (80%) does not encroach on the adjacent intervertebral foramen. Type II processes (12%) project in a superior posterolateral direction to decrease the foraminal diameter, while Type III uncinate processes (8%) lack incline of projection but are sufficiently high-riding to create foraminal encroachment (Tubbs et al. 2012). The uncinate process may be underdeveloped or absent at the sixth and seventh cervical vertebrae.

Transverse foramen

The transverse foramina (TF) are paired and usually contain the vertebral artery. The vertebral artery typically enters the TF at C6 in 95.6% of individuals (Wakao et al. 2013). The actual morphology of the TF is dependent on the presence of a vertebral artery at that level. Wakao et al. (2013) found that in patients with a vertebral artery that enters at C7, the C7 TF will be wider and correspondingly the pedicle will be smaller. Instrumentation of the C7 pedicle therefore requires an appreciation of the variant anatomy that can occur in this region.

The morphology of the transverse foramen can be highly variable (Taitz et al. 1978). Taitz et al. (1978) developed a five-tiered grading system to quantify both the morphology and orientation of the TF. The atlas had the highest mean diameter of the TF while C7 had the lowest. Absent (0.8%), duplicate (5.2%),

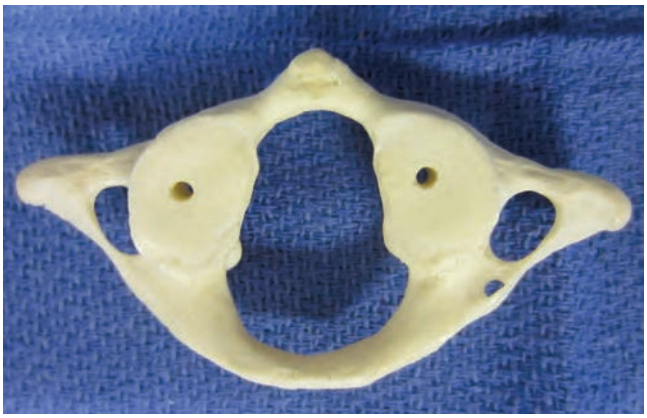

Figure 3.7 Accessory foramen of the transverse foramen. Note the defects in the central part of the articular processes are artifacts from postmortem articulation.

and triplicate (0.2%) foramina have also been observed (Taitz et al. 1978). Osteophytic encroachment of the TF is potentially a sequel of age-related spondylosis, but congenitally ossified TF have been described.

A posteriorly located accessory transverse foramen has a documented incidence of approximately 1% (Murlimanju et al. 2011). These foramen are typically smaller and they may be unilateral or bilateral. According to Murlimanju et al. (2011) only 0.3% of vertebrae exhibit three accessory transverse foramina (Fig. 3.7).

Spinous processes

The spinous processes of C2, C3, C4, and C5 are typically bifid. The C6 and C7 spinous process are occasionally bifid with two small lateral tubercles. Some individuals have cervical spines with nonbifid spinous processes. Only 9% of individuals have a nonbifid C2 spinous process while 1% have a bifid C7. Duray et al. (1999) performed a logistic regression analysis based on race and found that Caucasians have a statistically significant higher rate of bifid spinous processes, especially at C3 and C4 (Duray et al. 1999).

The vertebra prominens, the palpable prominence on the dorsum of the neck, is most commonly the C7 spinous process (70%). C6 (20%) and T1 (10%) may also be the most prominent spinous process.

Klippel–Feil syndrome

Neurologist Maurice Klippel and his resident Andre Feil described a case in which there was a congenital absence of cervical vertebrae. The thoracic cage was felt to be arising from the base of the cranium (Klippel and Feil 1975). The patient's autopsy revealed a fusion of cervical vertebrae that they labeled a cervicodorsal mass.

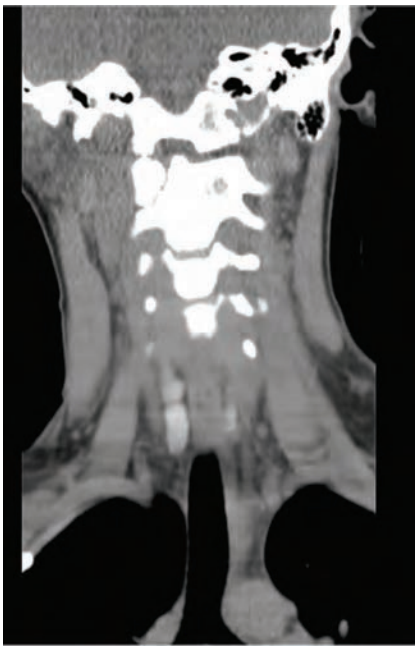

Figure 3.8 3D CT noting a fusion abnormality between C1 and C2. Also note the hemivertebra on the right side.

Congenital fusion of two or more cervical vertebrae is also commonly seen and is referred to as Klippel–Feil syndrome (Fig. 3.8). The classic triad of Klippel–Feil syndrome includes a short neck, low posterior hairline, and limited range of cervical motion. The majority of patients with a congenital fusion of the cervical vertebrae have a normal appearance and fewer than 50% exhibit this classic triad (Clark 2005).

Eight cervical vertebrae have been reported (Lane 1886). The laminae of the inferior cervical vertebrae frequently exhibit dorsally distinct tubercles from which fasciculi of the multifidus muscle arise. The nuchal ligament may have small ossicles associated with it. Segmentation anomalies of the cervical spine may result in the so-called butterfly vertebra.

Cervical ribs

Cervical ribs (discussed in more detail in Chapter 11) are present in approximately 2% of the population. These ribs are typically bilateral at the C7 vertebral level (40.3%). Demographically they occur more commonly in women (2.8%) and African-Americans (70.1%) (Viertel et al. 2012). Cervical ribs may represent a clinically insignificant anatomic variant although 10% of patients will develop or suffer from thoracic outlet syndrome.

The body of a cervical vertebra can be cleft in the sagittal or frontal plane. The pedicles may not be attached to bone anteriorly or posteriorly. The facet joints may be rotated.

References

Bagnall KM, Higgins SJ, Sanders EJ. 1988. The contribution made by a single somite to the vertebral column: experimental evidence in support of resegmentation using the chick-quail chimaera model. *Development* 103: 69–85.

Bergman RA. 1988. *Compendium of Human Anatomic Variation: Text, Atlas, and World Literature*. Baltimore: Urban & Schwarzenberg.

Billmann F, Le Minor JM, Steinwachs M. 2007. Bipartition of the superior articular facets of the first cervical vertebra (atlas or C1): A human variant probably specific among primates. *Anat Anz* 189: 79–85.

Cattell HS, Filtzer DL. 1965. Pseudosubluxation and other normal variations in the cervical spine in children. A study of one hundred and sixty children. *J Bone Joint Surg Am* 47: 1295–1309.

Christ B, Schmidt C, Huang R, Wilting J, Brand-Saberi B. 1998. Segmentation of the vertebrate body. *Anat Embryol (Berl)* 197: 1–8.

Clark CR, CSRSEC (eds) 2005. *The Cervical Spine, fourth edition*. Philadelphia: Lippincott Williams & Wilkins.

Devi BI, Shenoy SN, Panigrahi MK, Chandramouli BA, Das BS, Jayakumar PN. 1997. Anomaly of arch of atlas: A rare cause of symptomatic canal stenosis in children. *Pediatr Neurosurg* 26: 214–218.

Dubrulle J, Pourquié O. 2004. Coupling segmentation to axis formation. *Development* 131: 5783–5793.

Dunlap JP, Morris M, Thompson RG. 1958. Cervical-spine injuries in children. *J Bone Joint Surg Am* 40: 681–686.

Duray SM, Morter HB, Smith FJ. 1999. Morphological variation in cervical spinous processes: Potential applications in the forensic identification of race from the skeleton. *J Forensic Sci* 44: 937–944.

Fesmire FM, Luten RC. 1989. The pediatric cervical spine: Developmental anatomy and clinical aspects. *J Emerg Med* 7: 133–142.

Gore PA, Mortazavi M, Chang S, Tubbs RS, Theodore N. 2011. Pediatric cervical spine injuries: A comprehensive review. *Childs Nerv Syst* 27: 705–717.

Hu Y, Ma W, Xu R. 2009. Transoral osteosynthesis C1 as a function-preserving option in the treatment of bipartite atlas deformity: A case report. *Spine* 34: 418–421.

Jans C, Mahieu G, Van Riet R. 2009. Bipartite atlas mimicking traumatic atlantoaxial instability following a rugby tackle. *BMJ Case Reports* 2009.

Junewick JJ, Chin MS, Meesa IR, Ghori S, Boynton SJ, Luttenton CR. 2011. Ossification patterns of the atlas vertebra. *AJR Am J Roentgenol* 197: 1229–1234.

Karwacki GM, Schneider JF. 2012. Normal ossification patterns of atlas and axis: A CT study. *AJNR Am J Neuroradiol* 33: 1882–1887.

Kaushal P. 2010. Epitransverse process: A rare a rare outgrowth from atlas vertebra. *IJAV* 3: 108–109.

Klimo P Jr, Kan P, Rao G, Apfelbaum R, Brockmeyer D. 2008. Os odontoideum: Presentation, diagnosis, and treatment in a series of 78 patients. *J Neurosurg Spine* 9: 332–342.

Klippel M, Feil A. 1975. The classic: A case of absence of cervical vertebrae with the thoracic cage rising to the base of the cranium (cervical thoracic cage). *Clin Orthop* 109: 3–8.

Krishnamurthy A, Nayak SR, Khan S, Prabhu LV, Ramanathan LA, Ganesh Kumar C, Prasad Sinha A. 2007. Arcuate foramen of atlas: Incidence, phylogenetic and clinical significance. *Rom J Morphol Embryol* 48: 263–266.

Lane WA. 1886. Some variations in the human skeleton. *J Anat Physiol* 20: 388–404.

Lang J. 1992. Suboccipital Approach (and Other Approaches) to Aneurysms at the Craniocervical Junction. Stuttgart: Schattauer Verlagsgesellschaft.

Liang CL, Lui CC, Lu K, Lee TC, Chen HJ. 2001. Atlantoaxial stability in ossiculum terminale. Case report. *J Neurosurg* 95: 119–121.

Lustrin ES, Karakas SP, Ortiz AO, Cinnamon J, Castillo M, Vaheesan K, Brown JH, Diamond AS, Black K, Singh S. 2003. Pediatric cervical spine: Normal anatomy, variants, and trauma. *Radiographics* 23: 539–560.

Mallo M, Vinagre T, Carapuço M. 2009. The road to the vertebral formula. *Int J Dev Biol* 53: 1469–1481.

Murlimanju BV, Prabhu LV, Shilpa K, Rai R, Dhananjaya KVN, Jiji PJ. 2011. Accessory transverse foramina in the cervical spine: Incidence, embryological basis, morphology and surgical importance. *Turk Neurosurg* 21: 384–387.

Osti M, Philipp H, Meusburger B, Benedetto KP. 2006. Os odontoideum with bipartite atlas and segmental instability: A case report. *Eur Spine J* 15: 564–567.

Petraglia AL, Childs SM, Walker CT, Hogg J, Bailes JE, Lively MW. 2012. Bipartite atlas in a collegiate football player: Not necessarily a contraindication for return-to-play: A case report and review of the literature. *Surg Neurol Int* 3: 126.

Sakaura H, Yasui Y, Miwa T, Yamashita T, Ohzono K, Ohwada T. 2013. Cervical myelopathy caused by invagination of anomalous lamina of the axis: Case report. *J Neurosurg Spine* 19: 694–696.

Shaw M, Burnett H, Wilson A, Chan O. 1999. Pseudosubluxation of C2 on C3 in polytraumatized children: prevalence and significance. *Clin Radiol* 54: 377–380.

Taitz C, Nathan H, Arensburg B. 1978. Anatomical observations of the foramina transversaria. *J Neurol Neurosurg Psychiatry* 41: 170–176.

Thavarajah D, McKenna P. 2012. Congenital absence of the anterior arch of the atlas: A normal variant. *Ann R Coll Surg Engl* 94: 208–209.

Townsend EH Jr, Rowe ML. 1952. Mobility of the upper cervical spine in health and disease. *Pediatrics* 10: 567–574.

Tubbs RS, Rompala OJ, Verma K, Mortazavi MM, Benninger B, Loukas M, Chambers MR. 2012. Analysis of the uncinate processes of the cervical spine: An anatomical study. *J Neurosurg Spine* 16: 402–407.

Viertel VG, Intrapiromkul J, Maluf F, Patel NV, Zheng W, Alluwaimi F, Walden MJ, Belzberg A, Yousem DM. 2012. Cervical ribs: A common variant overlooked in CT imaging. *AJNR Am J Neuroradiol* 33: 2191–2194.

Wakao N, Takeuchi M, Kamiya M, Aoyama M, Hirasawa A, Sato K, Takayasu M. 2013. Variance of cervical vertebral artery measured by CT angiography and its influence on C7 pedicle anatomy. *Spine* 39: 228–232.

Wang JC, Nuccion SL, Feighan JE, Cohen B, Dorey FJ, Scoles PV. 2001. Growth and development of the pediatric cervical spine documented radiographically. *J Bone Joint Surg Am* 83: 1212–1218.

4 Thoracic vertebrae

Benjamin J. Ditty, Nidal B. Omar and Mark N. Hadley
University of Alabama at Birmingham, Birmingham, Alabama, United States

The thoracic spine comprises the longest segment of the human vertebral column. Unique to the thoracic spine are costovertebral articulations, which provide stability to thoracic vertebrae and are vital for the structural and functional integrity of the entire thorax. The tradeoff for the increased stability of the thoracic spinal column is that it affords less mobility than the cervical or lumbar spinal segments. However, it does play an important role in motions such as lateral flexion, axial rotation (more so in the upper thoracic vertebral segments), and flexion/extension (predominantly in lower thoracic vertebral segments) (Dvořák et al. 2008).

This chapter describes variations in the anatomy of human thoracic spinal vertebrae with differing degrees of clinical relevance. Although thoracic vertebrae tend to be relatively more uniform than cervical vertebrae, a number of morphologic variations have been characterized.

Embryology

Development of the thoracic spinal column begins with the formation of 12 pairs of thoracic somites derived from the paraxial mesoderm beginning at 20 days of gestation (Benzel and Stillerman 1999). The ventral aspect of each somite, known as the sclerotome, will condense around the notochord and neural tube to form a mesenchymal precursor to the spinal column that will later chondrify then ossify, with the exception of the cells in the caudal region of each sclerotome which contribute to the formation of the intervertebral discs (Benzel and Stillerman 1999). The notochord eventually regresses to form the nucleus pulposus of the intervertebral discs. It may persist as the persistent chorda dorsalis. Resegmentation of vertebrae occurs as the rostral aspect of each somite articulates with the caudal aspect of the somite above it (Benzel and Stillerman 1999).

In early embryonic development, all vertebrae possess primordial costal projections and consequently have the potential for rib formation (Benzel and Stillerman 1999; Herkowitz et al. 2006). Segmental expression of *Hox* genes is thought to be the determinant of completion of rib development from thoracic vertebrae (Benzel and Stillerman 1999). In cervical and sacral vertebrae, costal precursors fuse with the embryonic transverse processes; in lumbar vertebrae, costal precursors become the mature transverse processes, fusing with mammillary processes derived from the embryonic transverse processes (Herkowitz et al. 2006).

Spinal development is a dynamic process that continues long beyond the fetal period. Secondary ossification centers develop at puberty, and complete ossification of vertebrae is not achieved until around the age of 25 (Benzel and Stillerman 1999).

Vertebral bodies

Costal articulations

While the body of the first thoracic vertebra typically bears one entire facet for articulation with the head of the first rib it may bear, on one or both sides, two demi-facets as is typical in the 2–9th thoracic vertebra. If this is the case, the articulation of the first rib is with an inferior demi-facet from the seventh cervical vertebra and a superior demi-facet from the first thoracic vertebra (Cramer and Darby 2013).

In most specimens the ninth thoracic vertebra has only superior costal facets due to the 10–12th thoracic vertebrae each possessing a pair of full facets for articulation with their respective ribs. It is not abnormal for there to also be inferior demi-facets on the 9th thoracic vertebra for costal articulation with the 10th rib, in which case the facet on the 10th thoracic vertebra will assume a semilunar shape akin to a demi-facet (Cramer and Darby 2013).

Limbus vertebra

A limbus vertebra occurs when, in an immature skeleton, a fragment of the nucleus pulposus herniates through the ring hypophysis before fusion has occurred. This results in an ossified fragment, usually at the anterior superior edge of the vertebral body. This is commonly mistaken for a fracture of the superior endplate by less-experienced radiograph interpreters (McCarron 1987).

Failure of segmentation

The process of segmentation may fail to occur in the thoracic spine. When this occurs the intervertebral disc develops

Bergman's Comprehensive Encyclopedia of Human Anatomic Variation, First Edition. Edited by R. Shane Tubbs, Mohammadali M. Shoja and Marios Loukas.

incompletely. The constellation of two partially fused adjacent thoracic vertebral bodies with a small, dysmorphic, incomplete disc space should not be confused with the appearance of inflammatory spondylodiscitis (Keats and Anderson 2012). Vertebral cleavage can occur in the sagittal or frontal planes.

Butterfly vertebra

Butterfly vertebra within the thoracic spinal column, also referred to as anterior rachischisis or somatoschisis, are caused by a congenital defect in which the notochord persists in the developing spine. When this occurs, the vertebral body exists in two (usually equal) triangular-shaped halves, which give the affected vertebra the appearance of a butterfly on a frontal radiograph. These halves may also be referred to as hemivertebrae (Garcia et al. 1993). Hemivertebrae consist of the triangular vertebral body, a pedicle and transverse process, superior and inferior articular processes, and half of a lamina with half of a spinous process (Kim et al. 2008). In most cases of butterfly vertebra, the two hemivertebrae are ankylosed to the adjacent superior and inferior thoracic vertebral bodies (Garcia et al. 1993).

The body of the vertebra may fail to form and the thoracic bodies, in general, vary greatly in their shape. The aortic impression on the anterior aspect of the thoracic vertebrae may be indemonstrable (Frazer 1933).

The body of the second thoracic vertebra usually exhibits an identifying tubercle marking the attachment of a fasciculus of the medial portion of the longus colli muscle.

Pedicles

There is significant variability in pedicle shape and size between individuals and between thoracic vertebral levels within individuals (Panjabi et al. 1997). The pedicles may not be fused to bone anteriorly or posteriorly or may be absent. The superior intervertebral notch may be very shallow or absent (Frazer 1933).

Upper

In one study, three out of five pairs of adult T2 vertebral pedicles viewed in cross-section perpendicular to the long axis were teardrop-shaped posteriorly transitioning to a kidney shape anteriorly, with the convexity oriented medially. Variations in upper thoracic pedicle morphology were identified in which the superior edges of the posterior portions of the pedicles formed a narrow ridge while the anterior portions were square. In yet another observed variation, the pedicles were oval to teardrop-shaped throughout (Panjabi et al. 1997).

Middle

Middle thoracic vertebral pedicles (levels T6 and T7) tended to demonstrate greater uniformity than upper thoracic vertebral pedicles with a narrow teardrop or hybrid kidney/teardrop shape. Again, the convexity of the pedicles was directed medially. At mid-thoracic vertebral levels, the only remarkable variant identified was asymmetric pedicle length in one specimen (Panjabi et al. 1997).

Lower

In the lower thoracic spine, at vertebral levels T10 and T11, the pedicles are shaped similarly to those in the middle thoracic spine. At these lower thoracic, more weight-bearing levels, thoracic pedicle shape differs most dramatically near the vertebral body where pedicles can be relatively rectangular, oval, teardrop, or kidney shaped. Lower thoracic pedicle size variations are common. Lower thoracic pedicles may have the largest pedicle diameter within the thoracic spine or may be so small that the medial and lateral cortical surfaces of the pedicles are in contact with one another without intervening cancellous bone. Posteriorly, nearly all the pedicles in the lower thoracic spine take on a teardrop- or kidney-shaped appearance (Panjabi et al. 1997).

Facets

In individuals for whom the 12th pair of ribs is absent, it is common for the 12th thoracic vertebra to assume a morphology similar to a lumbar vertebra, with its inferior articular facet surface oriented more in the sagittal plane (Singer et al. 1988). The transition from thoracic-type facet articular projections, in which the articular surfaces are coronally oriented, to the lumbar-type facet articular projections, in which they are oriented in the sagittal plane, typically occurs at the level of T11 (Cramer and Darby 2013). The 10th facet is usually small but may also be absent (Frazer 1933).

When lumbar-type facet articular projections occur in the thoracic spine, they may occur unilaterally rather than bilaterally, with resulting articular asymmetry. These anatomic variations may be clinically relevant in the event of potential thoracic pedicle screw fixation. Surgeons must assess for these potential anatomic discrepancies prior to proceeding with surgical internal fixation and fusion.

Transverse processes

A transverse foramen through T1 has been described by Turner (1883) and Duckworth (1911). The transverse processes of the thoracic vertebrae may fail to ossify, resulting in an appearance that could be confused with a fracture of the tip of the transverse process on a radiograph. This was initially described in 1913 by Rhys, who described six cases in which radiographic evidence of separation or displacement of the distal transverse process did not correlate with an injury mechanism or was not preceded by an injury at all (Rhys 1913). Infrequently, articulations may form between adjacent transverse processes within the thoracic spine as described by Keats and Anderson (2012).

At the T10 vertebral level the transverse process may not articulate with the 10th rib (Cunningham 1903; Gray and

Johnston 1938; Morris and Anson 1966; Gehweiler et al. 1980; Cramer and Darby 2013).

Variability in the morphology of the transverse processes of the T10, T11, and T12 vertebrae has been described. At these levels the transverse processes may possess superior, inferior, and lateral tubercles which correspond to the mammillary and accessory tubercles and transverse processes typical of a lumbar vertebra (Cramer and Darby 2013).

The body of the second thoracic vertebra usually exhibits an identifying tubercle marking the attachment of a fasciculus of the medial portion of the longus colli muscle.

Laminae and spinous processes

The apophysis at the tip of a thoracic vertebral spinous process may fail to unify. This anomaly has no structural or functional significance but could be mistaken for a fracture on thoracic spinal imaging (Keats and Anderson 2012). The spinous process can be absent with the laminae uniting across the midline.

Spina bifida occulta may occur at any level in the thoracic spinal column. It may result in a double spinous process. In other cases it may create the appearance of a double spinous process, which is not to be confused with a bifid spinous process (Keats and Anderson 2012).

The tip of an individual thoracic spinous process may be much larger than those adjacent to it. When this occurs it may suggest a mass on thoracic spinal imaging (Keats and Anderson 2012).

Although fusion of two or more vertebrae is most often seen in the cervical spine, the thoracic region can also be affected.

References

Benzel EC, Stillerman CB (eds). 1999. *The Thoracic Spine*. London: Taylor & Francis.

Cramer GD, Darby SA. 2013. *Clinical Anatomy of the Spine, Spinal Cord, and ANS*. St Louis: Elsevier Health Sciences.

Cunningham DJ. 1903. *Text-book of Anatomy*. New York: William Wood.

Duckworth WL. 1911. Report on an abnormal first thoracic vertebra. *J Anat Physiol* 45: 232–238.

Dvořák J, Dvořák V, Gilliar W, Schneider W, Spring H, Tritschler T. 2008. *Musculoskeletal Manual Medicine: Diagnosis and Treatment*. New York: Thieme.

Frazer JE. 1933. *The Anatomy of the Human Skeleton*. London: J & A Churchill.

Garcia F, Florez MT, Conejero JA. 1993. A butterfly vertebra or a wedge fracture? *Int Orthop* 17: 7–10.

Gehweiler JA, Osborne RL, Becker RF. 1980. *The Radiology of Vertebral Trauma*. Philadelphia: Saunders Elsevier.

Gray H, Johnston TB. 1938. *Gray's Anatomy: Descriptive and Applied*, 27th edition. London: Longmans, Green.

Herkowitz HN, Rothman RH, Simeone FA. 2006. *Rothman-Simeone: The Spine*, fifth edition. Philadelphia: Saunders Elsevier.

Keats TE, Anderson MW. 2012. *Atlas of Normal Roentgen Variants that May Simulate Disease*, ninth edition. Philadelphia: Saunders Elsevier.

Kim DH, Betz RR, Huhn SL, Newton PO 2008. *Surgery of the Pediatric Spine*. New York: Thieme.

McCarron RF. 1987. A case of mistaken identity, limbus annulare mimics fracture. *Orthop Rev* 16: 173–175.

Morris H, Anson BJ. 1966. Morris' Human Anatomy: A Complete Systematic Treatise, 12th edition. New York: McGraw-Hill.

Panjabi MM, O'Holleran JD, Crisco JJ, Kothe R. 1997. Complexity of the thoracic spine pedicle anatomy. *Eur Spine J* 6: 19–24.

Rhys OL. 1913. Pseudo-fractures of transverse processes. *Brit Med J* 1: 1103–1104.

Singer KP, Breidahl DP, Day RE. 1988. Variations in zygapophyseal joint orientation and level of transition at the thoracolumbar junction. Preliminary survey using computed tomography. *Surg Radiol Anat* 10: 291–295.

Turner W. 1883. A first dorsal vertebra, with a foramen at the root of the transverse process. *J Anat Physiol* 17: 255–256.

5 Lumbar vertebrae

Ross Dawkins and Mark N. Hadley
University of Alabama at Birmingham, Birmingham, Alabama, United States

Embryology

An educated discussion on the anatomic variations of the lumbar requires an understanding not only of the normal anatomy, but more importantly of how that anatomy came to exist. We therefore begin this chapter with a review of the embryological development of the human spine.

One might say that gastrulation is the starting point for formation of the nervous system. It is the stage at which a groove known as the primitive streak develops on the epiblast surface of the bilaminar disc. This streak establishes the basic anatomical concepts of the human body, including symmetry, rostral and caudal ends, and dorsal and ventral surfaces. Cells of the epiblast on either side of the primitive streak travel towards it, migrate through it, and end up between the epiblast above and the hypoblast below. These mobile cells give rise to the embryonic mesoderm and endoderm, while remaining cells of the epiblast form the ectoderm (Youmans and Winn 2011).

As the primitive streak extends forward, a collection of cells known as the primitive node, or Hensen's node, forms at one end of the streak. The primitive node defines the rostral end of the streak. A group of specialized cells migrate through the primitive node and give rise to the notochodal process. Certain cells of the notochordal process align to form the notochordal plate, which then folds to form the notochord with a central canal (Moore et al. 2013). Although our interest here focuses on the vertebral column, recall that just dorsal to the notochord is a developing neuraxis, which starts as an ectodermal invagination whose edges meet to form a neural tube. This neural tube lies directly above and runs in parallel with the notochord. Mesodermal cells migrating from the primitive streak begin to compact alongside the notochord and differentiate into three sections: paraxial, intermediate, and lateral mesoderm. The paraxial mesoderm, lying closest to the notochord on either side, segments into masses known as somites. The somites are paired and flank the notochord, developing in a craniocaudal direction. By the end of the fifth week, 42–44 pairs of somites will have formed: 4 occipital, 8 cervical, 12 thoracic, 5 lumbar, 5 sacral, and 8–10 coccygeal somite pairs (Moore et al. 2013).

Each somite differentiates into two parts: a sclerotome and a dermomyotome. The dermomyotomes will go on to form muscle cells and overlying dermis of the skin. The sclerotomes form the spinal column. During the fourth week of embryogenesis, they begin to surround both the notochord and the neural tube. As the sclerotomal mesoderm begins to condense about the notochord, the longitudinal mass of tissue begins to display segmentation. First, segmental arteries arising from the developing aorta cut bilaterally across the condensing sclerotome. Any given segmental artery will lie between two sclerotomes. A second segmentation process occurs within each sclerotome, essentially cutting the sclerotome in half. Here, the sclerotomal fissure separates a cranial portion, which is loosely packed with cells, from a caudal portion, which is densely packed. Some of the cells from the densely packed caudal portion migrate cranially towards the fissure. These cells will form the annulus fibrosus of the intervertebral disc. The nucleus pulposus develops from remnants of the notochord. As the intervertebral disc is forming, the cranial portion of the sclerotome is fusing with the caudal portion of the adjacent scleorotome to form the vertebral centrum, which further develops into the vertebral body. Vertebral bodies are therefore derived from adjacent pairs of sclerotomes, while discs are derived from within a single sclerotome (Moore et al. 2013). The vertebral centrum allows bone to continually develop around it.

Recall that some of the mesodermal cells migrate dorsally from somites and travel around the lateral and dorsal sides of the neural tube. The condensed arches of cells form the vertebral pedicles, laminae, and spinous processes. Lateral projections of the arches form transverse processes, which have been reported to have no contact with the body. Craniocaudal thickenings of the arches form the articular processes. These structures, like the vertebral bodies, receive contributions from adjacent sclerotomes. In order to complete the ring of a vertebra, the centrum and two arches must fuse together (Moore et al. 2013).

Chondrification of the mesenchymatous vertebrae begins during the sixth week of development. Signals from the notochord and neural tube induce this process (Moore et al. 2013). Ossification occurs following chondrification, after which the notochord disintegrates. There are three primary areas of

Bergman's Comprehensive Encyclopedia of Human Anatomic Variation, First Edition. Edited by R. Shane Tubbs, Mohammadali M. Shoja and Marios Loukas.

ossification, one at the centrum and one on either side of the vertebral arch (Moore et al. 2013).

During the first two years of life, the neural arch halves unite dorsally. This union first occurs in the lumbar region shortly after birth and extends cranially, reaching the cervical regions by the second year. Fusion of the neural arch to the centrum begins first in the cervical region at three years of age. This process proceeds caudally and is completed in the sacrum around seven years of age.

Anatomic variations

The lumbar vertebrae, except for the fifth, probably show fewer variations of a congenital nature than any other vertebra. That being said, there exist a number of variations in vertebral anatomy that are not specific to, but can certainly be found in, the region of the lumbar vertebrae. We discuss these in addition to those variants more pertinent to the lumbar spine.

Vertebral body defects

Congenital block vertebra, or congenital synostosis, occurs as a result of a disturbance in segmentation of the somites during development of the vertebral column (Yochum 1987). This results in fusion of adjacent vertebral bodies, with fusion of the apophyseal joint in approximately 50% of cases. While this variant is more typical of the cervical spine, it is also known to occur in the lumbar spine. In some cases the two adjacent vertebrae fuse to form a solid block of bone. More often, a remnant of the intervening vertebral disc remains. A typical block vertebra has a decreased anterior/posterior diameter. As a result of the loss of the vertebral disc space the vertebral foramina are frequently narrowed with congenital block vertebrae, but can be normally sized or enlarged (Gehweiler et al. 1980; Taylor 2000).

Sagittal cleft vertebrae occur as a result of a failure of fusion of the two halves of the vertebral body. This is somehow associated with the embryologic extension of the notochord longitudinally through the vertebral column during ossification (Hollinshead 1982). Incomplete fusion of the two lateral chondral centers of the vertebral body results in a central sagittal constriction of the vertebral body (Taylor 2000). The sagittal cleft is created by the indentation of the endplate cortices (Yochum 1987). From the frontal view the body has the appearance of two triangular masses with opposing apices, hence the term butterfly vertebrae. The development of the ununited bodies is generally symmetrical (Yochum 1987). Furthermore, the cleft results in an increase in the interpediculate distance (Yochum 1987). The body may be cleft in the frontal plane. Enlarged fissures or Hahn's clefts may be seen. These are vascular channels within the vertebral body.

Lateral hemivertebrae appear as an absence of one lateral half of the vertebral body, and develop when one of the two lateral ossification centers of the vertebral body fails to grow. The apex of the lateral hemivertebra is directed medially. Normal disc spaces are usually present above and below the affected level (Yochum 1987). However, the endplates of the adjacent vertebrae are deformed, resulting in a trapezoid shape to those vertebrae. An isolated lateral hemivertebra will result in a scoliotic deformity, with the affected vertebra being located at the apex of the scoliotic curvature (Yochum 1987). It has been hypothesized that hemivertebrae can result from a lack of vascularization to the defective side (Hollinshead 1982).

Dorsal hemivertebrae appear as an absence of the anterior half of the vertebral body. The dorsal portion of the body tapers ventrally, and fibrous tissue replaces the absent ventral portion of the body. The adjacent vertebrae may demonstrate compensatory growth and come together in the defective area of the hemivertebra. Ventral hemivertebra is also a described anomaly. Dorsal and ventral hemivertebrae are much less frequent that lateral hemivertebrae (Taylor 2000).

The limbus bone is a small, triangular bony ossicle often adjacent to the anterior superior aspect of the vertebral body (Jaeger 1988). It is believed to result from a herniation of nuclear material through a secondary ossification center for the corner of the vertebral body. This results in nonunion of the secondary ossification center, and thus the presence of a bony fragment (Yochum 1987).

Nuclear impressions are invaginations in the vertebral endplates that result from notochordal remnants. They appear as broad curvilinear depressions of the endplate. They more commonly affect the inferior, rather than superior, endplate (Jaeger 1988; Taylor 2000). On a frontal view, the impressions create paramedian curvilinear indentations, creating the appearance of a double hump. This has been referred to as Cupid's bow contour (Yochum 1987; Taylor 2000).

Another vertebral disc variant, which can be confused with a nuclear impression, is a Schmorl's node. Vertical nucleus pulposus herniations, rather than notochordal remnants, are to blame for the endplate defects of Schmorl's nodes. Radiographically, a Schmorl's node appears as a squared-off, rectangular rim of sclerosis protruding through the endplate. It can be centrally or peripherally located. This is different from the defect of nuclear impressions, in which there is a smooth, wave-like cortical surface irregularity involving nearly all of the endplate (Yochum 1987).

Vertebral arch defects

Just as the notochord influences the development of the vertebral bodies, the neural tube produces signals integral to the regulation of vertebral arch development. Disruptions in arch formation can produce clefts in numerous parts of the vertebral arch. A retrosomatic cleft is found at the junction of the pedicle and vertebral body. It results as a failure of fusion between the ossifying neural arch and centrum. A cleft may also occur more posteriorly in the body of the pedicle itself. A retroisthmic cleft occurs on the lamina, behind the pars interarticularis.

One of the most-recognized neural arch cleft defects occurs in the area of the lamina or spinous process, and is known as spina bifida. Spina bifida occulta, or rachischisis, is a defect

in ossification at the spinous process or lamina (Hollinshead 1982; Jaeger 1988). The dorsal synchondrosis between the neural arches usually fuses during the first year of life. Failure of this fusion results in the formation of a dorsal cleft involving the spinous process or lamina. The size of cleft can vary from a small midline cleft to near absence of the vertebral arch. It is most commonly found in the lumbosacral region (Jaeger 1988).

When a spina bifida occulta defect occurs at the first sacral vertebra with an elongated spinous process of the fifth lumbar vertebra, this is known as a knife clasp deformity. The long spinous process may result from a fusion of the L5 spinous process with the first sacral tubercle (Jaeger 1988; Taylor 2000). An anterior/posterior radiographic view will demonstrate with spina bifida defect at S1 with a vertical enlargement of the L5 spinous process. A lateral view will show distal enlargement of the spinous process. This entity is so named due to the pain it induces when the patient extends the lumbar spine (Yochum 1987).

Spondylolysis is a vertebral arch cleft which occurs at the pars interarticularis. This disruption of the pars can be either unilateral or bilateral. There is debate as to whether a congenital etiology exists for this entity. Spondylolisthesis is defined as an anterior displacement of a vertebral body relative to the body immediately inferior. Approximately 90% of spondylolystheses involve the fifth lumbar vertebra (Yochum 1987). There are multiple types of spondylolisthesis. Those of interest here are the types that would result from a congenital deformity, as opposed to the acquired type. Dysplastic spondylolisthesis has a congenital implication with dysplasia in the neural arch of L5 or the sacrum, allowing anterior displacement of the former relative to the latter. If spondylolysis affects the bilateral pars interarticularis, the affected vertebra may become displaced. This is a subtype of isthmic spondylolisthesis. Some have stated that isthmic spondylolisthesis can result from poorly formed pars interarticularis (Youmans and Winn 2011). Again, given that a debate exists as to the possibility of a congenital etiology for sponylolysis, it is also unclear whether isthmic spondylolisthesis can be classified as a congenital variant. Of note, a higher incidence of spondylolysis and spondylolisthesis is associated with L5 spina bifida occulta (Taylor 2000).

Split cord malformation is a congenital anomaly where a longitudinal diastasis divides the spinal cord or cauda equina, depending on a thoracic or lumbar location. The division consists of either an osseous, cartilaginous, or fibrous band. Typically, there is an increased interpediculate distance. A total of 50% of cases are associated with other vertebral anomalies such as scoliosis, spina bifida occulta, and tethering of the spinal cord (Yochum 1987; Taylor 2000).

Agenesis of a vertebral pedicle is more likely to occur in the cervical spine, but has been documented in the lumbar region. Failure of development of the chondral center responsible for one side of the neural arch results in a unilaterally absent pedicle. The superior articular process and transverse process at the affected level may be dysplastic. In addition, the contralateral pedicle is often hyperplastic, which occurs more frequently in the lumbar spine opposed to the cervical spine (Yochum 1987).

If the chondral center responsible for the articular process fails to develop, then the rare entity of articular process agenesis occurs. The most common location is the inferior L5 articular process. In the place of the articular process is a nonossified, cartilaginous, or fibrous analogue (Jaeger 1988; Taylor 2000).

Nonfusion of secondary centers of ossification is known to occur in the lumbar vertebrae. One common site is the apophysis of the transverse process of the first lumbar vertebra. Another nonfusion site, which typically occurs in the lumbar region, is the inferior articular process apophysis. Found here are joint surfaces covered with cartilage. These often occur around the third lumbar vertebra. A triangular bony ossicle is found at the tip of the inferior articular process, referred to as Oppenheimer's ossicle (Jaeger 1988; Taylor 2000). A similar entity in the superior articular process is much less common (Jaeger 1988).

Variation in orientation of lumbosacral facet joints is known as tropism. The L1–2 to L4–5 facet joints are oriented in the sagittal plane. L5–S1 facet joints are oriented in the coronal plane. Tropism occurs when this convention is broken for either the right or left apophyseal joint at a given level. This most commonly occurs at the L4–5 and L5–S1 levels. On frontal radiographic views, normal lumbar spine facet joints are visible as linear radiolucencies between the superior and inferior facet. Tropism presents as an absence of the radiolucency on the affected side (Yochum 1987; Taylor 2000).

Rudimentary lumbar rib

The transverse processes in the lumbar spine are actually homologs of the ribs. Ribs of the lumbar ribs are actually more common that ribs of the cervical vertebrae (C7). The accessory process, a small tubercle projecting form the posterior surface of the transverse process medially, is the rudimentary true transverse process in that it serves as an attachment for spinal muscles along with the mammillary process on the superior and lateral aspect of the superior articular facet (Jinkins 2000). Rarely, an accessory process can be congenitally absent. This occurs more frequently in the fifth lumbar vertebra (Hollinshead 1982; Bergman et al. 1984). In contrast to an absent accessory process, a styloid process is defined as an elongated accessory process, exceeding a length of 3–5 mm. (Bergman et al. 1984). Occasionally, the mammillary and accessory processes are united by a bony bridge forming a foramen behind the transverse process. Variant supernumerary tubercles located lateral to the mammillary tubercle are known as the tubercle of Staurenghi.

A more common variation in this region of a lumbar vertebra is the presence of a rudimentary rib (gorilla rib) at the first lumbar vertebra, representing a congenital anomaly of the transverse process. The rib unites with the ventral surface of the transverse process or the tip of a short transverse process (Bergman et al. 1984). A transverse foramen may be present in the lumbar region, especially in L1 and L5.

Lumbosacral transitional vertebrae

Of all the vertebral transitional zones, the most commonly involved with anatomic variations is the lumbosacral. The typical human spine contains 24 presacral vertebrae. The 24th presacral vertebra, commonly identified as L5, may be partially or completely incorporated with the sacrum, either unilaterally or bilaterally. This is termed sacralization of L5 (Skinner 1927). Conversely, the first sacral vertebra, S1, can take on characteristics of a lumbar vertebra, including articulation rather than fusion with the remainder of the sacrum, lumbar-type facet joints, and a squared appearance in the sagittal plane. This is termed lumbarization of S1. Considered together, these variations are often referred to as a lumbosacral transitional vertebra (LSTV). The reported prevalence of LSTV falls within the range 4–30% (Konin and Walz 2010). There may be just four lumbar vertebrae in the absence of any fusion abnormalities.

There are varying degrees of sacralization of the fifth lumbar vertebra (O'Connor 1934). Castellvi et al. (1984) described a radiographic classification system identifying four types of LSTVs on the basis of morphologic characteristics as follows.

- Type I: unilateral (Ia) or bilateral (Ib) dysplastic transverse process, measuring at least 19 mm in width in the craniocaudad dimension.
- Type II: incomplete unilateral (IIa) or bilateral (IIb) lumbarization/sacralization with an enlarged transverse process that has a diarthrodial joint between itself and the sacrum.
- Type III: unilateral (IIIa) or bilateral (IIIb) lumbarization/sacralization with complete osseous fusion of the transverse process to the sacrum.
- Type IV: unilateral type II transition with a type III on the contralateral side (Castellvi et al. 1984).

Other characteristics of LSTV include a decreased disc height between the lumbar transitional vertebra and the sacrum as compared to a normal L5–S1 disc. In fact, this space may be completely devoid of any disc material. Conversely, when a lumbarized S1 is present, the S1–S2 disc height is greater than the typical rudimentary disc present in a normal spine (Nicholson et al. 1988). In addition to the disc space, the vertebral body displays morphologic changes with LSTV. With sacralization of L5, the lowest lumbar segment develops a wedged shaped. With lumbarization of S1, the highest sacral segment develops a squared appearance (Wigh and Anthony 1981). Finally, the facet joints of the transition point must be considered. With a sacralized L5 the facet joints are typically hypoplastic, if not all together nonexistent with complete fusion of L5–S1. With a lumbarized S1, S1–S2 facet joints can be identified, whereas a typical S1–S2 segment has osseous fusion (Konin and Walz 2010).

Transitional vertebrae often have enlarged transverse processes and may form a joint with the lateral mass of the sacrum. Such joints are termed assimilation joints.

References

Bergman RA, Thompson SA, Afifi AK. 1984. *Catalog of Human Variation*. Baltimore: Urban & Schwarzenberg.

Castellvi AE, Goldstein LA, Chan DP. 1984. Lumbosacral transitional vertebrae and their relationship with lumbar extradural defects. *Spine* 9: 493–495.

Gehweiler JA, Osborne RL, Becker RF. 1980. *The Radiology of Vertebral Trauma*. Philadelphia: Saunders Elsevier.

Hollinshead WH. 1982. *Anatomy for Surgeons*. Philadelphia: Harper & Row.

Jaeger SA. 1988. *Atlas of Radiographic Positioning: Normal Anatomy and Developmental Variants*. Norwalk: Appleton & Lange.

Jinkins JR. 2000. *Atlas of Neuroradiologic Embryology, Anatomy, and Variants*. Philadelphia: Lippincott Williams & Wilkins.

Konin GP, Walz DM. 2010. Lumbosacral transitional vertebrae: Classification, imaging findings, and clinical relevance. *Am J Neuroradiol* 31: 1778–1786.

Moore KL, Persaud TVN, Torchia MG. 2013. *The Developing Human: Clinically Oriented Embryology*. Philadelphia: Saunders.

Nicholson AA, Roberts GM, Williams LA. 1988. The measured height of the lumbosacral disc in patients with and without transitional vertebrae. *Brit J Radiol* 61: 454–455.

O'Connor DS. 1934. Anatomical variations in the fifth lumbar vertebra as factors in low-back pain. *Yale J Biol Med* 7: 147–150.

Skinner EH. 1927. Anatomical and postural variations of the lumbosacral spine. *Radiology* 9: 451–452.

Taylor JAM. 2000. *Skeletal Imaging: Atlas of the Spine and Extremities*. Philadelphia: Saunders.

Wigh RE, Anthony Jr RE. 1981. Transitional lumbosacral discs. Probability of herniation. *Spine* 6: 168–171.

Yochum TR. 1987. *Essentials of Skeletal Radiology*. Baltimore: Williams & Wilkins.

Youmans JR, Winn. 2011. *Youmans Neurological Surgery*. Philadelphia: Saunders Elsevier.

6 Sacrococcygeal vertebrae

R. Shane Tubbs[1] and Marios Loukas[2]
[1]Seattle Science Foundation, Seattle, Washington, USA
St George's University, School of Medicine, St Georges, Grenada
University of Dundee, Dundee, UK
[2]St. George's University, School of Medicine, St. Georges, Grenada

The sacrum and coccyx may be absent and the sacroccygeal intervertebral disc can be ossified (Zeligs 1940). Absence of the sacrum and coccyx, in part or complete, may be a part of the caudal regression syndrome. The coccyx may be duplicated (Mares and Bar-Ziv 1981).

The number of vertebrae in the sacrum may be increased by fusion of the first coccygeal, by (less often) addition of the last (fifth) lumbar (sacralization) (Fig. 6.1a, b), or by addition of both the last lumbar and first coccygeal vertebrae. The sacrum may be composed of six true sacral vertebrae. Although the cervical spine is the most consistent in having 7 vertebrae, the coccyx is the most variable. Ossification of the sacrococcygeal ligaments may result in a bony foramen of the fifth sacral nerves.

The number may be reduced to four by the "lumbarization" of the first sacral vertebra. In one study of 631 bodies, the sacrum was composed of five vertebrae in 77%, six in 21.7%, four in 1%, and seven in 0.2%. The lumbosacral junction is occasionally composed of a vertebra with characteristics of a lumbar vertebra on one side and a sacral on the other (so-called hemilumbarization or hemisacralization).

The articular surface of the sacrum may extend variably, over no more than the first two vertebrae or to the fourth sacral vertebra. Accessory articular facets may occur on the lateral sacral crest at the level of the first or second dorsal sacral foramen; these have been found to be unpaired or bilateral and to articulate with appropriate facets on the ilium. The sacrum may be malformed and take on the so-called scimitar appearance.

The sacral canal may be open dorsally because of failure of laminar fusion. Singh (2012) as did Smith (1902) (Fig. 6.2) reported a foramen through the ala and into the sacral canal. Fusion of the coccyx and sacrum occurs more often and earlier in males.

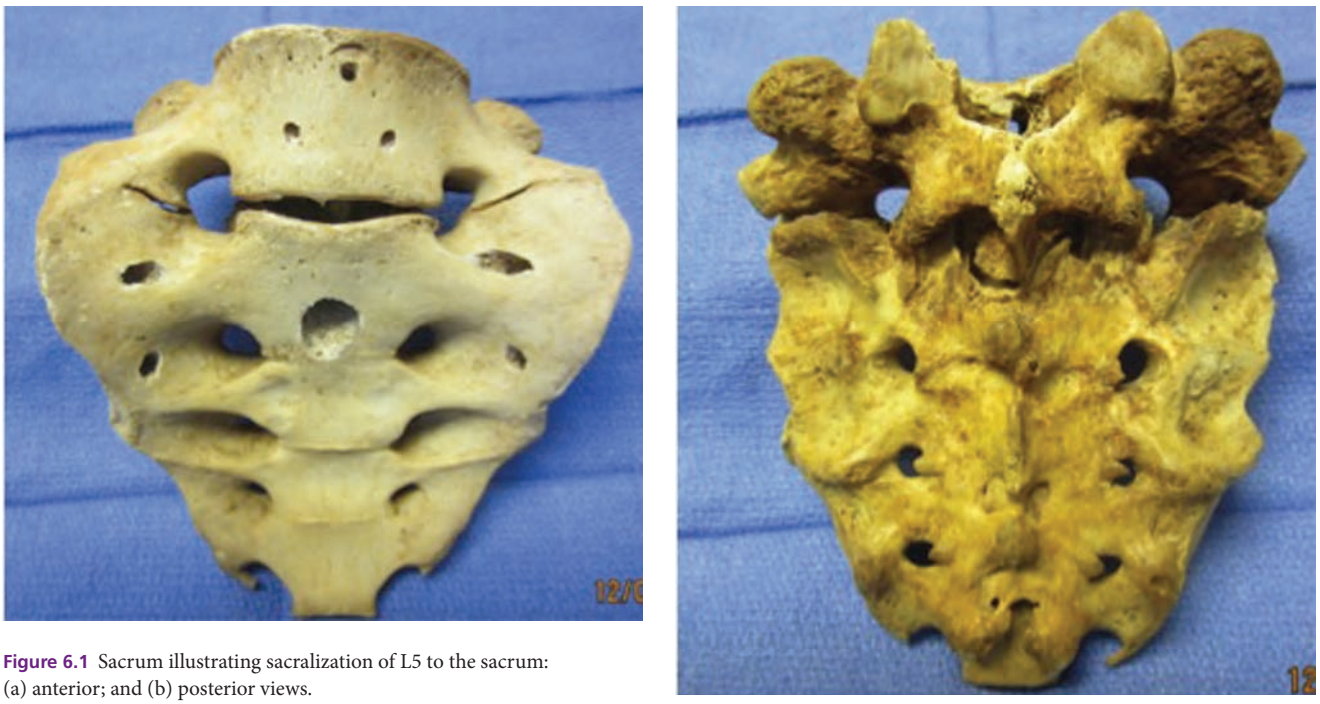

Figure 6.1 Sacrum illustrating sacralization of L5 to the sacrum: (a) anterior; and (b) posterior views.

Bergman's Comprehensive Encyclopedia of Human Anatomic Variation, First Edition. Edited by R. Shane Tubbs, Mohammadali M. Shoja and Marios Loukas.

Figure 6.2 Variant foramen through the superior aspect of the right sacrum.

Source: Smith (1902). Reproduced with permission from John Wiley & Sons.

The subdural and subarachnoid spaces extend into the sacral canal as far as the middle third of the body of the second sacral vertebra; however, in 46% of 56 cadavers, these spaces extend caudal to this level.

The coccyx may be very short or elongated. If the coccyx is "sacralized" then five sacral foramina may be present (Singh 2011). Fusion of the coccyx and sacrum takes place less often and later in life in the female than in the male.

Ribs may be associated with the sacrum or coccyx (Mares and Bar-Ziv 1981; Pais et al. 1978; Rashid et al. 2008). The development of the ribs reaches their full development in the thoracic region, whereas normally in the other parts of the spine the costal elements fuse with the lateral or transverse processes during weeks 4–12 of development. Any defect in fusion may result in a supernumerary rib (Pais et al. 1978).

References

Mares AJ, Bar-Ziv J. 1981. Sacral (pelvic) "rib" or coccygeal duplication? *Z Kinderchir* 34: 72–76.

Pais MJ, Levine A, Pais SO. 1978. Coccygeal ribs: development and appearance in two cases. *Am J Roentgenol* 131: 164–166.

Rashid M, Khalid M, Malik N. 2008. Sacral rib: a rare congenital anomaly. *Acta Orthop Belg* 74: 429–431.

Singh R. 2011. Sacrum with five pairs of sacral foramina. *IJAV* 4: 139–141.

Singh R. 2012. A new foramen on posterior aspect of ala of first sacral vertebra. *IJAV* 5: 29–31.

Smith EB. 1902. Two rare vertebral anomalies. *J Anat Physiol* 36: 372–374.

Zeligs IM. 1940. Congenital absence of the sacrum. *Arch Surg* 41: 1220–1228.

Further reading

Anderson RJ. 1883. Observations on the diameters of human vertebrae in different regions. *J Anat Physiol* 17: 341–344.

Armstrong JR, Crisp EJ, Freedman B, Gillespie HW, Golding FC, Jackson H, Lloyd K. 1950. Discussion on the significance of congenital abnormalities of the lumbosacral region. *Proc R Soc Med* 43: 635–640.

Badgley CE. 1941. The articular facets in relation to low-back pain and sciatic radiation. *J Bone Joint Surg* 23: 481–496.

Barton PN. 1948 The significance of anatomical defects of the lower spine. *Industr Med* 17: 37–40.

Blumel J, Evans EB, Eggers GWN. 1959. Partial and complete agenesis or malformation of the sacrum with associated anomalies. *J Bone Joint Surg (Am)* 41: 497–518.

Boucher B. 1957. Sex differences in the foetal pelvis. *Am J Phys Anthropol NS* 15: 581–600.

Brailsford JF. 1928/29. Deformities of the lumbosacral region of the spine. *Brit J Surg* 16: 562–627.

Colcher AE, Hursh AMW. 1952. Pre-employment low-back x-ray survey. A review of 1,500 cases. *Indstr Med* 21: 319–321.

Danforth MS, Wilson PD. 1925. The anatomy of the lumbosacral region in relation to sciatic pain. *J Bone Joint Surg* 7: 109–160.

Dassel PM. 1961. Agenesis of the sacrum and coccyx. *Am J Roentgenol* 85: 697–700.

Del Duca V, Davis EV, Barroway JN. 1951. Congenital absence of the sacrum and coccyx. *J. Bone Joint Surg (Am)* 33: 248–253.

Derry DE. 1911. Note on accessory articular facets between the sacrum and Ilium, and their significance. *J Anat Physiol* 45: 202–210.

Ehara S, El-Khoury GY, Bergman RA. 1988. The accessory sacroiliac joint. A common variation. *Am J Roentgenol* 150: 857–859.

Fawcett E. 1907. On the complete ossification of the human sacrum. *Anat Anz* 30: 414–421.

Fawcett E. 1937/38. The sexing of the human sacrum. *J Anat* 72: 633.

Freedman B. 1949/50. Congenital absence of the sacrum and coccyx. Report of a case and review of the literature. *Brit J Surg* 37: 299–303.

Gillespie HW. 1949. The signifcance of congenital lumbo-sacral abnormalities. *Brit J Radiol* 22: 270–275.

Girard PM. 1935. Congenital absence of the sacrum. *J Bone Joint Surg* 17: 1062–1064.

Goldstein R. 1947. Agenesis of sacrum and coccyx. *Acta Med Orientalia* 6: 202–204.

Greulich WW, Thhoms H. 1938. The dimensions of the pelvic inlet of 789 white females. *Anat Rec* 72: 45–51.

Hadley LA. 1950. Accessory sacroiliac articulations with arthritic changes. *Radiology* 55: 403–409.

Hamsa WR. 1935. Congenital absence of the sacrum. *Arch Surg* 30: 657–666.

Harris HA. 1953. Ossification in the lumbo-sacral region. *Brit J Radiol* 6: 685–688.

Harrison RG. 1901. On the occurrence of tails in man, with a description of the case reported by Dr. Watson. *Johns Hopkins Hosp Bull* 12: 96–101.

Heyns OS, Kerrich JE. 1947. The number of vertebrae in the fetal Bantu sacrum. *Am J Phys Anthropol* 5: 67–78.

Katz JF. 1953. Congenital absence of the sacrum and coccyx. *J Bone Joint Surg (Am)* 35: 398–402.

Keith A. 1921. The disappearance and reappearance of the human tail. *Nature* 106: 845.

Lanier VS, McKnight HE, Trotter M. 1944. Caudal analgia: An experimental and anatomical study. *Am J Obst Gynec* 47: 633–641.

Letterman GS, Trotter M. 1944. Variations of the male sacrum. Their significance in caudal anesthesia. *Surg Gynecol Obstet* 78: 551–555.

Lewin T. 1968. Anatomical variations in lumbo-sacral synovial joints with particular references to subluxation. *Acta Anat* 71: 229–248.

Lichtor A. 1947. Sacral agenesis. *Arch Surg* 54: 430–433.
Mitchell GAG. 1936/37. The significance of lumbosacral transitional vertebrae. *Brit J Surg* 24: 147–158.
Nathan H, Arensburgh B. 1972. An unusual variation in the fifth lumbar and sacral vertebrae: A possible cause of vertebral canal narrowing. *Anat Anz* 132: 137–148.
Newell JL. 1934. A case of multiple congenital anomalies of the Müllerian and genito-urinary systems with absence of the coccyx. *New England J Med* 210: 1217–1218.
Phesant HC, Swenson PC. 1942. The lumbosacral region. A correlation of the roentgenographic and anatomical observations. *J Bone Joint Surg (Am)* 24: 299–306.
Piontek J. 1971. Variation of the level of closure of the sacral canal in man. *Folia Morphol (Warsaw)* 30: 460–464.
Pirkey EL, Purcell JH. 1957. Agenesis of lumbosacral vertebrae. A report of two cases in living infants. *Radiology* 69: 726–729.
Roller GT, Pribram HFW. 1965. Lumbosacral intradural lipoma and sacral agenesis. *Radiology* 84: 507–512.
Rowe GG. 1950. Anomalous vertebrae from the lumbo-sacral column of man. *Anat Rec* 107: 171–179.
Russell HE, Aitken GT. 1963. Congenital absence of the sacrum and lumbar vertebrae with prosthetic management. *J Bone Joint Surg (Am)* 45: 501–508.
Sinclair JG, Duren N, Rude JC. 1941. Congenital lumbosacral defect. *Arch Surg* 43: 473–478.
Smith ED. 1959. Congenital sacral anomalies in children. *Aust NZ J Surg* 29: 165–176.
Southworth JD, Bersack SR. 1950. Anomalies of the lumbosacral vertebrae in five hundred and fifty individuals without symptoms referable to the low back. *Am J Roentgenol* 64: 624–634.
Sugar 0. 1987. How the sacrum got its name. *JAMA* 257: 2061–2063.
Taylor RG. 1939. Anomalies of the lumbosacral articulations. *JAMA* 113: 463–465.
Trotter M. 1926. The sacrum and sex. *Am J Phys Anthropol* 9: 445–450.
Trotter M. 1937. Accessory sacroiliac articulations. *Am J Phys Anthropol* 22: 247–261.
Trotter M. 1940. A common anatomical variation in the sacro-iliac region. *J Bone Joint Surg* 22: 293–299.
Trotter M. 1947. Variations of the sacral canal: Their significance in the administration of caudal analgesia. *Curr Res Anaesth Analgesia* 26: 192–202.
Trotter M. 1964. Accessory sacroiliac articulations in East African skeletons. *Am J Phys Anthropol NS* 22: 137–142.
Trotter M, Letterman GS. 1944. Variations in the female sacrum. Their significance in continuous caudal anaesthesia. *Surg Gynecol Obstet* 78: 419–424.
Trotter M, Lanier PF. 1945. Hiatus canalis in American Whites and Negroes. *Human Biol* 17: 368–381.
Turner W. 1886a. The sacral index of the pelvic brim as a basis of classification. *J Anat Physiol* 20: 125–143.
Turner W. 1886b. The sacral index in various races of mankind. *J Anat Physiol* 20: 317–323.
Weisel H. 1954. The articular surfaces of the sacro-iliac joint and their relation to the movement of the sacrum. *Acta Anat* 22: 1–14.
Willis TA. 1923. The lumbo-sacral vertebral column in man, its stability of form and function. *Am J Anat* 32: 95–123.
Young M, Ince JGH. 1939/40. Transmutation of vertebrae in the lumbosacral region of the human spine. *J Anat* 74: 369–373.

7 Scapula

Peter J. Ward
West Virginia School of Osteopathic Medicine, Lewisburg, West Virginia, United States

Body of the scapula

The body of the scapula is typically triangular with distinct medial, superior, and lateral borders. The medial border meets the superior at the pointed superior angle of the scapula. The superior border meets the lateral border at the glenoid fossa, which articulates with the head of the humerus. The lateral border meets the medial border at the pointed inferior angle of the scapula.

The fossae for the supraspinatus and infraspinatus muscles are located on the scapula's posterior aspect and the bone in this region can become quite thin (Fig. 7.1a). Foramina through the body of the scapula, particularly in the infraspinatus fossa, have a reported incidence of between 0.9 and 3.4% (Vallois 1926; Gray 1942). These defects can be seen radiographically and remain unchanged over time. They are problematic if the resulting radiolucency is mistaken for a lesion of the lung (Citgay and Mascatello 1979; Prescher 2000; De Wilde et al. 2004).

An inconstant bone has been described residing immediately inferior to the inferior angle of the scapula (Fig. 7.2a). The presence of this bone simulated a radiopaque lung lesion leading to its discovery during a medical visit (Adler 1941; Kohler and Zimmer 1968; McClure and Raney 1975 quoting). Another unusual and incidental finding involving the body of the scapula was the case of a 42-year-old Chinese man whose scapula was shown radiographically to be missing its inferior one-quarter with a bifurcated inferior body (Fig. 7.2b). There was no history of injury or disability and the patient had presented for treatment of nausea, vomiting, and hiccups (Khoo and Kuo 1948).

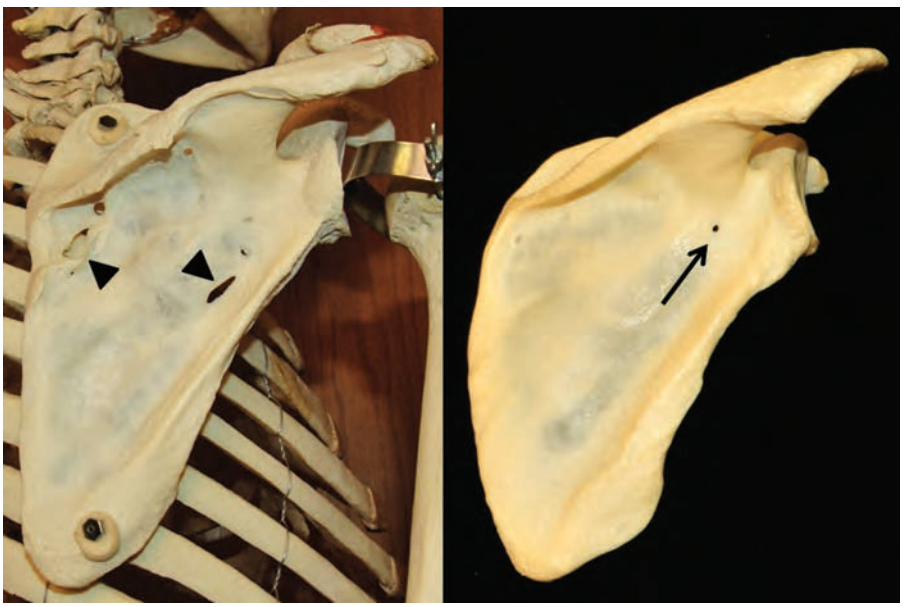

Figure 7.1 Defects of the body of the scapula. Abnormally large defects (arrowheads) are different from large nutrient foramina of the scapula (arrow).

Bergman's Comprehensive Encyclopedia of Human Anatomic Variation, First Edition. Edited by R. Shane Tubbs, Mohammadali M. Shoja and Marios Loukas.

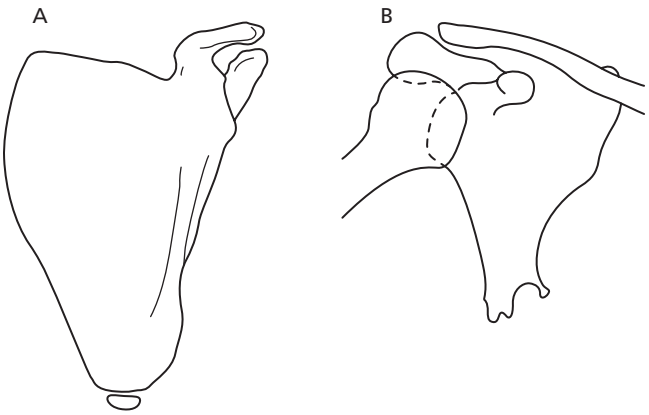

Figure 7.2 (a) Position of the infrascapular bone. (b) Rare dysplasia of the scapular body.

Source: McClure and Raney (1975). Reproduced with permission from Wolters Kluwer Health.

Scapular articulations with ribs

Typically the anterior surface of the scapula is smooth and articulates indirectly with the posterior thoracic wall via the scapulothoracic joint. The anterior surface of the scapula has sometimes been reported to have distinct synovial articulations with the ribs that restrict its motion. This has been reported occurring near the inferior angle, superior angle, and superior border of the scapula (Gruber 1864, 1872; Fontan 1912; Kajava 1924). The reported incidence of costal facets on scapulae has been reported as 5.6–7.2% (Vallois 1926; Gray 1942).

Curvature of the scapular body

The degree of concavity varies considerably and may impact the ease with which the scapula moves along the posterior thoracic wall (Dwight 1887). The angle formed by connecting the scapula's superior angle, base of the scapular spine, and inferior angle (Fig. 7.3) falls within the range 124–162° (Lehtinen et al. 2005; Aggarwal et al. 2011). The largest angle was associated with a tubercle of Luschka.

Figure 7.3 Different curvatures of the scapular body: (a) flat; (b) moderately curved; and (c) markedly curved.

Tubercle of Luschka

The tubercle of Luschka is an extension of bone from the superior angle of the scapula. It is not an osteochondroma or other bony tumor, but an extension of the scapula in the vicinity of the levator scapulae muscles (Lehtinen et al. 2005). A study of scapulae in the Huntington collection at the Smithsonian museum found 42/700 (6.0%) scapulae that displayed a prominent tubercle of Luschka (Edelson 1996). The authors also describe how the presence of the tubercle of Luschka may be associated with "snapping scapula." This condition causes a palpable and audible click as the scapula moves across the posterior ribcage (Parsons 1973; Percy et al. 1988).

Lateral border of scapula

The lateral border of the scapula is often a relatively direct line running from the inferior aspect of the glenoid to the inferior angle. However, there is variability associated with the prominence of the attachment site for the teres major muscle (Dwight 1887; Hrdlička 1942a–c). The prominence of this attachment site can vary from a slightly raised region of the lateral border to a "rhino-horn" projection. In one study a very prominent horn was seen in 22% of scapulae from the Huntington collection of the Smithsonian and 7/700 (1.0%) of those specimens had the projection veering medially and anteriorly towards the body, potentially restricting scapular motion (Edelson 1996). A sulcus for the circumflex scapular artery as it crosses the lateral border of the scapula has been reported as being absent in 14.5–40.0% of specimens (Kajava 1924; Vallois 1932; Bergman et al. 1988). The latissimus dorsi sometimes attaches to the dorsal surface of the inferior angle of the scapula.

Medial border of scapula

The medial border of the scapula can be convex (Fig. 7.4a), straight (Fig. 7.4b), or concave (Fig. 7.4c) (Graves 1910, 1921; Vallois 1928; Hrdlička 1942a, c). The reported variation of these features is fairly consistent: convex, 54.3–61.3%; straight, 20.8–27.0%; concave, 9.9–18.7%; and unclassifiable in 0.2% of the specimens studied (Graves 1921; Gray 1942).

Inferiorly, instead of a pointed inferior angle there may be a flat inferior border of the scapula (Fig. 7.4d). The medial border may also veer laterally (Fig. 7.4e) immediately superior to the scapular spine (Dwight 1887; Vallois 1928; Hrdlička 1942a). Medial angulation of the superior angle was seen superior to the spine of the scapula in 60/700 (8.5%) of scapulae from the Huntington collection of the Smithsonian (Edelson 1996).

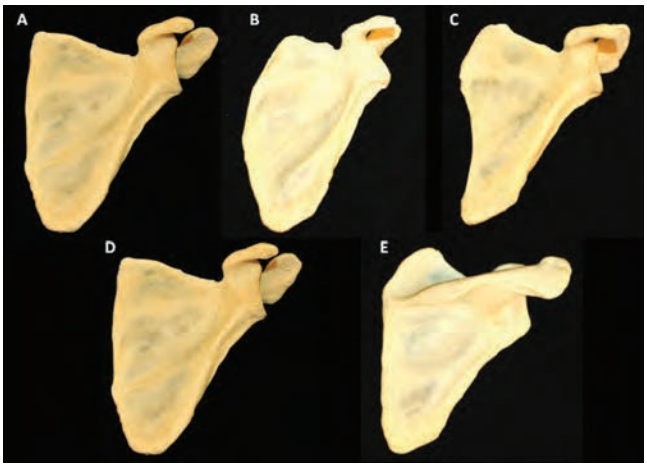

Figure 7.4 Medial and inferior borders of the scapula: (a) straight medial border; (b) convex medial border; (c) concave medial border; (d) distinct horizontal inferior border; and (e) sharp lateral inclination of medial border superior to spine of the scapula.

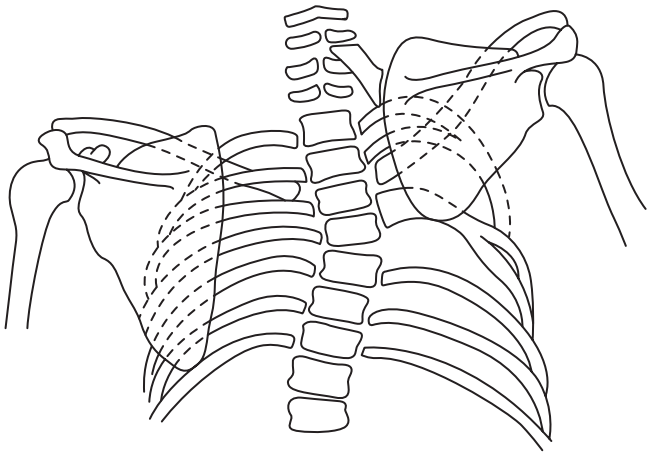

Figure 7.5 Undescended scapula with omovertebral bone.

Source: McClure and Raney (1975). Reproduced with permission from Wolters Kluwer Health.

Rarely, a bony bridge known as the omovertebral bone (Fig. 7.5) may exist between the medial border or the superior angle of the scapula and the spinous and transverse processes of the cervical vertebrae (McClure and Raney 1975; Bergman et al. 1988). This omovertebral bone was found in 54% of the subjects enrolled in a surgical study of Sprengel's deformity, congenital high scapula. Two cases demonstrated a synovial articulation between the omovertebral bone and scapula (Khairouni et al. 2002).

Superior border of scapula

The superior border is the most variable of the scapula's borders. The variations associated with the scapular notch and the coracoid process will be discussed separately. Aside from those two features the superior border can appear horizontal (Fig. 7.6a), moderately oblique (Fig. 7.6b), markedly oblique (Fig. 7.6c), deeply saddle-shaped (Fig. 7.6d), concave or semilunar (Fig. 7.6e), or wavy (Fig. 7.6f) (Hrdlička 1942a).

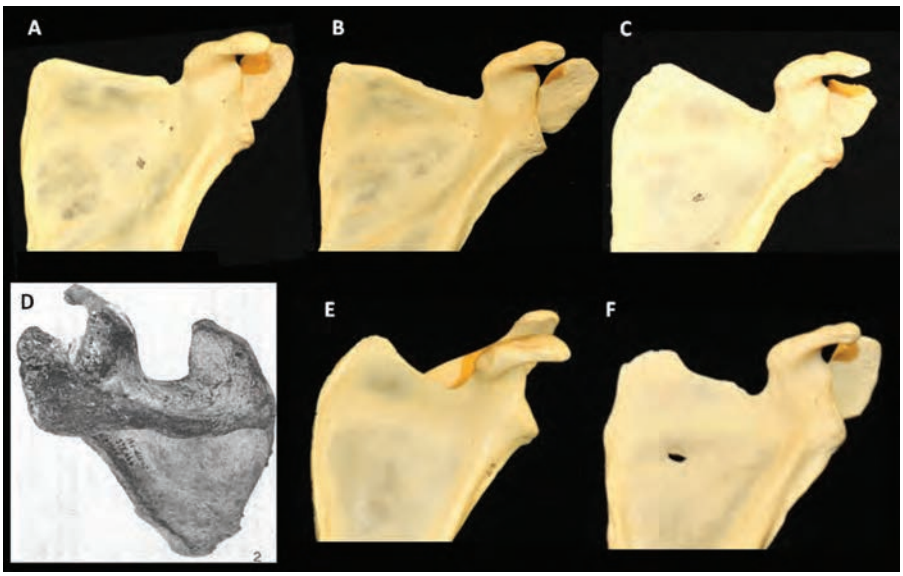

Figure 7.6 Types of superior scapular border: (a) horizontal; (b) moderately oblique; (c) markedly oblique; (d) saddle-shaped; (e) deeply concave; and (f) wavy.

Source (d): Hrdlička (1942c). Reproduced with permission from John Wiley & Sons.

Scapular notch

The differences in the appearance of the scapular notch contribute to the variability of the superior border of the scapula. Sometimes it is not present or only exists as a slight depression along the superior border (Fig. 7.7a). When present, it has been described as: J-shaped with the origin of medial border of notch notably inferior to origin of lateral border (Fig. 7.7b); deep U-shaped with the origins of medial and lateral borders of notch roughly equal (Fig. 7.7c); V-shaped with the inferior aspect of the notch forming an acute angle (Fig. 7.7d); the notch nearly surrounded by bone; or the notch wholly surrounded by bone (Fig. 7.7e) (Hrdlička 1942a). The frequency of each type of scapular notch varies widely between studies, which may be due to the subjective distinctions made by different authors. The reported variances are: J-shaped, 22%; deep U-shaped, 13.2–62.5%; V-shaped, 20–25%; slight indentation, 26.8%; and not present, 18% (Vallois 1926; Prescher 2000; Iqbal et al. 2010). An alternative set of terms (Type I = no notch; Type II = notch longest in transverse diameter; Type III = notch longest in vertical diameter; Type IV = bony foramen; and Type V = notch and a bony foramen) was proposed in a study by Natsis (2007a).

As noted above, the scapular notch is occasionally bridged by bone instead of the superior transverse scapular ligament (McClure and Raney 1975; Bergman et al. 1988; Osuagwu et al. 2005; Khan 2006). In these cases there is a circular suprascapular foramen that typically surrounds the suprascapular nerve. The reported rates of ossification of the superior transverse scapular ligament fall within the range 1.5–12.5% (Poirier and Charpy 1911; Kajava 1924; Vallois 1926, 1932; Gray 1942; Edelson 1995b; Prescher 2000; Bayramoğlu et al. 2003). One study in a Brazilian population had an unusually high incidence of 30.8% (Silva et al. 2007). The suprascapular foramen is more common in aged scapulae and in white males (Edelson 1995b).

In a study of 32 dissected scapulae, the superior transverse scapular ligament was described as bipartite (5/32), fan-shaped (17/32), or ossified (4/32), with the suprascapular nerve passing through the opening (Bayramoğlu et al. 2003).

Coracoid process

The coracoid process is located immediately lateral to the scapular notch on the superior border of the scapula. It forms from distinct centers of ossification that may fail to unite with the rest of the scapula. In this case it will exist as a separate bone (Bergman et al. 1988). The muscles associated with the coracoid process may also vary, giving it an unusual appearance. The pectoralis minor muscle, which typically inserts on the distal coracoid, may send muscle fibers superior to the coracoid process to insert on the scapular neck or humerus instead. In these cases, there is often a distinct groove on the superior aspect of the coracoid process (Seib 1938; Bergman et al. 1988).

The coracoclavicular ligaments that span the space between the superior aspect of the coracoid process and the inferior distal clavicle can sometimes ossify (Fig. 7.8a) to become a strut of bone (Nutter 1941; McClure and Raney 1975). One radiographic study of this condition found that in 12/1000 (1.2%) instances of this bony strut there was a distinct coracoclavicular joint (Fig. 7.8b) complete with cartilaginous articular surfaces (Nutter 1941). Other instances of this variation show either complete ossification between the coracoid and clavicle or a mix of fibrous and osseous material (McClure and Raney 1975).

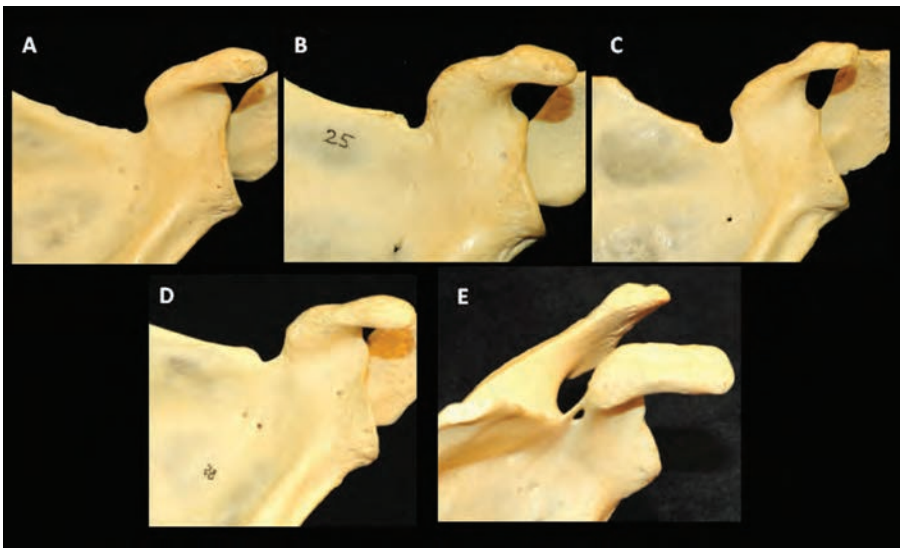

Figure 7.7 Variations of the scapular notch: (a) notch is almost wholly absent; (b) J-shaped; (c) deep U-shaped; (d) V-shaped; and (e) fully ossified superior transverse scapular ligament.

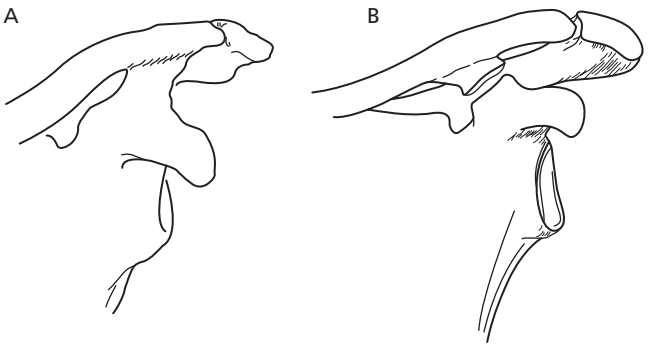

Figure 7.8 Osseous connections between the coracoid process of the scapula and the clavicle: (a) coracoclavicular bridge; and (b) coracoclavicular articulation.

Source (a): McClure and Raney (1975). Reproduced with permission from Wolters Kluwer Health.

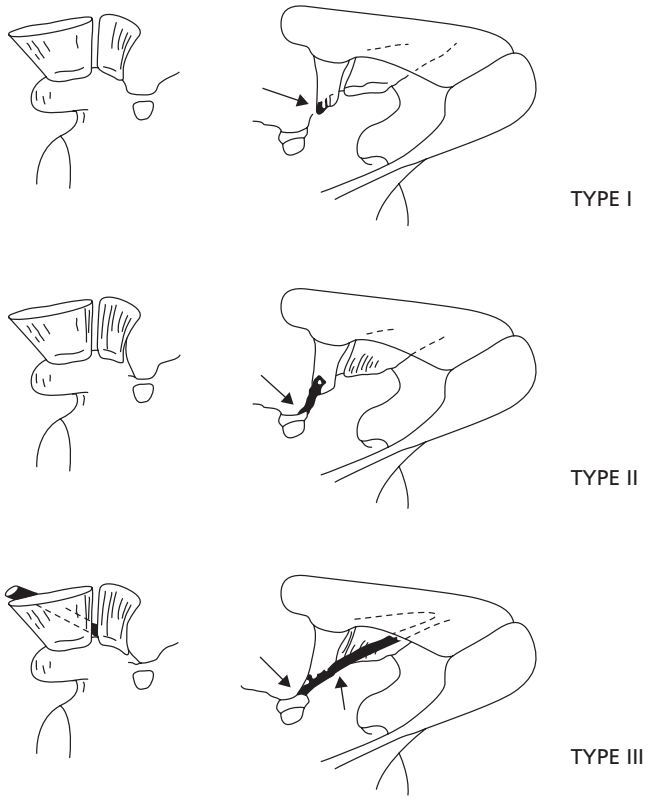

Figure 7.9 Proposed classification of the coracoclavicular ligament based on its variant scapular attachments. Type 1: conoid and trapezoid ligaments separate from superior transverse scapular ligament. Type II: ligamentous bridge between conoid and superior transverse scapular ligament. Type III: a ligamentous band extending from superior transverse scapular ligament across trapezoid ligament.

Source: Harris et al. (2001). Reproduced with permission from Elsevier.

An anterior coracoscapular ligament has been described spanning the medial side scapular notch to the medial aspect of the coracoid process (Avery et al. 2002; Bayramoğlu et al. 2003). It was seen in 16/27 cadavers (11/16 bilateral) that were examined and was distinct from the superior transverse scapular ligament in all cases. The suprascapular nerve passed inferiorly in all cases, the suprascapular artery passed superiorly in all cases, and the suprascapular vein passed superiorly in 81% of the cases. It was also possibly the ligament described in two case studies which described a split superior transverse scapular ligament in the vicinity of the medial coracoid base (Alon et al. 1998) and spanning the supraspinous fossa to the base of the coracoid process (Fabrizio 2012).

Three variations of the coracoclavicular ligaments have been reported. Type I coracoclavicular ligaments (9/18) had the conoid ligament originate from the posterior dorsal coronoid process and dorsal coronoid precipice (Fig. 7.9a). Type II ligaments (6/18) were similar but had fibers confluent with the superior transverse scapular ligament (Fig. 7.9b). Type III ligaments (3/18) had a fascicle running from the superior transverse scapular ligament to fuse with the trapezoid ligament (Fig. 7.9c) (Harris et al. 2001).

A bifid coracoid process was noted alongside a duplicated acromion in one case study (McClure and Raney 1974). A single case study has also described a feature referred to as the os coracosternale vestigale. In this instance, a 7-month-old boy presented with an elevated right shoulder that was rotated anteriorly across the superior shoulder. A bony connection between the coracoid process and the sternum was found, presumably a remnant of mesenchymal tissue that normally disappears during development (Finder 1936).

Shape of the glenoid fossa

The glenoid fossa is a concave depression where the scapula articulates with the round head of the humerus. The presence of a glenoid notch in the anterio-superior rim of the glenoid cavity gives the cavity an indented, piriform shape (Fig. 7.10a) instead of an oval appearance (Fig. 7.10b). The reported rates of these shapes vary widely, likely as a result of subjective distinctions made by different authors. In study of 1149 scapulae (Gray 1942) there were four types described: piriform with a glenoid notch (92.4%); round (0.4%); oval (6.8%); and unclassifiable (0.3%). Another study of 236 scapulae (Prescher and Klümpen 1997) found two shapes only: piriform (54.6%) and oval (45.4%). Yet another study of 90 scapulae (Coskun et al. 2006) strongly notched piriform shapes less frequently (28%) than oval (72%). The same authors showed some glenoid cavities exhibiting two notches (on the anterior and posterior aspects of the superior glenoid rim) but did not give a rate of incidence.

An unclassifiable or irregular glenoid fossa can be caused by dysplasia of the scapular neck. The inferior aspect of the glenoid cavity may be hypoplastic (Fig. 7.11a) with a dentate or notched

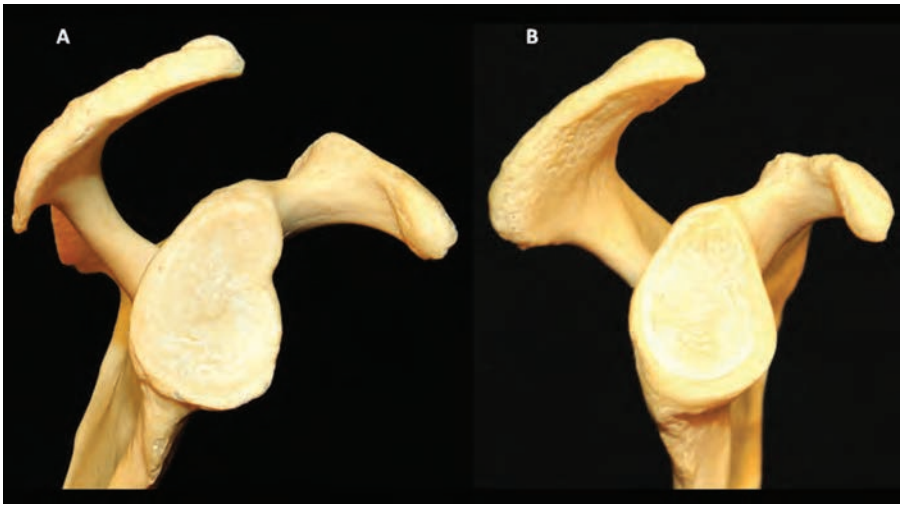

Figure 7.10 Different appearances of the glenoid fossa: (a) piriform with glenoid notch on anterior aspect of the fossa; and (b) oval without glenoid notch.

border (Brailsford 1953; Sutro 1967; McClure and Raney 1975). This occurs infrequently and is typically bilateral (Resnick et al. 1982). In very rare cases the glenoid cavity may be convex and the humeral head is slightly concave (Fig. 7.11b) (Brailsford 1953; McClure and Raney 1975).

The anterior superior aspect of the glenoid labrum is sometimes detached from the glenoid fossa, creating a small sublabral foramen (Cooper et al. 1992; Williams et al. 1994; Tirman et al. 1996). This variation may be mistaken for a lesion of the glenoid labrum, resulting in unnecessary surgery. In a retrospective study a sublabral foramen was seen in 24/200 (12%) of arthroscopic videos (Williams et al. 1994). These researchers found that 18/24 of these patients also had a cord-like middle glenohumeral ligament. They also noted the Buford complex in 3/200 (1.5%) of the subjects. The Buford complex is the combination of a cord-like middle glenohumeral ligament along with the absence of the anterosuperior glenoid labrum (Williams et al. 1994; Tirman et al. 1996).

The inferior transverse scapular ligament (sometimes called the spinoglenoid ligament) has been described as arising from the lateral scapular spine and inserting onto the rim of the glenoid fossa or glenohumeral joint capsule. It likely serves to keep the suprascapular neurovascular bundle intact as it crosses from the supraspinous fossa to the infraspinatus fossa (Prescher 2000; Demirkan et al. 2003; Plancher et al. 2005). However, one study set a very rigorous definition for what constituted a true ligament and found an unambiguous inferior transverse scapular ligament in only 2/75 shoulders examined (Demaio et al. 1991). A thickened aponeurosis was seen in its place in 10/75 specimens. Kharay and Sharma (2010) reported an ossified spinoglenoid ligament.

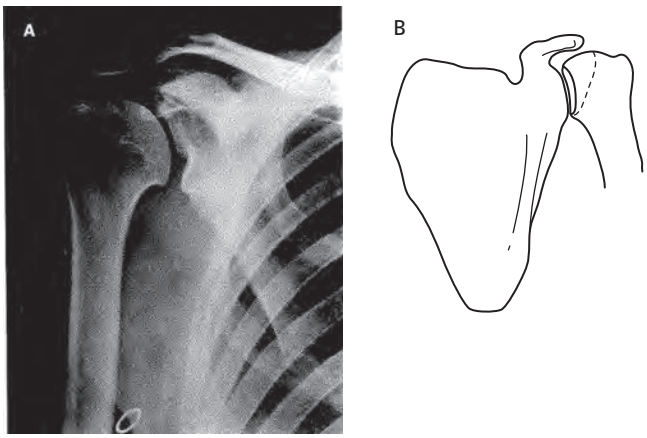

Figure 7.11 Irregular glenoid fossa and scapular neck dysplasia: (a) dentated/notched inferior glenoid fossa; and (b) hypoplasia of scapular neck, irregular notched glenoid articular surface, and widening of lower part of joint space.

Source (a): Sutro (1967). Reproduced with permission from J. Michael Ryan Publishing.

Shape of acromion

The spine of the scapula separates the supraspinous and infraspinous fossae and extends laterally to end in a bony strut that articulates with the distal clavicle. Viewed from above, the shape of the acromion has been described as falciform (Fig. 7.12d), triangular (Fig. 7.12c), quadrangular (Fig. 7.12a), or intermediate (Macalister 1893). Widely varying rates of occurrence have been reported: falciform (5.7–46.9%); triangular (8.3–61.3%); quadrangular (1.3–55.8%); and intermediate (5.1–61.2%). The wide variances in the percentage of scapulae in each category likely reflects a lack of agreement on what makes each type unique rather than pure morphologic variation (Kajava 1924; Vallois 1932; Gray 1942; Bergmann et al. 1988; Edelson 1995a). Other authors have described the superior aspect of the acromion as cobra-shaped, square, and intermediate (Edelson and Taitz 1992). One study using this nomenclature investigated 90 Turkish scapulae and found 31% cobra-shaped, 13% square, and 56% intermediate (Coskun et al. 2006).

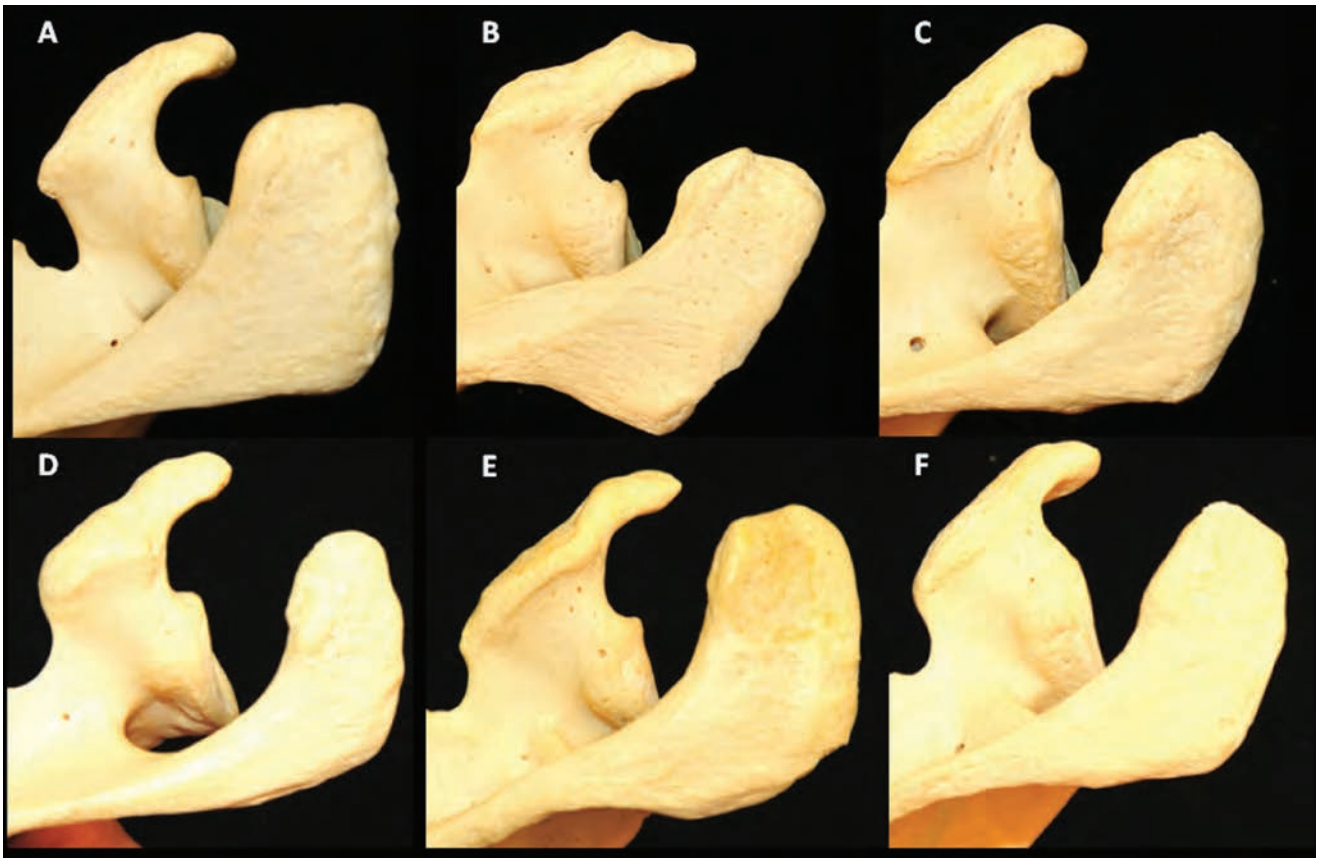

Figure 7.12 Shape of acromion from a superior view: (a) quadrangular; (b) quadrangular with prominent posterior angle; (c) triangular; (d) falciform (small posterior corner); (e) quadrangular (falciform tendency); and (f) triangular (falciform tendency).

When viewed laterally, the inclination of the acromion can vary significantly (Dwight 1887). This shape has been described as flat (Fig. 7.13a), curved (Fig. 7.13b), or hooked (Fig. 7.13c) (Bigliani et al. 1986). A fourth shape was later described wherein the acromion is curved with an inferiorly convex middle third (Fig. 7.13d) (Gagey et al. 1993; Natsis et al. 2007b). The reported incidence of each type of lateral acromial shape is tremendously variable: flat (10–43%); curved (25–89.8%); hooked (0–40%); and inferiorly convex (1.6–2.6%) (Bigliani et al. 1986; Epstein 1993; Gagey et al. 1993; Nicholson et al. 1996; Coskun et al. 2006; Natsis et al. 2007b). This variability may be due to differences in how each author viewed the scapulae as well as differences in terminology related to outgrowths from the distal acromion; these include such diverse terms as plaques, hooks, enthesophytes, beaks, osteophytes, spurs, etc. (Chambler and Emery 1997). One study of 394 scapulae (Getz et al. 1996) did apply a consistent quantitative algorithm of categorizing each acromial shape and found: flat (22.8%); curved (68.5%); and hooked (8.6%). While several studies did not find any connection between age and acromial shape (Getz et al. 1996; Nicholson et al. 1996), another study of 830 scapulae did find that hooked scapulae increased in proportion over time and that hooked acromia were present bilaterally in 73% of the specimens studied (Edelson 1995a). The author stated that the presence of an enlarged facet for the acromioclavicular joint may be what some authors have previously identified as a "hook."

The lateral shape of the acromion is of clinical interest primarily because of its potential role in rotator cuff dysfunction. Hooked acromia were found in much higher proportion in a population of patients with rotator cuff impingement or full-thickness tears of the supraspinatus tendon (Epstein et al. 1993). Likewise, lowering the coracoacromial arch by hooking of the acromion or inferior angulation of the coracoid process is associated with degenerative changes (Edelson and Taitz 1992). The coracoacromial ligament attaches to the acromion in four ways: on the inferior aspect of the acromion away from its apex (Fig. 7.14d) (22.2%); inferiorly at the apex (Fig. 7.14c) (21.6%); at the apex in line with the inferior aspect of the acromion (Fig. 7.14b) (49.5%); or at the apex but not in line with the inferior aspect (Fig. 7.14a) (8.7%). There were also hybrid types (Gagey et al. 1993). Curved or hooked acromia are also more likely to have enthesophytes near the location of the coracoacromial ligament (Gagey et al. 1993; Natsis et al. 2007b). The incidence of anterior acromial spurs increases from 7% in specimens under 50 years to 30% in specimens over 50 years (Nicholson et al. 1996).

Regarding very rare variations affecting the shape of the acromion, there is a case study of a German's miner who had an acromion that extended laterally and inferiorly to the level of the surgical neck of the humerus (Arens 1951; McClure and Raney 1975).